

FEASIBILITY IN DEVELOPING SMART STRUCTURES
FOR USE IN WIND TURBINE BLADES

by

James Craig Blockey

A thesis submitted in partial fulfillment
of the requirements for the degree

of

Master of Science

in

Mechanical Engineering

MONTANA STATE UNIVERSITY
Bozeman, Montana

July 2008

©COPYRIGHT

by

James Craig Blockey

2008

All Rights Reserved

APPROVAL

of a thesis submitted by

James Craig Blockey

This thesis has been read by each member of the thesis committee and has been found to be satisfactory regarding content, English usage, format, citation, bibliographic style, and consistency, and is ready for submission to the Division of Graduate Education.

Dr. Doug Cairns

Approved for the Department of Mechanical and Industrial Engineering

Chris Jenkins

Approved for the Division of Graduate Education

Dr. Carl A. Fox

STATEMENT OF PERMISSION TO USE

In presenting this thesis in partial fulfillment of the requirements for a master's degree at Montana State University, I agree that the Library shall make it available to borrowers under rules of the Library.

If I have indicated my intention to copyright this thesis by including a copyright notice page, copying is allowable only for scholarly purposes, consistent with "fair use" as prescribed in the U.S. Copyright Law. Requests for permission for extended quotation from or reproduction of this thesis in whole or in parts may be granted only by the copyright holder.

James Craig Blockey

July 2008

ACKNOWLEDGEMENTS

During the course of writing this thesis, assistance was never in short supply. Assistance came in many forms ranging from recommendations to machining work to LabVIEW programming to mental support. Without this help the completion of this thesis would not have been possible. There are numerous individuals and organizations that deserve to be acknowledged, including, but not limited to Dr. Doug Cairns, for heading my thesis committee, for trusting me to work on this project and helping throughout the process of my Masters Degree. Dr. John Mandell, for the time he spent reviewing my thesis and work and being a member of my thesis committee. Robb Larson, for the time he spent helping with LabVIEW programming and for spending the time to be on my thesis committee. Jon Ehresman, for the work he did in developing the prototype and always being prepared for a barbeque or floating trip to help clear the mind. James Schmitt, for his constant suggestions and advice, for pushing me to expand my thinking and time spent helping with the prototype. Nathan Palmer for his work with the test specimens and the SEM; for doing the elbow work and keeping me up to date with the projects that were rooted in the work presented in this thesis. John Parker for his help running the ME 251 lab, the cutting and mixing work he assisted me with, as well as the regular advice and recommendations he provided. Cali and the girls from Spectators for always being willing to provide support, sustenance and affirmation. All my friends, family and others who helped or simply tolerated the hours spent at the computer finishing this project and thesis.

TABLE OF CONTENTS

1. INTRODUCTION	1
2. BACKGROUND	8
3. CONTROL SURFACES.....	10
Introduction	10
The Creation of Lift	10
Current Power Control Mechanisms.....	12
Previous Design Attempts and Design Alternatives.....	15
Design Alternatives	15
The Gurney Flap.....	17
History.....	17
Function of the Gurney Flap.....	20
Variables in the Design of the Gurney Flap	22
Flap Height	23
Flap Location	24
Mounting Angle	25
Final Considerations of the Gurney Flap	26
4. THE PROTOTYPE	27
Introduction	27
System Requirements.....	27
System Overview	28
Detailed Description	30
Testing Procedures	32
Prototype-Stage 1	34
Prototype-Stage 2	40
Prototype-Stage 3	43
Program Changes.....	45
System Testing	49
Prototype-Stage 4	57
The Programs.....	57
Inclusion of a Damper	60
Adding a Power Boost	64
System Testing	67
Addition of the Pressure Transducer.....	70
Conclusion:.....	72
Active Control Surfaces and Prototype Conclusions and Future Work	73

TABLE OF CONTENTS-CONTINUED

5. SENSORS	76
Introduction	76
Sensor Options and Selection	78
The Different Sensors	79
Metal Foil Strain Gauges	80
Piezoelectric Strain Gauges	83
Fiber Optic Strain Gauges	84
Other Strain Gauges	87
Sensor Selection	89
The Fiber Optic Sensor and Fiber Bragg Gratings	90
The Fiber Bragg Grating	90
Creating and Manufacturing the Fiber Bragg Grating	91
Applying FBGs to Sensors	94
Interrogation Methods	96
Time-Division Multiplexing	96
Wavelength-Division Multiplexing	98
Interrogation Conclusion	100
Considerations of Embedded FBG Based Strain Gauges	101
Reliability of Embedded FBGs	102
Mechanical Failure	102
Optical Degradation	105
Color Center Model	106
Densification Model	107
Power-Law and Log-Time Models	108
Effects of Embedded Optical Fibers on Laminates	114
Effect on Static Strength	115
E.J. Friebele et al.-1999 [60]	115
Jose Silva et al.-2005 [61]	118
Effects on Fatigue Strength	119
Surgeon and Wevers 1999 and 2001 [62, 63]	119
Jose Silva et al.-2005 [61]	124
Effects of Embedded Fiber Optics Conclusion	125
Sensors Conclusion	127
6. CONCLUSIONS AND FUTURE WORK	132
Conclusions	132
Active Control Surfaces	132
The Prototype	132
Sensors	133

TABLE OF CONTENTS-CONTINUED

Future Work	135
Active Control Surfaces	135
The Prototype	136
Sensors	138
Closing Remarks	140
REFERENCES CITED	142
APPENDICES	148
APPENDIX A	149
APPENDIX B.....	158
APPENDIX C.....	162

LIST OF TABLES

Table	Page
1. Numerous different tests were performed during the course of the development of the prototype, these tests and their purposes are discussed to clarify the later discussion.....	32
2. This shows the average stopping distance of the actuator when attempting the desired test lengths. This series of tests had no buffer zone.....	41
3. This shows the average stopping distance of the actuator when attempting the desired test lengths. This series of tests allowed a 2mm buffer zone, before the desired displacement, in an attempt to prevent overshoot.....	42
4. A listing of the tests conducted to examine the maximum velocity, deceleration and overshoot of the actuator, at various actuation distances.....	52
5. Data collected from tests examining the sampling rate of the DAQ system, during full speed actuation of the flap.....	55
6. Tests were run to an actuation distance of 45 mm, with varying combinations of Boost and Damping; the closer the average test stopping distance was, to 45 mm, the better the results.....	67
7. Numerous tests were run to an activation distance of 45 mm, to examine the effect of changing the buffer zone size and the boost zone size; the closer the average final stopping distance was to 45 mm, the better the results.	68
8. Tests were run to various distances throughout the activation limits of the prototype. The top value is the distance the following series of tests was run to.	69
9. The tests conducted by Freible et al. were as shown, the fiber orientation represents each individual test conducted, the previous columns describe the method of the test.....	115
10. The results of the experiment showed that optical fiber orientation, with respect to the surrounding plies, has a significant effect on the degradation of a laminate.	117
11. Three point bending tests showed there to be little variation of both the stiffness and the modulus of rupture of the specimens with and without embedded optical fibers.	118

LIST OF TABLES-CONTINUED

Table	Page
12. The cycles to failure for the different sets of specimens revealed a stark contrast in the life expectancies of laminates with embedded optical fibers, depending on the direction of the surrounding plies.	121
13. A listing of all the major components used in the construction and testing of the prototype throughout the development process.	159

LIST OF FIGURES

Figure	Page
1. A diagram showing the increase in size of wind turbines built from 1985 to 2007 [2].	1
2. A wind turbine failure can be catastrophic, with devastating results. Tips of the blades can reach speeds in excess of 150 mph and pieces of the blades can be thrown over 1300 ft.	2
3. All modern aircraft utilize active control surfaces; the B2 Spirit bomber is an aircraft which revolutionized the possibilities and capabilities of the use of active control surfaces.	3
4. The North Wind 250 was developed in the early 1990s by Northern Power Systems. Its design incorporated an aileron style load control system.	4
5. The Gurney flap can be found in many applications, including some production vehicles such as the Mitsubishi Lancer Evo.	5
6. A Fiber Bragg Grating is a pattern printed onto an optical fiber, which reflects a specific wavelength of light.	6
7. The Brush wind turbine was the first to use wind energy for the generation of electrical power. © The Charles F. Brush Special Collection	8
8. The yearly production of renewable energy in the U.S., between 1984 and 2006.	9
9. The basis of the basic explanation of the creation of lift, as described by Bernoulli's Equation; based on the shape of the airfoil.	11
10. Without proper load control mechanisms severe damage and even destruction of a wind turbine can occur.	12
11. The transition to turbulent flow and boundary layer separation due to angle of attack and air velocity.	13
12. The flap patented by Zaparka was mounted near the trailing edge of an airfoil and was capable of being raised or lowered to adapt the airfoil to a given condition [13].	17
13. In 1971, Bobby Unser was the first to drive a car equipped with a Gurney Flap.	18

LIST OF FIGURES-CONTINUED

Figure	Page
14. An example of the original Gurney flap used on the All American Racers Eagle racing cars in 1971 [14].....	19
15. The effect of Gurney Flap mounting location on the generated lift [2].....	20
16. A demonstration of the recirculation region created in front of a Gurney flap and the vortex is formed behind the flap [24].....	21
17. Three of main variations made to a Gurney flap, are flap height, flap distance from the trailing edge and flap mounting angle [26].	22
18. Increasing the height of a Gurney flap will cause an increase in the generated lift as well as the drag [26].	23
19. By increasing the distance a Gurney flap is mounted away from the trailing edge of an airfoil, the lift is decreased, while drag effects are relatively scattered [26].	24
20. Minor decreases in lift are seen when flap angles are reduced, however there is also a significant decrease in drag on the airfoil [26].	25
21. In this prototype, the third stage seen here, the various main components can be seen: A) The linear actuator, B) The Gurney flap and C) The relay assembly can just be seen behind the actuator. The batteries are kept separate from the rest of the assembly.....	29
22. The piano hinge flap design has many benefits, including simplicity, with few moving parts, durability and a low profile.	30
23. The stage one prototype, utilizing both the mechanical and virtual flap.	34
24. The program required for the operation of the 'virtual' flap was relatively basic, monitoring an input and generating a single output. Several main components are labeled here.	35
25. The user interface for the Stage-1 Prototype mechanical flap. The program required many more controls than the 'virtual' flap.	37

LIST OF FIGURES-CONTINUED

Figure	Page
26. The program required for controlling the flap mechanism of the prototype was much more complex than that for the 'virtual' flap, requiring multiple levels of logic as well multiple inputs and outputs to monitor flap location and extend and retract the flap.....	38
27. Tests consistently showed better performance from the system when a LP was used instead of the LVDT. A series of tests were run to find the overshoot with the extensometers, when looking at three extension values; 10mm, 20mm and 30mm.....	41
28. Rigid supports were added to eliminate the need for additional linkages to support the actuator and other hardware.	44
29. The front panel of the control program was designed to be as user friendly as possible by being simple to use and provide a great deal of information to the user at the same time.	46
30. The first half of the control program, largely the input and data manipulation components of the program. The connections to the second half of the program are labeled A-E, along the right side of the program.	47
31. The second half of the program contains mostly the logic systems, safety switches and the output controls. The connections to the first half of the program can be seen on the left hand side of the program, labeled A-E.	48
32. The Stage 3 Prototype showed excellent deployment times, deploying to the full 89mm in only 190ms.	49
33. The actuator accelerates very quickly and attains a high maximum velocity; however the time required to decelerate is significantly longer, contributing to overshoot.	51
34. The slope of the deceleration region is relatively linear, which helps in predicting overshoot.....	52
35. Deceleration rates vary only slightly between all of the tests, even allowing for varying initial velocities.	53
36. The slow data acquisition rate achieved by the control program and DAQ caused large gaps in the data, during extension.....	55

LIST OF FIGURES-CONTINUED

Figure	Page
37. The use of the Math Script Node created a much cleaner, simpler and ostensibly better program, which may have been easier to understand but, in operation, proved, to be even slower than previous programs.	59
38. The logic structure of the control program was completely re-examined and re-thought, culminating in a much smaller and simpler control program than had previously been developed.	61
39. Tests showed a dramatic reduction in the extension of the actuator after power-off, with the inclusion of the damper.	62
40. Tests showed a 'burble' at the onset of the test, this was likely the result of a small amount of air in the damper.	63
41. At 12V the actuator ran slower, allowing for more precise control of the actuator, but took longer for full activation.	65
42. The Boost voltage design allowed for a stepped voltage, dropping from 24V to 12V as the actuator approached the desired location, as is demonstrated by the change in slope.	66
43. A plot of the pressure derived actuation distance and actuator location shows an excellent correlation between the two values.	71
44. The base of the tower and the nacelle have many sensors, the blades, however, still have no sensors.	76
45. The metal foil strain gauge is a simple gauge and is one of the oldest and best understood mechanisms for measuring strain.	80
46. As seen in this SEM image, embedded metal foil strain gauges can cause localized resin rich zone and debonding.	82
47. A stress applied to a piezoelectric material causes positive and negative charges to be created on the surface of the material.	83
48. In the first image an embedded optical fiber is shown, as can be seen, the fibers are small enough to be embedded directly in a laminate. The second image shows two strain gauge rosettes, the one on the right utilizes fiber optics while the rosette on the left utilizes metal foil strain gauges this demonstrates an advantage of multiplexing.	85

LIST OF FIGURES-CONTINUED

Figure	Page
49. Active Fiber Composites (AFCs) and Macro Fiber Composites (MFCs) are made by embedding PZT fibers in a polymer matrix, layered between a set of interdigitated electrodes.	88
50. In this SEM image, it can be seen that MFCs utilize a rectangular PZT fiber, which is much easier to manufacture and greatly reduces the costs of MFCs, compared to AFCs.	89
51. When light travelling down an optical fiber reaches a FBG, only a select wavelength of light is reflected back down the optical fiber.....	90
52. The holographic method utilizes two intersecting coherent beams of ultraviolet light to create an interference pattern.....	92
53. With a phase mask UV light passes unimpeded through a diffraction grating which suppresses the 0 order while the +/- 1 orders each contain approximately 40% of the diffracted light, creating the interference pattern.....	93
54. With a TDM interrogator, signals are differentiated by signal return time, the further away from the interrogator a FBG is located, the more time is required for the signal from the sensor to return.	96
55. With a WDM interrogator each FBG reflects only its individual Bragg Wavelength, by monitoring that wavelength, the interrogator is capable of differentiating the individual FBGs.	98
56. Damage to the optical fiber during handling and manufacturing is a major concern in the survivability of FOSs.....	101
57. The general construction of an optical fiber includes a silicone coating which is applied over the top of a silica cladding.....	103
58. (A) Stripping of the coating, covering the fiber core and cladding can reduce the mean strength of the fiber by over 50%. (B) Once stripped, the creation of the FBG further reduces the strength of the fiber, the mean value can be reduced by as much as 56%.....	104
59. The power-law correlation developed by Edrogan et al. to describe the optical decay of FBGs, written in non-hydrogen loaded fibers.	109

LIST OF FIGURES-CONTINUED

Figure	Page
60. The log-time model accomplishes a much better correlation, compared to the power-law model, with experimental data for hydrogen loaded fibers.	111
61. Embedding an optical fiber in a laminate, results in a large resin pocket surrounding the optical fiber, which can compromise the strength of the laminate.	114
62. The decrease in stiffness of the specimens tested at 450 MPa was substantial, more than a 10% decrease before 200k cycles.	120
63. The second set of experiments conducted by Surgeon and Wever showed rapid crack growth in the D set of specimens, validating the damage initiation caused by locating an optical fiber at the -45/90 interface.	123
64. A replica of an early Persian, vertical style, windmill.	150
65. Dutch windmills, typical of later European style windmills with more advanced blade designs.	151
66. The Brush wind turbine was the first to use wind energy for the generation of electrical power. © the Charles F. Brush Special Collection.	152
67. The 1300 MW Seminole Generating Station, a coal-fired power station, located in Florida, approximately 50 miles from Jacksonville. Courtesy Seminole Electric Cooperative.	154
68. The yearly production of renewable energy in the United States between 1984 and 2006.	155
69. During the 1990s government funded research into wind energy increased, providing an important key in the advancement and resulting expansion of wind generated electricity [2].	156
70. The complete virtual flap control program.	163
71. Input Control.	164
72. Output control and pressure logic.	164
73. The output control.	164
74. The complete Stage 1 Prototype control program.	165

LIST OF FIGURES-CONTINUED

Figure	Page
75. Input control	168
76. Data manipulation and logic	168
77. The logic boxes	169
78. The first half of the Stage 2 and 3 Prototype control program. The connections to the second half of the program can be seen on the right hand side of the program, labeled A-E.	170
79. The second half of the Stage 2 and 3 Prototype control program. The connections to the first half of the program can be seen on the left hand side of the program, labeled A-E.	171
80. The input controls, utilizing the DAQ Assist.	173
81. The data manipulation module and user controls.	173
82. Output control and logic box, utilizing logic switches.	174
83. Data write to file output box and control screen display box.....	174
84. Program safety switches and display box.....	175
85. The complete Stage 4 Prototype Math Script based program.	176
86. The input and data manipulation of the Math Script box version of the Stage 4 Prototype control program.....	178
87. The output control and voltage control-logic box portion of the program.....	179
88. The shift register and data writing node.....	179
89. The complete Stage 4 Prototype control program based on logic switches....	180
90. The logic portion of the program, utilizing the logic switches again, completely restructured, allowing faster operation, but becoming cluttered and difficult to follow.	182
91. The output voltage control and output DAQ, no longer utilizing the DAQ Assist.	183

LIST OF FIGURES-CONTINUED

Figure	Page
92. The input section, no longer utilizing the DAQ Assist.	183
93. The expression nodes, used to manipulate data.....	183

GLOSSARY

AFC-Active Fiber Composite

DAQ-Data Acquisition, can refer to the data acquisition unit as well

FBG-Fiber Bragg Grating

FOS-Fiber Optic Sensor

LP-Linear Potentiometer extensometer

LVDT-Linear Variable Differential Transformer extensometer

MFC-Macro Fiber Composite

PID-Proportional-Integral-Derivative

PZT-Piezoelectric Transducer

TDM-Time Division Multiplexing

WDM-Wave Division Multiplexing

Activation Time-Time required for the flap to go from zero extension to full extension.

Annealing-A process of heating and cooling an optical fiber with a Bragg grating, to eliminate electrons at lower energy levels, forming a stable Bragg grating, at temperatures below the annealing temperature.

Buffer Zone-The user controlled zone before and after the desired flap location where the actuator is able to stop. Any displacement reading of the actuator, within this zone, or movement of the desired displacement where the actuator remains within the zone, will result in a zero output voltage.

Boost Zone-The user controlled zone before and after the desired flap location, outside of the buffer zone, where the actuator will operate at 12 V, outside of this zone the actuator will operate at 24 V.

Bragg Wavelength-The wavelength of maximum reflectivity of a specific Bragg grating period.

Chord-The figurative line running from the leading to the trailing edge of an airfoil.

Desired Displacement-A user input displacement or a displacement derived from an input pressure, which the actuator is desired to achieve.

H-Bridge-A common relay assembly to reverse the direction of an electric motor, utilizing four SPST relays.

Overshoot-The distance between the final stopping location of the actuator and the desired stopping location.

Power-Off-The instant when power to the actuator is shut off, by the control program.

Stopping Distance-The distance traveled by the actuator after power-off.

ABSTRACT

Recently the use of wind as an alternative energy source has developed quickly. The length of the blades is a leading factor in the power output of a wind turbine and as a result, blade length has grown at a similar pace to the growth of the industry. The rapid expansion in use and size of wind turbines is not without its problems, though. As the industry has changed and grown, the overall design of the blades has remained relatively stagnant. This is evident in two primary areas, power control and health monitoring. Power control mechanisms are generally unchanged, utilizing either pitch control or active stall designs. While effective, these systems are neither efficient nor fast acting and can contribute to higher maintenance requirements. Current wind turbine blades also have no sensors built into them. The nacelle and tower utilize many sensors, but the blades themselves have none, leading to blades which are incapable of any real time health monitoring. The application of smart structures will enable the in situ monitoring of the blade and allow the blade to adapt to changing wind loadings

Smart structures are those which apply an array of sensors to continuously monitor the state of the structure and are capable of using those sensors to appropriately react to achieve a desired state. This paper will examine the application of smart structures to the wind energy industry. It will be shown that a fiber optic, Fiber Bragg Grating sensor is the best type of sensor for wind energy. One of the main contributing factors is the capability of the sensors to multiplex, which means many sensors can be located along a single optical fiber and different types of sensors can be run on the same optical fiber. The blades will 'react' to changing conditions through the use of an actuated Gurney style flap. The flap will be used to shed the wind loads from the blade in high wind scenarios. These systems working together will provide an effective and efficient method of advancing the design of the wind turbine blade to a level appropriate for the systems expected today and in the future.

INTRODUCTION

The production of electricity from wind energy has grown immensely in the last 10 years; from 1996 to 2006 the production increased nearly 10 fold and there are no signs of the growth slowing. Between 2004 and 2006 alone, production more than doubled [1]. Along with the increase in total power production, as can be seen in Figure

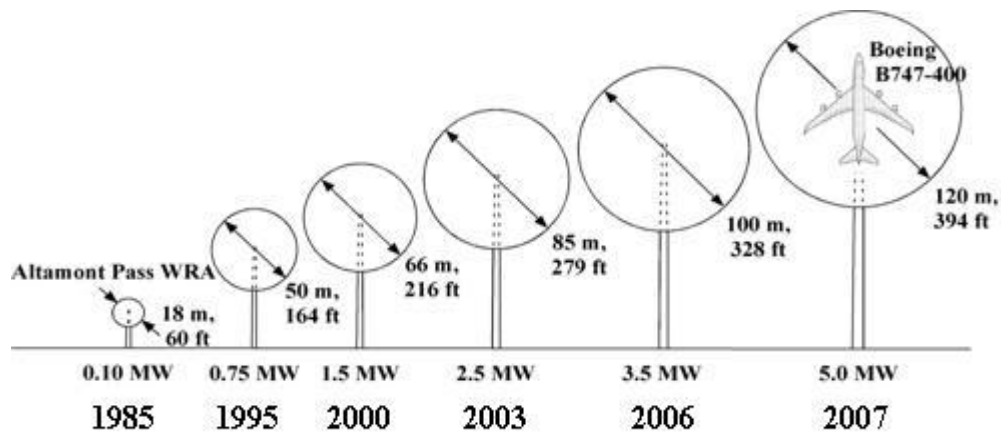


Figure 1: A diagram showing the increase in size of wind turbines built from 1985 to 2007 [2].

1, the size of the wind turbines has rapidly grown as well. The driving force behind the increasing size of the wind turbine is the quest to achieve higher power output capacity from new wind turbines. The total power output is heavily dependent on the length of the blade as seen in Equation 1. In this equation it can be seen that the two dominating factors are wind velocity and blade length, and outside of choosing appropriate locations for the wind turbines, blade length is the only one of these factors that can be controlled,

$$P = \frac{1}{2} \cdot \rho \cdot C_p \cdot N \cdot \pi R^2 \cdot V^3 \quad 1$$

Where, P is the output capacity of the wind turbine, R is blade length, V is wind velocity, ρ is air density, C_p is coefficient of performance, and N is electrical and mechanical efficiency.

The growth in the size of the blades hasn't come without consequence, the enormity and weight of the blades built today has pushed the limits of current materials and technology. The weight of the blades, reaching up to 23 tons for modern blades [2], increased surface area and wind loading and rapidly changing wind speed and directions



Figure 2: A wind turbine failure can be catastrophic, with devastating results. Tips of the blades can reach speeds in excess of 150 mph and pieces of the blades can be thrown over 1300 ft.

combine to result in greatly increased stresses and strains on the blades, and cause those strains become much more difficult to control [3]. The high stresses placed on the blades can result in devastating failures as seen in Figure 2. Taking precautions to avoid failures becomes increasingly important every year as new wind turbines continue to be built in new areas, often close to communities, and the number of incidents continues to increase. Blade failures are the main documented incident with 118 failures documented between 1992 and 2007, of those, 76 have occurred since 2002 [4]. These failures can send debris

flying for over a quarter mile, causing damage to structures, obstructing roadways and threatening human life.

For the industry to grow safely and prevent or limit the number of incidents, there are some advancements which must occur. One of these is for the blades to be able to



Figure 3: All modern aircraft utilize active control surfaces; the B2 Spirit bomber is an aircraft which revolutionized the possibilities and capabilities of the use of active control surfaces.

adapt more quickly to changing wind conditions. Currently blades use two different methods of protecting themselves from high wind conditions and gust scenarios: active stall and pitch control, with brake systems to then bring the rotor to a stop. Both of these systems are effective when used with appropriate blades and in certain conditions; however they are inefficient and slow acting. To safely allow larger wind turbines to be built, active control surfaces will need to be utilized. Active control surfaces are

mechanisms which are capable of adapting the surface of an airfoil to changing conditions to achieve a desired result. The use of active control surfaces is not a new one; the aerospace industry has used it for decades (Figure 3) and research has been done in the past on adapting such control surfaces to wind energy [5] (Figure 4). However, no major, large scale wind turbine currently uses such a system. Application of a properly designed system would allow the wind turbine to adapt itself to changing wind conditions to maximize the power output of the system and activate fast enough to protect itself from damage without relying solely on use of the brakes or blade pitching.



Figure 4: The North Wind 250 was developed in the early 1990s by Northern Power Systems. Its design incorporated an aileron style load control system.

One viable system for achieving an active control surface on a wind turbine blade is a device known as a Gurney flap. The Gurney flap is a small flap of material mounted near the trailing edge of an airfoil which affects the resulting lift on the airfoil. The Gurney flap has been used for years in automobile racing and can often be found on modern day production performance cars as seen in Figure 5. By creating a Gurney flap which can be activated near the trailing edge of the suction side of an airfoil, during high wind and gust conditions, the overall lift on the blades can quickly be reduced. When used in conjunction with current pitch control

systems, this could allow for operation in higher winds and operation at maximum capacity for longer periods, allowing for greater power output from each wind turbine. It could also allow for reduced use of pitch control and braking mechanisms and, when necessary, allow more time for the blades to pitch and brake, increasing the reliability of the wind turbine.

To further protect the next generation of wind turbines, sensing ability is going to play an important role. Currently on a wind turbine, there are a large number of sensors



Figure 5: The Gurney flap can be found in many applications, including some production vehicles such as the Mitsubishi Lancer Evo.

built into the base of the tower and into the nacelle, but no sensors are located through the length of the blades. This creates a critical gap in information for existing wind turbines. One of the primary sensors which will be required is strain gauges, without them, it is difficult to impossible to create an accurate lifecycle history for a blade and to monitor

the health of the blade. Placing the sensors in a blade, would allow for in situ monitoring of the blade, increasing both the safety of the blade as well as the efficiency of the system. The sensing system could then also be used to provide information for the control of the active control surfaces.

Many different sensors exist, however one system above the others, suits the needs of a wind turbine for multiple purposes, better, the fiber optic sensor (FOS). FOSs utilizing Fiber Bragg Gratings (FBGs), as seen in Figure 6, provide many advantages that no other sensor currently can. FBG sensors use small shifts in reflected wavelengths to determine strains, which then can be interpreted into many different quantities including strain, pressure and temperature, values which would be important in a wind turbine. The

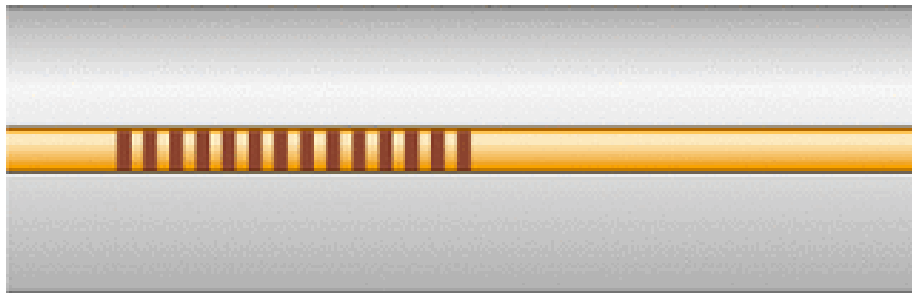


Figure 6: A Fiber Bragg Grating is a pattern printed onto an optical fiber, which reflects a specific wavelength of light.

adaptation of these sensors into a wind turbine blade would allow an important step in the advancement of the wind turbine and help provide another level of safety.

Alone these technologies provide valuable advancements, but together can create a powerful, stable, self adapting system. When these two technologies combine they form what is known as a smart structure. For nearly 20 years now, smart structures have been defined as structures which have the ability to sense, diagnose and actuate in order

to perform a function [6]. In the case of the mechanisms discussed here, the various sensors built into the blades would be used to regulate the control surfaces by appropriate activation of the flaps. The application of smart structures to wind turbines is a key step in advancing the technology of the systems which are currently used.

Wind energy has slowly become a mainstream technology, but many challenges remain before it can be considered a truly viable option in mass power generation. These challenges are broad, to begin with, wind energy will have to prove to be safe, reliable and profitable if the growth seen during the last ten years will continue into the future. To accomplish this, the incorporation of smart structures into wind turbine blades is an important step that will need to occur. The adaptation of smart structures can help make wind turbines into safer more reliable systems which can continue to flourish and become an ever more important asset in the search for green energy.

BACKGROUND

As the sun heats the earth, it heats different regions at different rates; causing a pressure gradient in the atmosphere. Air which is heated more rapidly rises, drawing in cooler air; resulting in wind, which creates an immense source of energy [7].

The first known use of a windmill was in China around 200 B.C., where it was utilized for pumping water. By the 1300s, windmills had made their way to the middle-

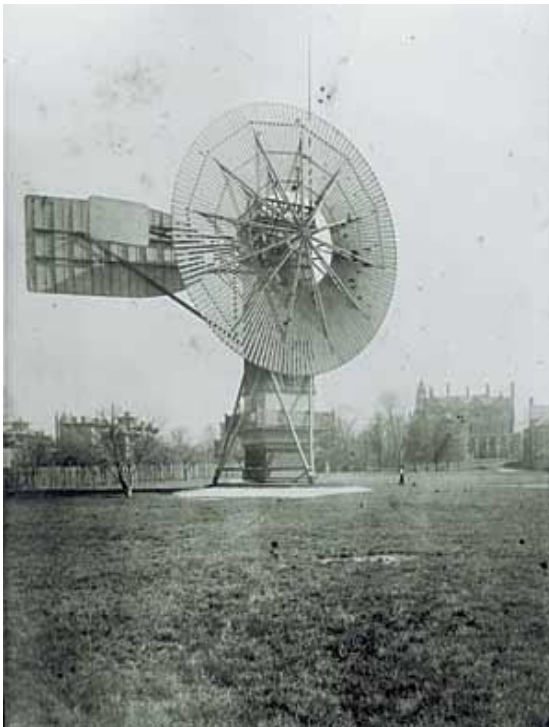


Figure 7: The Brush wind turbine was the first to use wind energy for the generation of electrical power. © The Charles F. Brush Special Collection

east and finally to Europe, where their uses and designs continued to expand and evolve [8]. The first use of wind for electrical generation was in 1887, in Cleveland, OH, where Charles Brush built the first wind turbine (Figure 7) [9].

During the course of the next 100 years, the use of wind turbines fluctuated greatly; the rising and falling use often following the development of other power generation methods and the cost of fossil fuels [9]. This trend continued until the 1980s when the fear of reliable and

inexpensive fuel and energy pushed the drive for alternative sources of energy [10, 11].

This led to the expanded development and use of wind energy, which began to quickly grow in the mid and late 1980s (Figure 8), largely encouraged by government subsidies,

loans and tax benefits [11]. The growth slowed until the late 1990s, when the use of wind energy began to develop into an economically viable [12], source of energy and entered the public conscious as a valuable resource in the drive for an environmentally friendly method of achieving national energy independence. An expanded discussion of the history and growth of wind energy can be found in Appendix A.

The growth during the last 10 years has brought wind energy to the point where it currently resides; a viable and important source of energy, which has the potential to change the way in which power is generated around the world. For this to happen, developments will need to occur; including the development of active control surfaces, which can provide an effective method of load control, and the application of sensors which can provide real time blade condition information. Together, they will enable bigger and more efficient wind turbine blade designs. This will lead to increased power output and better reliability, making wind a more viable energy source than at any other point in its long history.

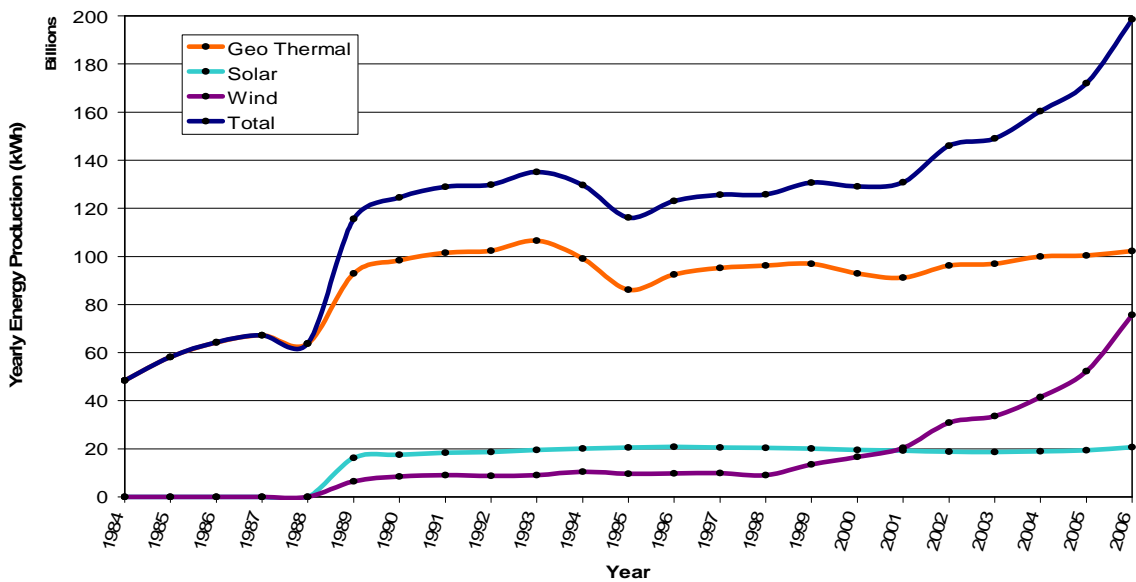


Figure 8: The yearly production of renewable energy in the U.S., between 1984 and 2006.

CONTROL SURFACES

IntroductionThe Creation of Lift:

An airfoil, as described by Merriam-Webster's Dictionary, is "a body (as an airplane wing or propeller blade) designed to provide a desired reaction force when in motion relative to the surrounding air [13]." An airfoil can be many types of devices, from a hand out a car window to the wing of a Boeing 747; the basic ideas are the same. A basic explanation for how lift is created, is that as air passes over the surfaces of an airfoil, the air on one surface moves faster than on the other causing lift. This is the result of conservation of energy, as described by Bernoulli's Equation (Equation 2). The

$$P_1 + \frac{1}{2} \cdot \rho \cdot V_1^2 + \rho_1 \cdot g \cdot h_1 = P_2 + \frac{1}{2} \rho \cdot V_2^2 + \rho_2 \cdot g \cdot h_2 \quad 2$$

Where P is pressure, V is velocity, ρ is density, g is gravity and h is the vertical height. A subscript of 1 denotes the initial value and 2 denotes the final value.

equation can simplified, allowing for two assumptions, first, that there is no change in elevation allowing the ρgh values to cancel and second, that the flow is incompressible, making ρ become constant. Both of these assumptions are technically incorrect, but they allow for a simplified understanding of the affects of the equation and the affects are generally small enough to allow for the assumptions in this basic explanation. The results of this simplification can be seen in Equation 3. Here it can be seen that if there is

$$P_1 + \frac{1}{2} \cdot \rho \cdot V_1^2 = P_2 + \frac{1}{2} \rho \cdot V_2^2 \quad 3$$

an increase in velocity, on side 2 then there must be a corresponding drop in pressure, on side 2 for the equation to remain balanced. To achieve this, an airfoil is designed with a curved, suction side surface, over which air moves at an increased velocity and more flat pressure side, over which the air travels over at a lower velocity. The result of this is that the air traveling over suction side of the airfoil, with a higher velocity, experiences a drop in pressure compared to the pressure side, creating a pressure imbalance and resulting in lift (Figure 9).

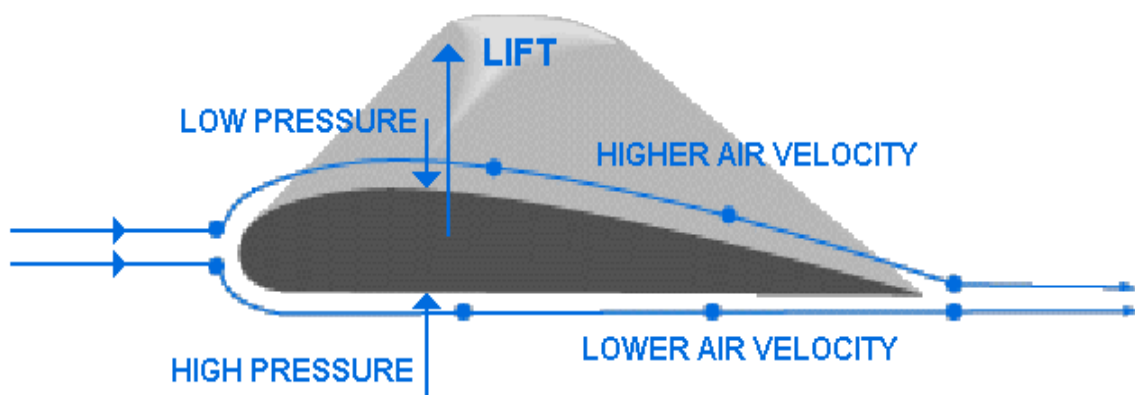


Figure 9: The basis of the basic explanation of the creation of lift, as described by Bernoulli's Equation; based on the shape of the airfoil.

In current wind turbine designs, the generated lift is completely dependent on the aerodynamic shape of the blades, not control surfaces, as in other airfoils. Note that this is not the full or only explanation for how lift is created, many other influences and ideas exist, however they will not be discussed as they do not hold any significance to the topics to be discussed later and a basic understanding, presented here, is sufficient for the purposes of this paper.

Current Power Control Mechanisms:

Control surfaces are an essential component of any modern aircraft. Without them, modern flight would not be possible. While invaluable to aircraft, control surfaces have yet to take hold in wind energy. Yet, mechanisms for controlling the power from a wind turbine are essential. Excessive wind loadings can cause many problems, including damage to the gearboxes, generators and blades (Figure 10). Wind speeds are constantly varying and must be adapted for. Currently in wind energy there are two main methods which are utilized for power control; passive stall and pitch control, also utilized is a



Figure 10: Without proper load control mechanisms severe damage and even destruction of a wind turbine can occur.

combination of these two methods, known as active stall. These two methods utilize two very different methods of alleviating excess loadings from a blade.

To understand the operation of a passive stall wind turbine, it's important to first understand what stall is. As air travels across the surface of an airfoil, the flow is laminar over most of the airfoil, meaning it is smooth and attached to the airfoil. However, at a point, the flow transitions into a turbulent flow as seen in Figure 11, the flow separates from the airfoil and begins to swirl. When this occurs, it reduces the lift on the airfoil, so for an efficient airfoil design, the transition to turbulent flow must occur as late as possible. Two

significant factors that influence the transition to turbulent flow are air velocity and angle of attack. Initially, as the magnitude of either of these factors increases, the lift created will gradually increase, however the transition point, to turbulent flow, on the wing will also begin to creep forward. As the wind velocity or angle of attack continues to increase a point is reached where any further increases will begin to induce a stall, reducing the effective lift of the airfoil. A passive stall wind turbine blade is designed to take advantage of this effect. As wind speeds increase, the blade is specifically designed to progressively stall, reducing the lift on the blade and allowing for safe operation in varying wind conditions [14].

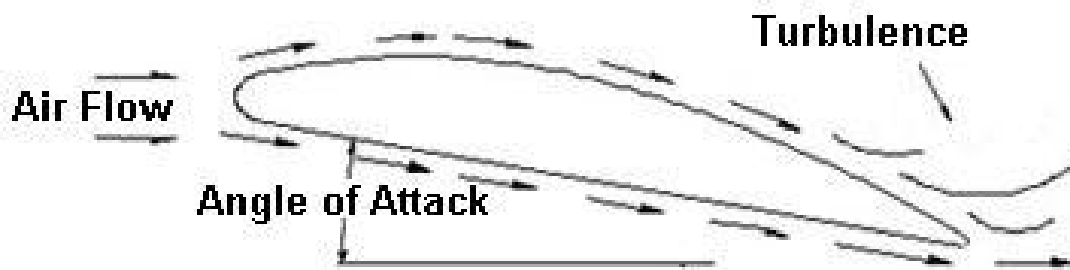


Figure 11: The transition to turbulent flow and boundary layer separation due to angle of attack and air velocity.

A pitch control wind turbine utilizes blades which are able to rotate along their longitudinal axis. As the wind speed increases, the rotational velocity of the hub is continuously monitored. As the velocity of the hub increases, a control system initiates a mechanism which rotates the blades out of the wind or reduces the angle of attack of the blade. As mentioned; as the angle of attack of an airfoil increases, the lift on the airfoil increases as well, up to a point where the airfoil stalls. By reducing the angle of attack of

the blades, the lift on the blades is reduced as well, slowing the rotational velocity of the turbine and preventing damage to the system. This also allows for a system which can adjust itself to acquire the maximum efficiency and power output, by continuously changing the angle of the blade for given wind conditions.

An active stall wind turbine is then a combination of these two systems. Similar to a pitch control design, the blades are able to rotate along their longitudinal axis and the rotational velocity of the hub is continuously monitored. However, as the wind velocity increases, rather than rotating the blades out of the wind, or decreasing the angle of attack, the blades are pitched into the wind, an increased angle of attack, causing an induced stall, similar to the passive stall system [14].

While these systems are effective at protecting the wind turbine from excessive wind loadings, they each have flaws. The passive stall design requires extensive and complicated aerodynamic analysis. In use, the passive stall design experiences a decrease in power generation as the wind speeds increase and the turbine transitions into a deeper stall [14], reducing the efficiency of the wind turbine. The pitch control and active stall systems utilize hydraulics or stepper motors to rotate the blades [14]. As a result the systems are complicated to design, heavy and increase the maintenance requirements of the turbine. Also, rotating the blades is a slow process, affecting the ability of the turbines to react and protect themselves from rapidly changing wind conditions. To resolve these problems another type of load control system is needed.

Previous Design Attempts and Design Alternatives:

In the early to mid 1990s several contracts were awarded by the National Renewable Energy Laboratory for the development of next generation wind turbines [15]. Under these contracts several different designs originated for load control on wind turbines. One of these methods was an aileron control system developed by Northern Power Systems and Zond Systems Inc., known as the North Wind 250 and Z-40, respectively. The North Wind 250, shown previously in Figure 4, was a 250 kW twin blade system, while the Z-40 was a 500 kW turbine with 3 blades, both utilizing large ailerons, similar to an aircraft wing [16]. Another design attempted by several companies, including Advanced Wind Turbine Inc. and Atlantic Orient Corp. was the aerodynamic tip brake. The tip brake was a magnetically activated brake, which when deployed would be flung out to create drag to slow the rotation of the rotor [17, 18]. While these systems all reached advanced stages of testing, most of them never reached large scale production and in several cases the companies which developed the systems have since collapsed. The sole turbine which was extensively produced was the 50 kW AOC 15/50, built by Atlantic Orient Corporation, now Atlantic Orient Canada Inc., who has been building the turbines since the mid 1990s. However, the small size of the AOC 15/50 has diminished the effect it has had on the large scale wind industry.

Design Alternatives: In addition to the designs which had previously been attempted, there are several other possibilities for power control on a wind turbine blade. Two of the options, which will be examined, are a Gurney flap and a virtual flap, both of which would be attached to the trailing edge of the blade. The Gurney flap, and variants,

will be examined in much more detail and will be the primary case studied. The virtual flap will be examined in a brief proof of concept manner, but not beyond that. The concept of both methods is to disturb the flow of air over the suction side of the airfoil and create boundary layer separation. The difference between the two concepts is that the virtual flap uses high pressure air, blown from a row of nozzles to create the same effect as a mechanical flap.

The Gurney Flap

History:

In 1931 Edward Zaparka patented a device for increasing lift on an airfoil. His device consisted of a small flap, which was attached to the trailing edge of an airfoil (Figure 12). The flap had a series of linkages which allowed the flap to be deployed when needed and retracted when it wasn't. As Zaparka described it in his patent,

“My invention relates to a variable lift airfoil arrangement whereby the lift coefficient per unit area is increased and an improved lateral control provided ... As one embodiment of my invention, I provide means to modify the circulation or relative hypothetical velocity around the wing or airfoil in such a way that the normal amount of effective circulation is increased, and, moreover, may be varied at will during flight ... Discontinuity of airflow near the trailing edge is prevented, and the conditions of airflow at the upper surface of the wing are very much improved [19].”

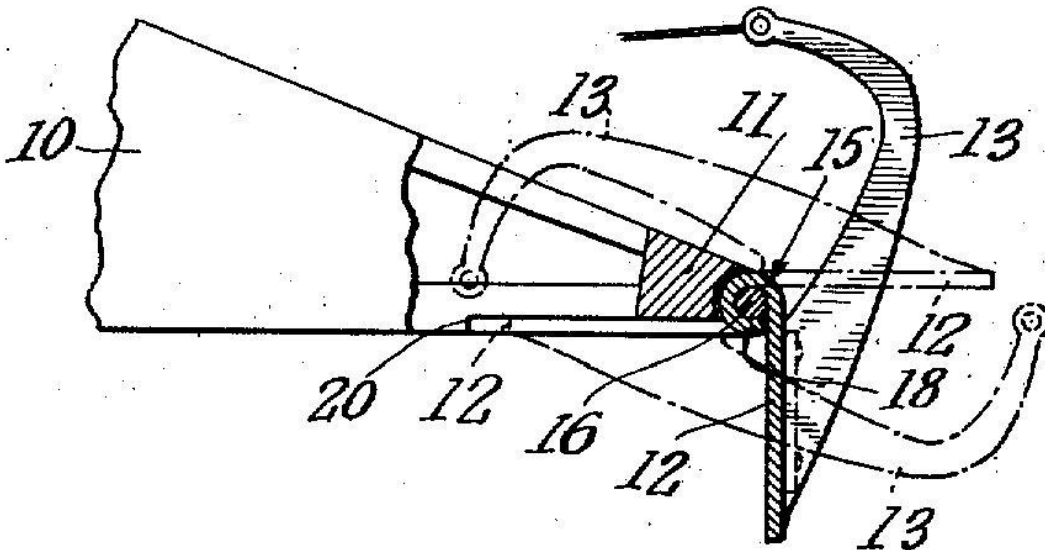


Figure 12: The flap patented by Zaparka was mounted near the trailing edge of an airfoil and was capable of being raised or lowered to adapt the airfoil to a given condition [13].

The device itself was quite basic, but the concepts behind the design were well ahead of their time and came to be used, in one form or another, on aircraft ever since. While more complex adaptations of Zaparkas flap were created, the simple effectiveness of his flap would not be closely examined again for another 40 years.

In 1971, far from the airstrip, on a Phoenix racetrack Dan Gurney was faced with a problem, his race team was testing a new car and results were showing a car whose handling was poor and speeds that were too low. The car didn't have sufficient down force [20]. His driver, Bobby Unser (Figure 13), challenged him to find an answer to the



Figure 13: In 1971, Bobby Unser was the first to drive a car equipped with a Gurney Flap.

problem. For inspiration Gurney looked to the work of Richie Ginther. Ginther was a racer and developer during the 1950s and 60s [21]. During a portion of that time he worked as a development driver for Ferrari, where he is credited as being the first to use a spoiler. Gurney had seen the success Ginther had had

using spoilers on his Ferraris and came up with the idea to attach a small vertical flap, or spoiler, to the rear wing of the race car. After 45 minutes Gurney had built and attached the flap to the wing as seen in Figure 14, and Unser went back out for several more test laps around the track.

Unfortunately the lap times showed no improvement from the prior times and it was assumed that the flap was a failure. When Unser came back in however, he informed Gurney that the problem this time was too much down force, affecting the cars balance and hurting performance. Once extra down force was added to the front of the car and a balance was achieved Gurney had achieved his goal of down force, improved the cars performance and had found an advantage, available to his team alone.

Gurney and his team kept the true function of the flap a secret from the other teams, responding to inquires that the flap was to protect the hands of the help from the sharp trailing edge of the wing or to provide additional structure to the wing. However, he did share the secret with McDonnell Douglas Corp. Robert Liebeck, who was a

consultant from McDonnell Douglas, hired to assist in car designs, was the first to analyze the Gurney Flap aerodynamically. His numerical analysis and wind tunnel tests showed that the flap, located at the trailing edge of an airfoil, not only increased the lift on the airfoil, but also reduced the drag on the airfoil [22]. The complete results of his work were presented at the AIAA 9th Fluid and Plasma Dynamics Conference in July 1976 and Published in the September 1978 Journal of Aircraft. Since Liebeck published his results, the use of the Gurney Flap has expanded into many fields, including the



Figure 14: An example of the original Gurney flap used on the All American Racers Eagle racing cars in 1971 [14].

automotive industry and fixed and rotary wing aircraft and provides a viable option in the development and application of active control surfaces for wind turbine blades.

Function of the Gurney Flap:

The Gurney flap, as mentioned, is a small strip of material which is mounted at the trailing edge of an airfoil. Typically mounted on the pressure side of the airfoil, a Gurney flap is an almost counterintuitive way of creating additional lift on the airfoil. While, most commonly used to generate additional lift, it is predicted that the Gurney flap can also be located on the suction side of the airfoil to reduce the lift generated by the airfoil (Figure 15) [23]. While the general principals of how the flap affects the lift generated by the airfoil should remain intact, the following discussion, will consider a pressure side mounted flap.

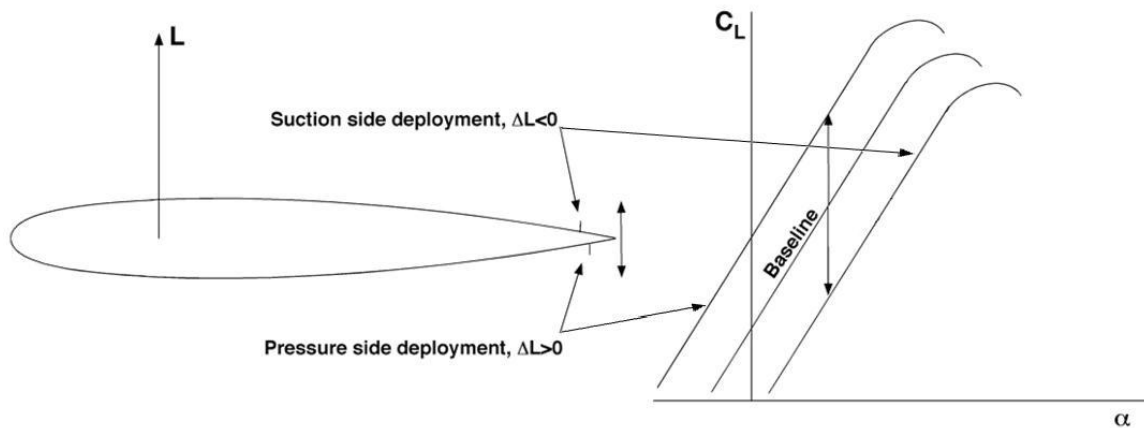


Figure 15: The effect of Gurney Flap mounting location on the generated lift [2].

By mounting a Gurney flap at the trailing edge of an airfoil, several affects combine to generate the overall effectiveness of the flap. In front of the flap, a recirculation region is created. Behind the flap, a strong clockwise rotating vortex is

formed; earlier predictions had predicted that two counter rotating vortices were formed, however, later work , has shown only one strong clockwise rotating vortex [24], as seen in Figure 16. These combine to dramatically affect the lift generated by an airfoil. A low pressure region is created behind the trailing edge of the airfoil which causes an increase in the downward momentum of the air and delays boundary layer separation from the suction side. As well there is a reduction in the size of the upper-surface recirculation and an increase of the air velocity over the suction side surface [24]. On the pressure

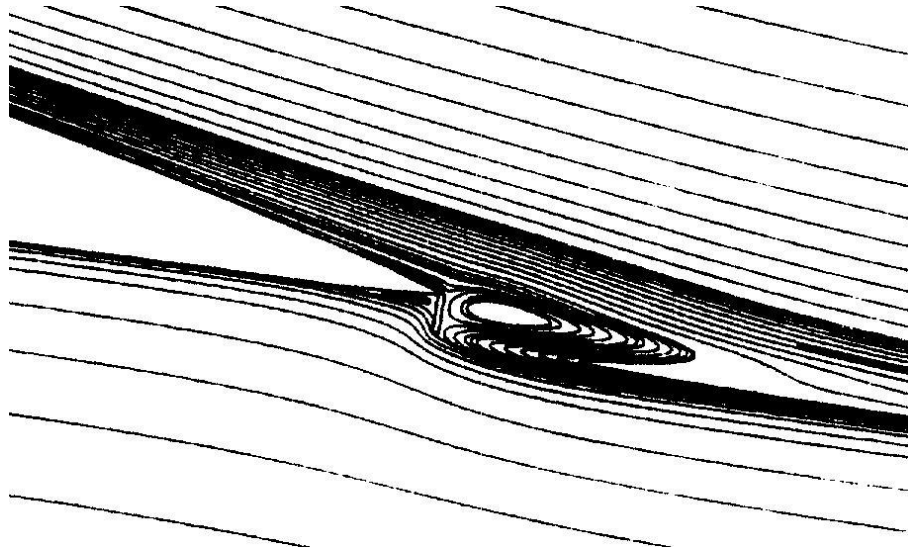


Figure 16: A demonstration of the recirculation region created in front of a Gurney flap and the vortex is formed behind the flap [24].

side, the recirculation region hastens boundary layer separation, effectively reducing the air velocity over the pressure side surface [25]. The combined effects lead to a dramatic increase in lift generated by the airfoil, with minimal consequences.

Utilizing a Gurney flap has several other effects on an airfoil, besides simply increasing the lift generated. One of these effects is an increase in drag. Initially, the research showed an actual decrease in drag from installing the Gurney flap [22], later

research has shown this not to be true, by installing a Gurney flap certain drag penalties will occur [24]. Generally these drag penalties can be kept relatively small with respect to the lift gains. As previously mentioned, as the angle of attack of an airfoil becomes lower, the lift that is generated by the airfoil is reduced. Installing a Gurney flap decreases the zero lift attack angle of an airfoil [25]. What this means is that an airfoil can be angled further into the flow of air, before the lift on the airfoil becomes zero. In line with this is a reduction in the stall velocity of the airfoil.

Variables in the Design of the Gurney Flap:

There are many variations that can be made to the Gurney flap to affect the effectiveness of the flap. Three of these have vital importance to the prototype that was assembled to model the use of the Gurney flap on a wind turbine blade (Figure 17), these are; flap height, flap distance from the trailing edge and the mounting angle of the flap.

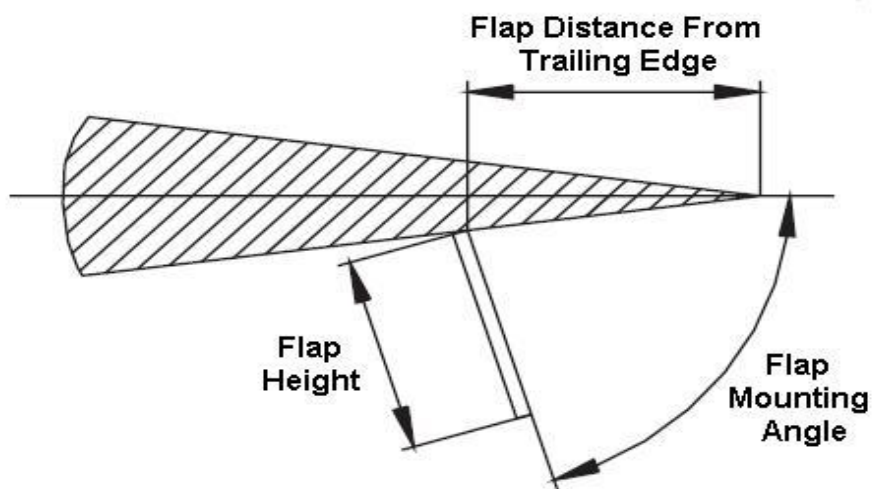


Figure 17: Three of main variations made to a Gurney flap, are flap height, flap distance from the trailing edge and flap mounting angle [26].

Flap Height: Flap height is a critical component when examining the lift and drag generated on an airfoil by including a Gurney flap. When examining flap height, the height is given as a percentage of the chord length. For example, if a Gurney flap with a height of 4 cm is mounted on an airfoil with a chord length of 1 m, it would have a height of 4%. Liebeck had predicted in his work that a flap of height of 2% would provide the best results; beyond that height, significant drag would begin to be introduced [22]. Later research would prove this to be true, as can be seen in Figure 18. Even at low flap heights, 0.5%-1%, significant increases in lift are seen and as flap height increases, the lift generated by the airfoil continues to increase as well. Below a flap height of 2%, the increase in drag, while present, does not increase significantly, above 2%, however, the drag begins increasing more rapidly. These results remained relatively consistent throughout the range of angles of attack [26]. While a flap taller than 2% will provide greater lift, it must be determined whether the drag penalties are acceptable.

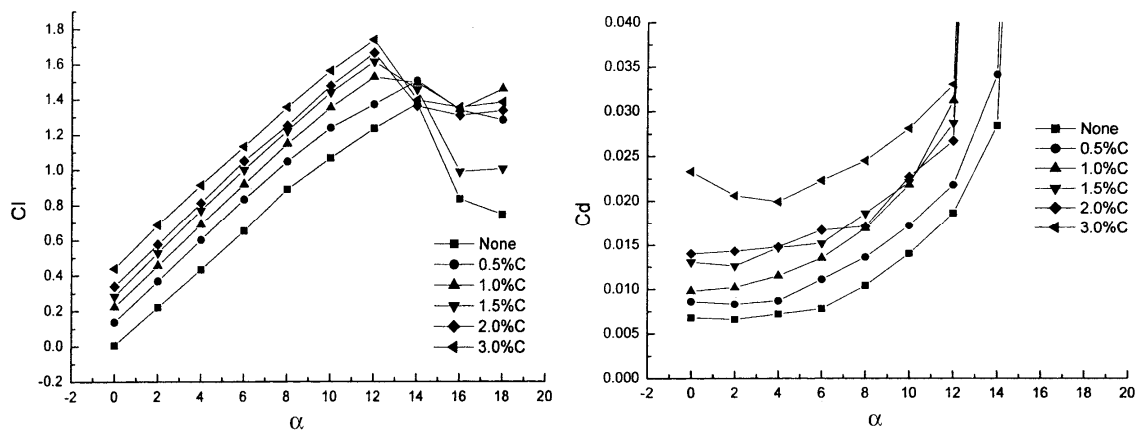


Figure 18: Increasing the height of a Gurney flap will cause an increase in the generated lift as well as the drag [26].

Flap Location: Typically a Gurney flap is located as close as possible to the trailing edge of an airfoil, however this is not always possible and the affect must be taken into account. Research done by Wang et al. examined just that, they examined a Gurney flap of 1.5% height mounted at locations of 0%, 2%, 4% and 6% of the chord length, away from the trailing edge of a NACA0012 airfoil. The results showed a decrease in lift generated by the Gurney flap, the further the flap was mounted from the trailing edge. Lift results were relatively constant with a minor drop in effectiveness with each increment away from the trailing edge (Figure 19). Drag results were relatively scattered with respect to attack angle. At low attack angles an actual decrease in drag, compared to a flap mounted at the trailing edge, could be seen in the 2% and 4% conditions, however, the advantage evaporated and a significant increase in drag was seen for the 4% and 6% flaps when the angle of attack between 2° and 10°. Beyond 10°, all values coincided relatively well, but clear definition is difficult. Overall, the data provides an expectation of increased drag, regardless of mounting location and a decrease in lift, the further a flap is mounted from the trailing edge of the airfoil.

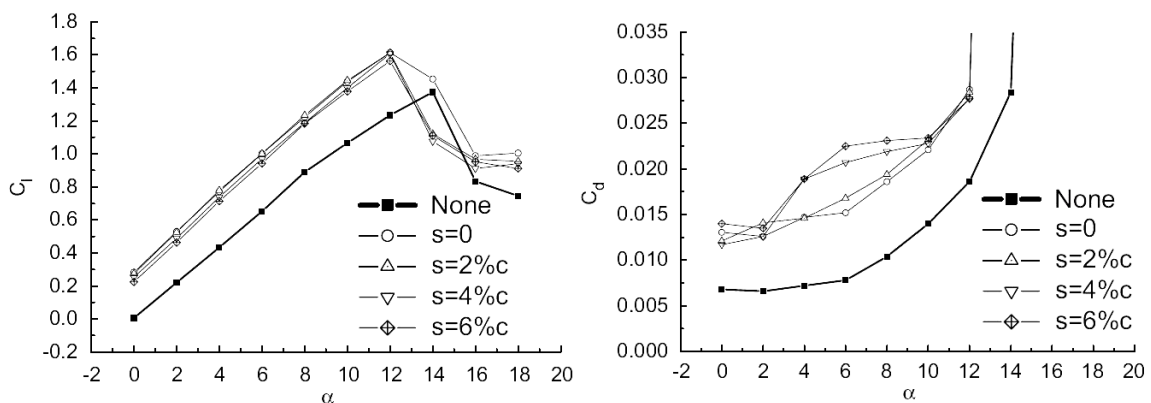


Figure 19: By increasing the distance a Gurney flap is mounted away from the trailing edge of an airfoil, the lift is decreased, while drag effects are relatively scattered [26].

Mounting Angle: Typically a Gurney flap is mounted perpendicular to the surface of the airfoil to which it is attached. Examining the effect of different mounting angles provides important information for applications where drag is important or where a flap can or must be mounted at an angle. This was examined by Wang et al. as well; the research examined the effect of a 1.5% height Gurney flap mounted at angle of 45, 60 and 90, with 90 being perpendicular to the airfoil. The results (Figure 20) could be considered somewhat common sense, the swept back angle of the flaps mounted at less than 90 showed a decrease in both lift and drag. The reduction in drag was fairly significant; at lower angles of attack, a drop of over 30% was seen. At higher attack angles, the decrease in drag was not as dramatic, but remained significant. The decrease in lift generated, was relatively small in comparison to the overall affect of the flap and remained fairly constant throughout the range of attack angles. In general, the significant decreases in drag seen at lower flap angles may be considerable enough to compensate for the loss of lift, in certain situations.

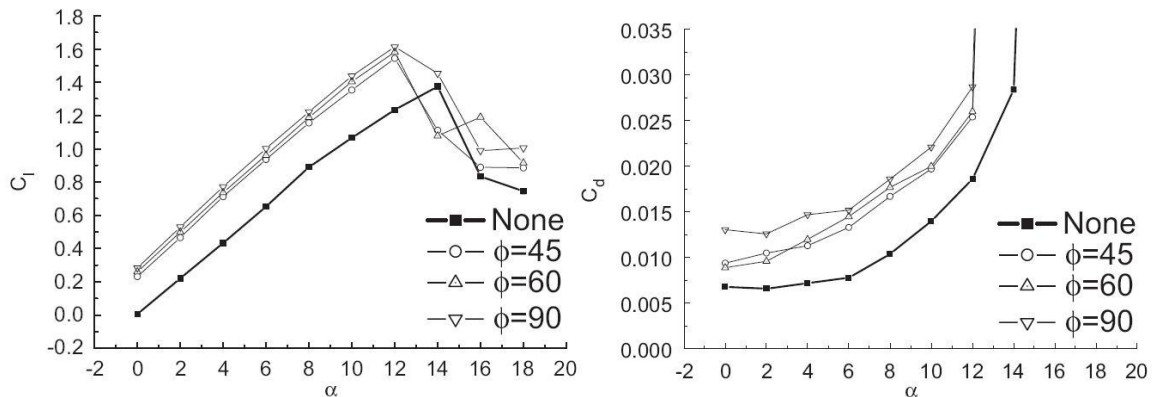


Figure 20: Minor decreases in lift are seen when flap angles are reduced, however there is also a significant decrease in drag on the airfoil [26].

Final Considerations of the Gurney Flap:

The Gurney flap provides an excellent method of affecting the lift generated by an airfoil. The small size and simplicity makes it a viable option for load control on a wind turbine blade. In a typical scenario where a Gurney flap is used, to increase the lift on an airfoil, drag is generally considered a bad thing, in the situation here, where the idea is to shed wind loadings and reduce lift, drag is not necessarily the enemy. With that in mind, where a typical Gurney flap will have a height of around 2% of the chord length, on a wind turbine, this height can be greatly increased and a flap of height 10%, may be acceptable, the increased load shedding would likely be of much more significance than the increase in drag.

While there are other variables, other than those mentioned here, that come into play in the function of a Gurney flap, the particular variables, discussed above, play an important role in the subsequent work. To test the function and application of the Gurney flap, a prototype was needed for proof of concept purposes and eventually, wind tunnel testing. The piano-hinge design of the prototype which was assembled and will be discussed, beginning in the next section, was such that these variables are of key importance.

THE PROTOTYPE

Introduction

The prototype is actually a series of proof of concept mechanisms, assembled to demonstrate the ability to deploy a Gurney flap within set boundaries. The prototype was built in four different stages; a flat plate with open-closed control, a flat plate with set distance controls and two different versions of a blade section with set distance controls. The function and differences of the individual systems will be discussed in further detail below. The basic concept of the prototypes was to use a control system to monitor an input or set of input quantities which were then used to determine the deployment of a Gurney flap and function within set system requirements.

System Requirements:

When building the prototype several goals were set, ranging from performance standards for actuation to the physical dimensions of the prototype:

- ∅ The flap must be capable of fully actuating within 500ms
 - An actuation time of 500ms enables the system to quickly and precisely control changing wind conditions.
- ∅ The control system must utilize LabVIEW data acquisition software
 - LabVIEW is a widely used and understood operating system that lends to a control system with some sort of universality.
- ∅ The system must be robust and autonomous

- The system must be able to adapt to rapidly changing conditions and be able to operate without error, compensating for sometimes unexpected conditions.
- ∅ The system must be examined for both its ability to be incorporated into new and existing wind turbine blades
 - Many systems are currently in operation or being developed, which could benefit from the capabilities provided by active control systems, in addition to a next generation of wind turbines.
- ∅ The prototype must be approximately 60cm x 60cm in size
 - Dimensions must be controlled in order that the prototype can be easily transported and possibly tested in a wind tunnel.
- ∅ The system must be such, that a production version could be built to provide the reliability necessary for use during the lifetime of a wind turbine blade.
 - On a wind turbine, very high life cycles are expected, as well as greatly varying loads, the system must be reliable enough to handle these conditions and not compromise the longevity of the wind turbine.

System Overview:

With the given system requirements, a system was designed that could best accomplish the set goals. To create the simplest system, with the fewest moving parts, a piano hinge flap design was utilized. A linear actuator was selected, to deploy the flap. A LabVIEW control system was programmed to monitor input values and control output voltages. The output voltages controlled a series of relays, which then controlled the

power to the actuator; power came from a 24V battery, power source. The actuator was then capable of controlling the flap extension and retraction. The separate components can be seen below in Figure 21

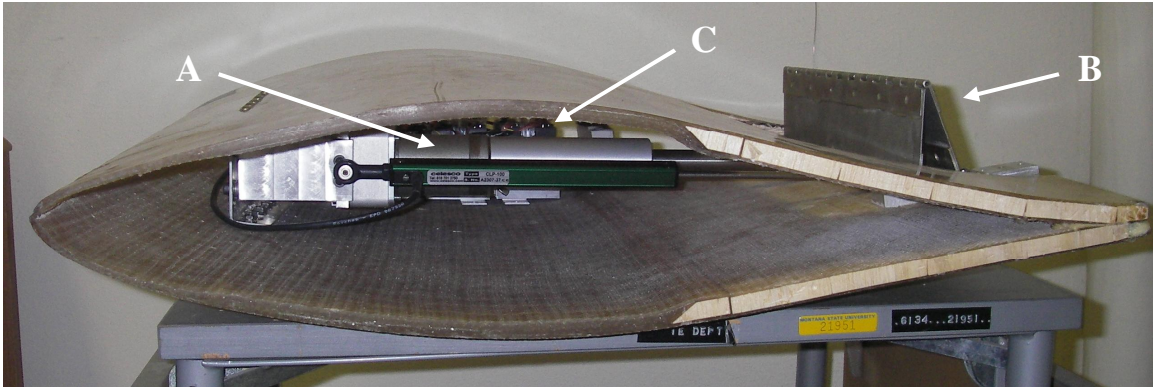


Figure 21: In this prototype, the third stage seen here, the various main components can be seen: A) The linear actuator, B) The Gurney flap and C) The relay assembly can just be seen behind the actuator. The batteries are kept separate from the rest of the assembly.

Detailed Description:

One of the primary factors in the choice of a piano hinge style flap was its simplicity (Figure 22). By utilizing a piano hinge for the flap, the flap can be actuated without the use of high maintenance items, such as linkages, springs or cables. This leads to a simple actuation system, with as few moving parts as possible, which tends toward a more reliable design and allows for one axis of motion. This also lends to a very low profile, allowing all the components to fit within the confined space seen at the trailing edge of the blade. The shape of the flap leads to a durable and strong flap capable of handling any loads the flap would see under typical operation and some incidental strikes.

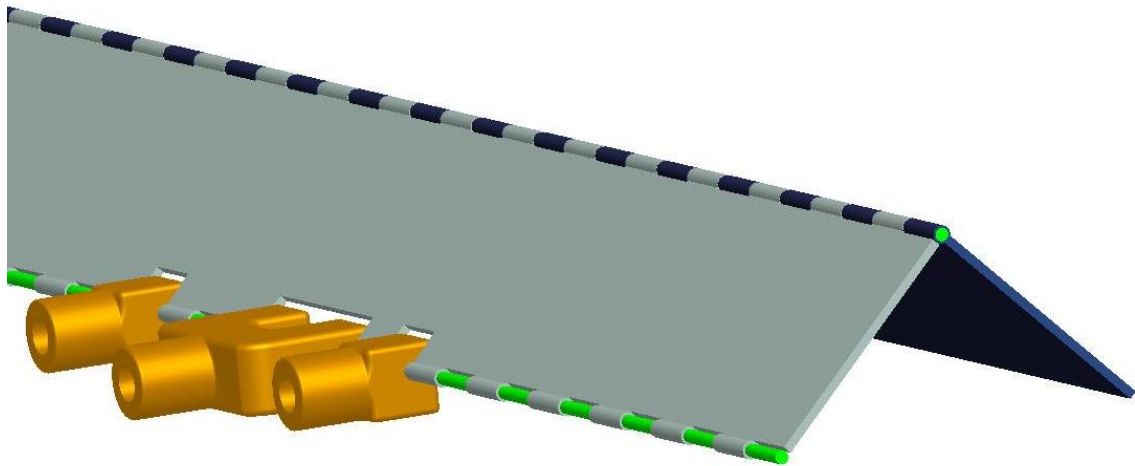


Figure 22: The piano hinge flap design has many benefits, including simplicity, with few moving parts, durability and a low profile.

With the piano hinge flap, a linear actuator is necessary to extend and retract the flap. The actuator that was chosen was an Ultra Motion, 24V DC, 'Bug' series actuator. The 'Bug' actuator was chosen for its high velocity capability while under a load and slim profile. To power the actuator a 24V DC power source was needed, this was

accomplished by wiring two Interstate YB7-A 12V batteries in series. This enabled the powering of both 24V and 12V devices, and running the actuator at 12V to achieve slower operation; this would become beneficial later.

For directional control of the actuator a series of relays was utilized. Initially a circuit utilizing two double pole, double throw and one single pole, double throw, contact type relays, was built. The relays were inexpensive, yet acted quickly and effectively; attributes which would prove valuable during early stages of circuit design. Later the contact relay circuit was replaced by a solid-state relay H-bridge, utilizing four single pole, single throw relays. The solid-state relays were chosen for many reasons, including their faster action times, excellent reliability and the fact that there is no concern of arcing, allowing for safer operation of the actuator.

During the course of the prototypes, several other components were added. One of the first components that would be added was an extensometer. Two different extensometers would be added and examined, a Celesco CLP-100 linear potentiometer and an Omega LD621-50 linear variable displacement transducer. The extensometers were added to allow displacement monitoring and control of the prototype. Also, added during the process of prototype construction was an ACE Control HB-15-150-AA-P linear damper, used to help control the motion of the actuator, during rapid acceleration, stopping and direction changes. At several different times during the prototyping process, a pressure transducer was utilized to control deployment of the flap. The pressure transducer was included to act as a wind speed monitoring device. A complete description of the components, used during prototyping, can be found in Appendix B.

Testing Procedures

During the course of the development of the prototypes, numerous different tests were conducted, often these tests were only found to be necessary when a given situation would arise. Some tests would be conducted throughout the development process and others would be conducted one time. The reasons and goals of these tests were various and will be discussed here to clarify the following discussion of prototype development (Table 1).

Table 1: Numerous different tests were performed during the course of the development of the prototype, these tests and their purposes are discussed to clarify the later discussion.

Test	Purpose	Procedure
Time of Full Actuation	To examine time required for full deployment of the flap, to ensure the flap was capable of deploying within the limits set by the system requirements.	In the Stage 1 Prototype, the activation time was monitored by examining a graph displaying the output voltages and determining the change in time between power on and power off. For the rest of the prototypes a simple secondary program was utilized which monitored only displacement, to allow high sampling rates. The actuator was controlled by manually contacting the leads to the batteries. The results could then be examined to determine the time of full actuation.
Extensometer Signal Noise	To examine the clarity in the signal received by the DAQ of the LP and LVDT to determine which sensor would provide the cleanest signal.	The sensors were connected, parallel to one another and the actuator; the flap was then run by hand, both by physically extending and retracting it and by manually contacting the leads to the batteries. The signal from the extensometers was recorded and plotted to show the degree of signal noise in the extensometers.

Table 1 Continued

<p>Overshoot</p> <p>Overshoot Cont.</p>	<p>Overshoot tests were done to examine the distance between an input activation distance and the final stopping distance of the actuator. These tests demonstrated the degree to which the prototype could be expected to accurately perform and how repeatable the results were.</p>	<p>The control program was modified to not send an output voltage which would retract the actuator, this was done to demonstrate the distance to which the actuator would activate while eliminating any chatter in the prototype, where the actuator bounces back and forth around a desired displacement without stopping within an allowed buffer zone. A desired distance was manually input, for the actuator to achieve and the final stopping distance was recorded, the flap was manually repositioned to a zero displacement.</p>
<p>Actuator Velocity and Stopping Distance</p>	<p>The tests were run to examine the maximum velocity achieved by the actuator as well as to determine the distance the actuator traveled once the power to it was shut off.</p>	<p>The tests were performed similar to the tests for deployment time. The same, simpler program was utilized and the actuator was extended by manually contacting the leads from the actuator to the batteries. However, the tests were not run to full extension, but instead the flap was only partially extended. The data was examined and the derivative of the extension data provided a velocity chart, which was then used to find the maximum velocity, as well, by monitoring when the velocity begins to drop, it allowed the determination of the time and distance traveled by the actuator from the time the power is shut off to when the actuator stops.</p>
<p>Sampling Rate</p>	<p>The sampling rate tests were performed to see what sampling rates were being achieved by the control program and DAQ.</p>	<p>The tests were performed by utilizing data from the Velocity and Stopping Distance tests and running tests to the matching extensions, with the control program, when a matching set of data was achieved, the data points recorded by the control program were matched to displacement values from the Velocity test data and the time index of those tests was used to determine the sampling rate of the control program.</p>

Prototype-Stage 1

The first stage of the prototype was a basic on-off system, built on a flat plate, for proof of concept purposes. Being an on-off system meant there were two possible flap positions, fully deployed or fully retracted. This prototype also incorporated the ‘virtual’ flap into it as seen in Figure 23. The virtual flap consisted of a 12 inch steel tube, with a series of 1/8 inch holes drilled in the side of it, which was then connected to an air

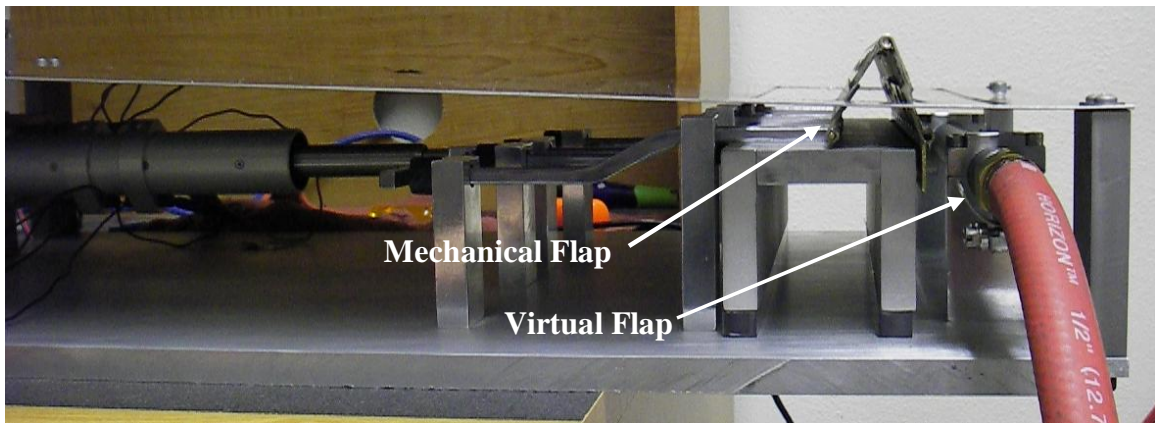


Figure 23: The stage one prototype, utilizing both the mechanical and virtual flap.

compressor. When activated, high pressure air was forced through the holes, meant to disrupt the flow of air over the airfoil and forcing premature boundary layer separation; creating a ‘virtual’ flap with the air. Activation of the flap and ‘virtual’ flap was controlled by a pressure transducer, which was meant to monitor air pressure changes, due to changing wind speeds. The pressure transducer was an Omega PX209-15G5V sensor. The system was monitored and controlled by a LabVIEW program. The program was built in LabVIEW 6.0 and used a National Instruments SCXI-1000DC chassis with an SCXI-1200 card with an attached SCXI-1302 card. The program monitored the pressure and when pressure levels reached high enough levels, the program sent an output

voltage to a series of relays which then sent the necessary output power to engage the desired flap; each mechanism was operated separately due to DAQ limitations.

The 'virtual' flap utilized a 24V AC solenoid sprinkler control valve to control the flow of air and was connected to a relay, which was used to control the power needed to open and close the valve. The program built, seen in Figure 24, was relatively simple, monitoring only the pressure from the pressure transducer and outputting on one channel, to control the single relay. When a set pressure level was acquired, the program would output 5V to the relay which would engage and allow the 24V AC required to open the

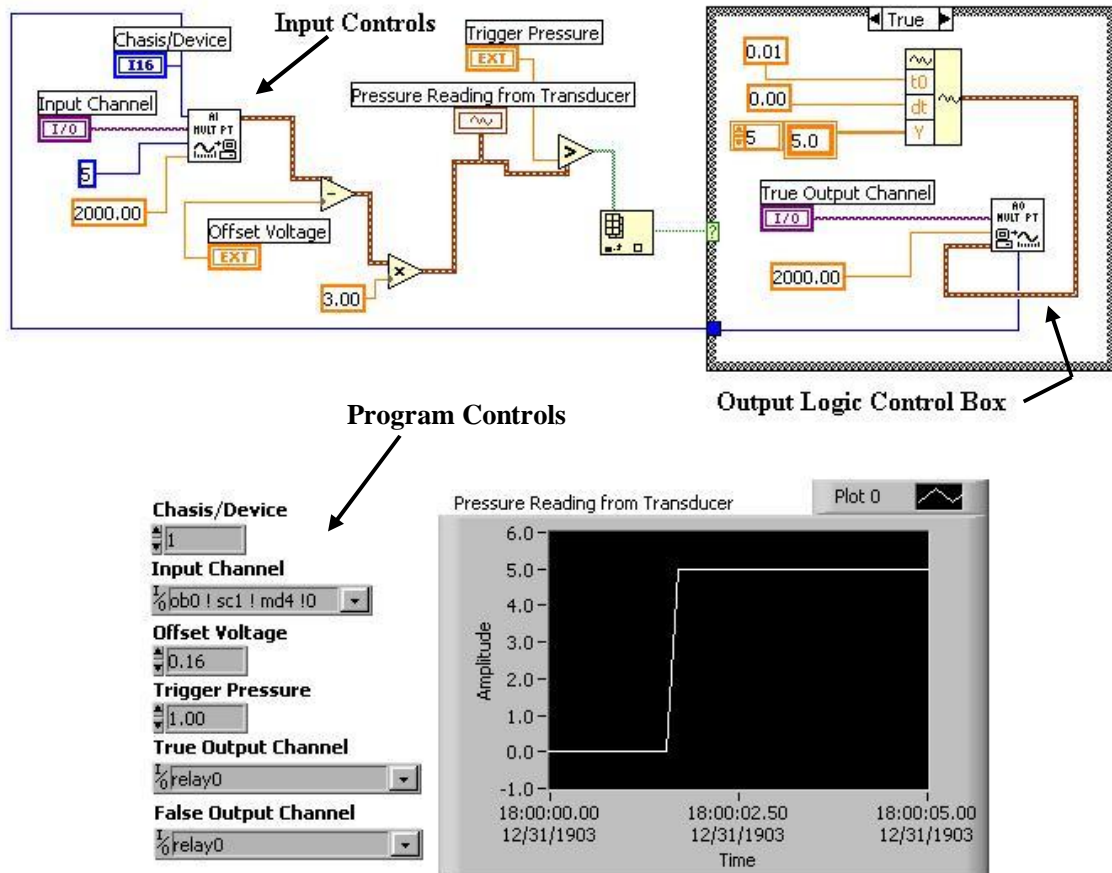


Figure 24: The program required for the operation of the 'virtual' flap was relatively basic, monitoring an input and generating a single output. Several main components are labeled here.

valve and release air from the air compressor. The system had several beneficial attributes; it was fast acting, the time required to react was limited simply by the computer running the program and the time required for the valve to open; the system was simple, the valve was the only moving part, making it reliable and reducing maintenance; the program required to operate the system was simple to design and operate; also, the design would much more easily be retrofit into existing blades.

Unfortunately there are several major drawbacks which would need to be overcome; mainly the effectiveness of the system is unproven and untested. A great deal of research would need to be done to prove the 'virtual' flap to be an effective method of reducing lift. Also, a method of distributing the air throughout the length of the blade would need to be designed, which could maintain constant air pressure to the flaps while keeping weight to a minimum.

The mechanical flap was a much more complex system, requiring extensive machining, programming and problem solving. The basic idea of the system was similar; a LabVIEW program continuously monitored the air pressure and when a sufficient level was reached, engaged a series of relays. With the on-off design, no extensometers were required, but it was necessary to stop the power to the actuator when full extension was achieved. To do this, two magnetic switches were utilized, in conjunction with a magnet located on the output shaft of the actuator. The switches were located at either limit of actuation and connected to a AA battery, when the magnet passed beneath the switch, it completed a circuit, sending a voltage to the DAQ, which could be monitored by LabVIEW and used to discontinue the output to the activated relays (Figures 25 and 26).

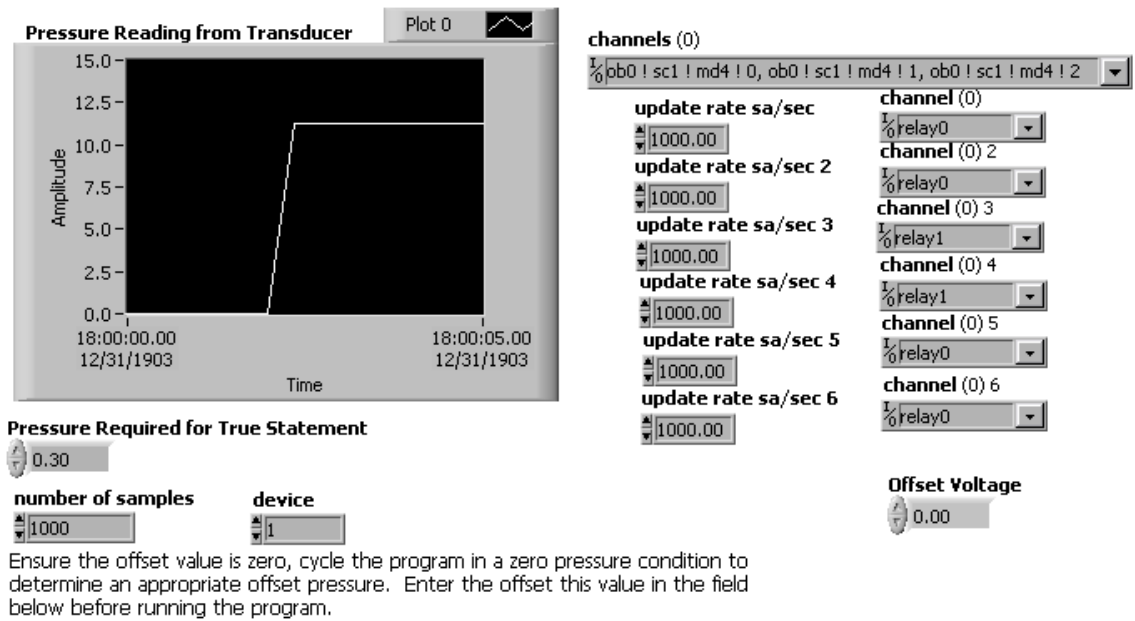


Figure 25: The user interface for the Stage-1 Prototype mechanical flap. The program required many more controls than the 'virtual' flap.

A more complete explanation of each programs that were built, for each stage of the prototypes can be found in Appendix C.

Although, the system worked quite well, there were several problems that had to be closely examined for complete and reliable system operation. The magnetic switches proved to be a sensitive point in the function of the system. The switches had a very limited region over which they could be activated, which presented several problems, the first being overshoot. With the limited range over which the switches would activate, the momentum of the actuator would carry it past the point at which the switch was activated and the system would then send power to the actuator again. This would cause power to continue going to the actuator when it was past the limits of movement and could have caused damage to the actuator or belt, if the power was not monitored externally. This problem was solved by including rubber dampers which fulfilled several functions. First,

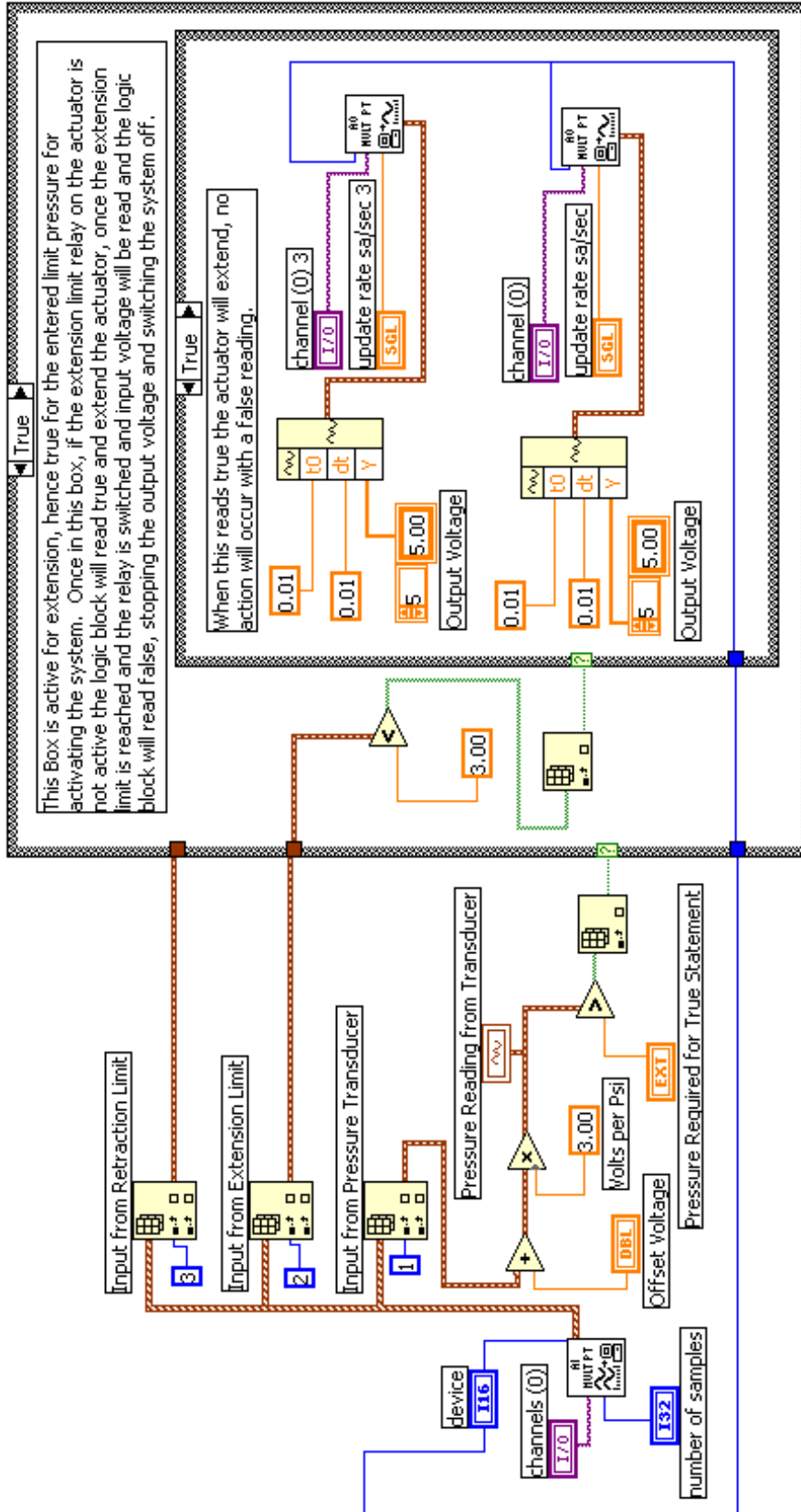


Figure 26: The program required for controlling the flap mechanism of the prototype was much more complex than that for the 'virtual' flap, requiring multiple levels of logic as well multiple inputs and outputs to monitor flap location and extend and retract the flap.

they slowed the movement of the flap when it was reaching its limits and the switches were activated, also the dampers lessened the impact of the actuator when it reached the limits. While the dampers generally solved the issues, the placement of the switches was still critical.

A second major problem of the system was its ability to adapt to changing conditions, mainly when a pressure load was removed while the flap was still being extended. When this occurred, the flap would continue extending until the extension limit was reached, however, rather than shutting the power down, it would continue to attempt to extend the actuator. The fix for the problem was in the LabVIEW program, which was reexamined in detail. The logic system of the program had to be completely restructured so as to be able to adapt to mid-motion changes. Once completed the program was robust enough to handle all conditions which were applied.

Once fully functioning, the prototype was tested for its deployment time, which was consistently around 580 ms [27], very near the desired 500 ms, for full extension. The prototype, from a proof of concept standpoint, was very effective. It demonstrated the ability to monitor an input pressure and utilize that pressure to create an output voltage, which controlled a relay circuit, which successfully controlled the actuator and flap. For an initial stage of design, the prototype was very effective.

Prototype-Stage 2

The second stage of the prototype utilized the flat plate system again, but rather than simply using an on-off design, it attempted partial deployment. This meant that the input pressure was converted to a displacement, by the control program, which then deployed the flap. Rather than simply being fully extended or retracted, there was the ability to extend the flap to any location. To achieve this, a key component was needed, an extensometer. Two different types were examined, a CLP-100 linear potentiometer (LP) from Celesco and a LD621-50 LVDT from Omega. These sensors were attached beside the actuator and were examined to determine the best sensor for the application.

The programming of the partial deployment system was vastly different from the development of the previous programs. As mentioned, rather than simply using a pressure limit to engage or disengage the flap, that pressure had to be converted into a displacement, which was then used to control the flap location. Also, the flap now had to rely on the program to fully control its location, rather than being able to rely on mechanical limits to stop the flap. This proved to be the main challenge in the design of the program and the system as a whole. Early tests quickly showed a significant problem with overshoot. Similar to the previous Stage 1 Prototype, once the power was removed from the actuator, the momentum carried the actuator beyond the desired point. For testing purposes a program was built which enabled a desired displacement value to be input, rather than utilizing a pressure value. As shown in Figure 27, one series of tests was performed to examine both the magnitude of overshoot and also compare the results from the LP and LVDT. These tests showed a significant overshoot in all cases, ranging

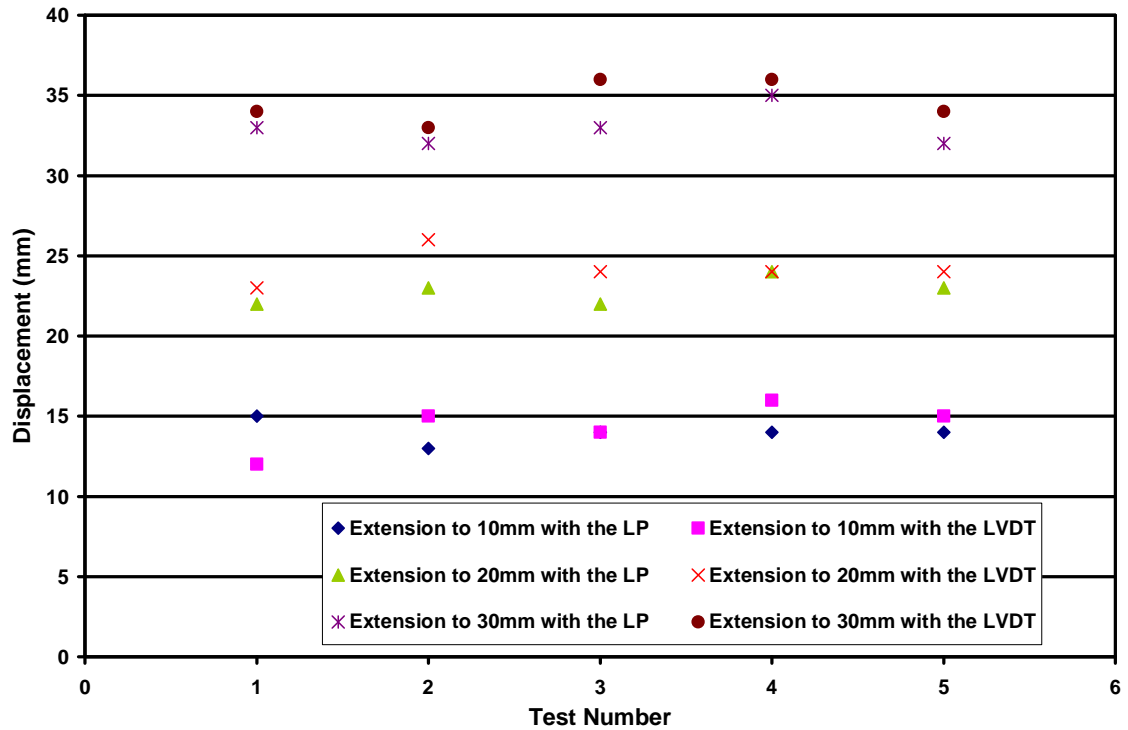


Figure 27: Tests consistently showed better performance from the system when a LP was used instead of the LVDT. A series of tests were run to find the overshoot with the extensometers, when looking at three extension values; 10mm, 20mm and 30mm.

from 2.8 to 4.4 mm, in all cases, a consistently better performance with the LP was seen as compared to the LVDT, in tests run to 10, 20 and 30mm. In the tests, the LVDT outperformed the LP in only three instances and on average stopped the actuator 0.4, 1.4 and 1.6mm after the LP in the respective distances examined, as seen in Table 2.

Another set of tests were run, allowing the program to shut off the voltage to the actuator 2mm before the desired distance was reached, compensating for a portion of the

Table 2: This shows the average stopping distance of the actuator when attempting the desired test lengths. This series of tests had no buffer zone.

Test Length	10mm	20mm	30mm
LP	14.0	22.8	33.0
LVDT	14.4	24.2	34.6

overshoot. These results showed a significant improvement in the results, as can be seen in Table 3. However, acquiring the exact desired displacements remained difficult and elusive. In the tests, the LP continued to show better performance than the LVDT.

Table 3: This shows the average stopping distance of the actuator when attempting the desired test lengths. This series of tests allowed a 2mm buffer zone, before the desired displacement, in an attempt to prevent overshoot.

Test Length	10mm	20mm	30mm
LP	10.0	20.0	32.2
LVDT	11.4	22.2	35.4

Several other tests were performed examining the differences between the LP and LVDT, to determine which would be the best sensor for the prototypes. These tests included examining the cleanliness of the output signal. Several tests showed the advantage to be with the LP again. The signal from the LVDT consistently showed a much higher noise level in the signal. This could be due to the sensitivity of a LVDT to magnetic fields and the proximity of the sensor to the motor of the actuator or the magnet it contained, regardless a sensor which is not sensitive to an electromagnetic field, is essential to any component that would be built into a wind turbine blade. As well the LP is significantly less money than the LVDT. All these factors combined into choosing the LP as the best sensor for moving forward with the prototypes.

While generally effective, the Stage 2 Prototype showed a major area which would continue to plague the prototypes throughout the testing process, overshoot. It also showed the ability to build a program which was capable of controlling the flap displacement, rather than the previous on-off design. However, the flat plate system was just a midpoint in the partial deployment system design.

Prototype-Stage 3

The third stage of the prototype moved from the flat plate into a section of blade, which offered a better representation of the final application and allowed for the possibility of wind tunnel testing. Partial flap deployment continued to be used on the Stage 3 Prototype; however the overall design and dimensions of the prototype were vastly improved from the previous systems. In an attempt to get faster action from the prototype and limit overshoot, several improvements were made.

The first change made was to switch from a mechanical relay to a solid state relay. Solid state relays are much faster acting, protect equipment better, are silent and are much more reliable, all advantages in the proposed application. Unfortunately, solid state relays are also much more expensive when compared to their mechanical counterparts, but with the experience which had been gained in wiring a circuit, the relays were also much more likely to not need to be replaced. To protect the relays a typical blade or cylinder fuses are insufficient, as their comparatively slow reaction time can allow the relay to be destroyed by a short circuit, before the fuse is able to melt. To circumvent this, a semiconductor fuse and fuse box was needed, and was wired into the circuit. The circuit which was built, was an H bridge, requiring four relays, as solid state relays typically only come in a single pole single throw design. The second major improvement was moving from the LabVIEW 6 based data acquisition (DAQ) system to LabVIEW 8. With the move, the previous DAQ unit was replaced by a new National Instruments NI USB-6229 DAQ unit. The new unit incorporated a faster USB connection to the computer, higher sampling rates and more output and input channels.

These combined to create a system which was faster acting and more capable of controlling the prototype, more rapidly.

The changes made to the control system were not the only changes to the system which had to be taken into account. The mechanism itself was simplified, the main change being the elimination of the linkages from the actuator to the flap, which could be seen previously in Figure 23, these linkages had been included to provide vertical stability to the flap. By adding more rigid supports to the actuator, these linkages were no longer needed and were able to be removed (Figure 28). Another change was the overall dimensions of the flap, previously, full extension was 43mm, with the new prototype, a flap height of 10% was chosen, this increased the maximum extension, to 89mm. The greater area allotted inside the blade also allowed for mounting all of the relays inside the prototype, rather than separate from it. The entire system was completely rewired to adapt to the new hardware and present a cleaner appearance.



Figure 28: Rigid supports were added to eliminate the need for additional linkages to support the actuator and other hardware.

Program Changes:

With the new system a new control program was required as well; this program was much more intense when compared to the previous programs. The program had to take into account four relays, compared to the previous two. It was structured to utilize only the LP and was set up for the set displacement actuation. The solid state relays also required the inclusion of several safety factors to prevent system damage; solid state relays are very sensitive to shorts and with the required four relays and the H bridge design, a short can easily be created, which would blow the fuse. To present a more functional program which would operate continuously and safely, safety checks were required. Also, to prevent damage to the actuator and flap, a safety was required to ensure that excessive desired displacement values didn't exceed the mechanical restraints of the system. Extensive time was also spent to enable the simplest operation and to create the shortest possible learning curve, for anyone else who would attempt to run the program. All this was packaged into the leanest and fastest possible program. Many iterations of the program were created during the evolution to the final Stage 3 Prototype program, and the final program utilized several key features which were new to the programs. Two of the major features were the replacement of the logic boxes with true/false logic switches, which simplified the program, allowing for faster running speeds, and the inclusion of a while loop, which allowed for a higher sampling rate. The final program was the fastest Stage 3 program produced, yet was still much larger and more complicated compared to the previous programs (Figures 29-31).

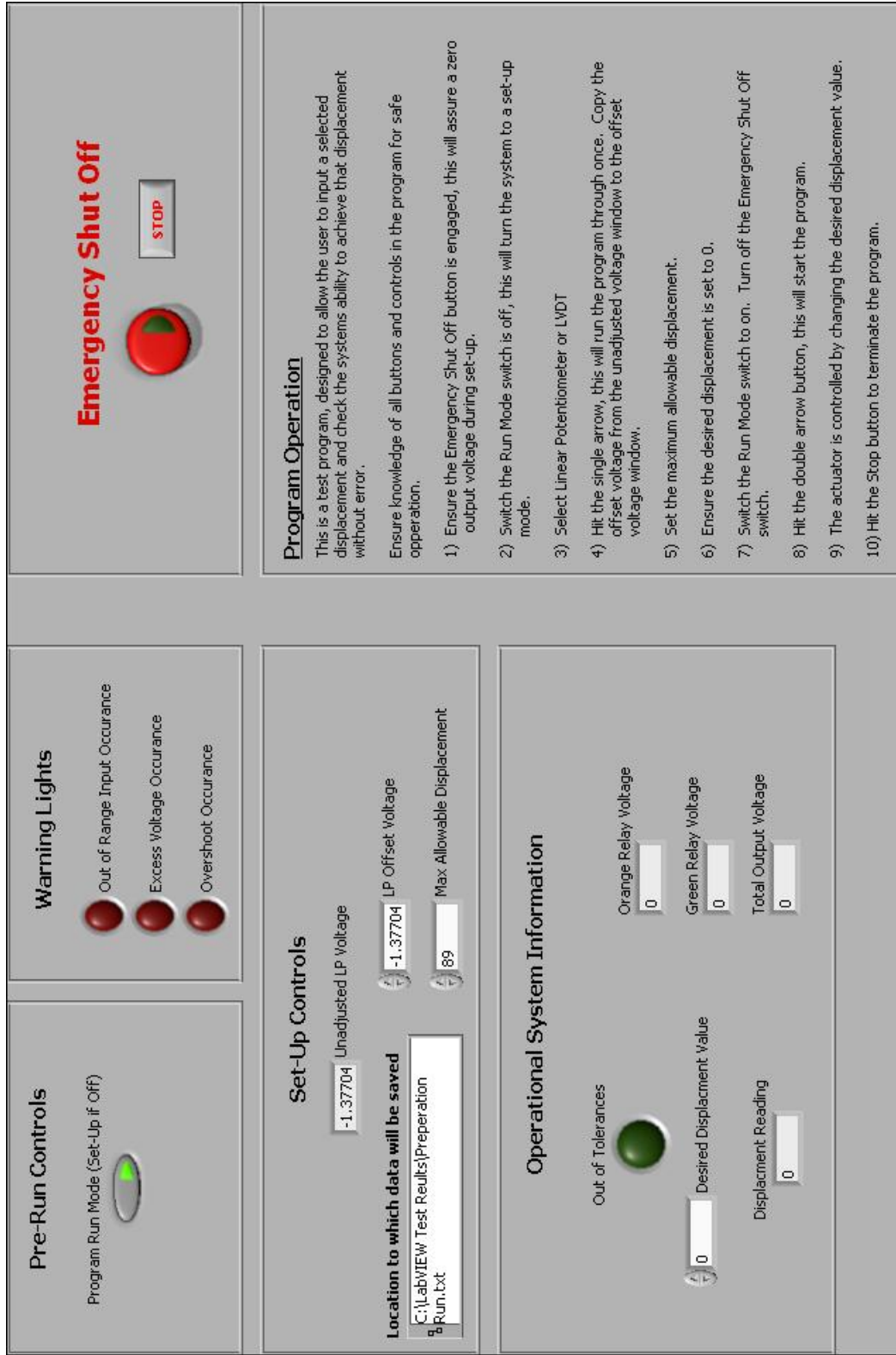


Figure 29: The front panel of the control program was designed to be as user friendly as possible by being simple to use and provide a great deal of information to the user at the same time.

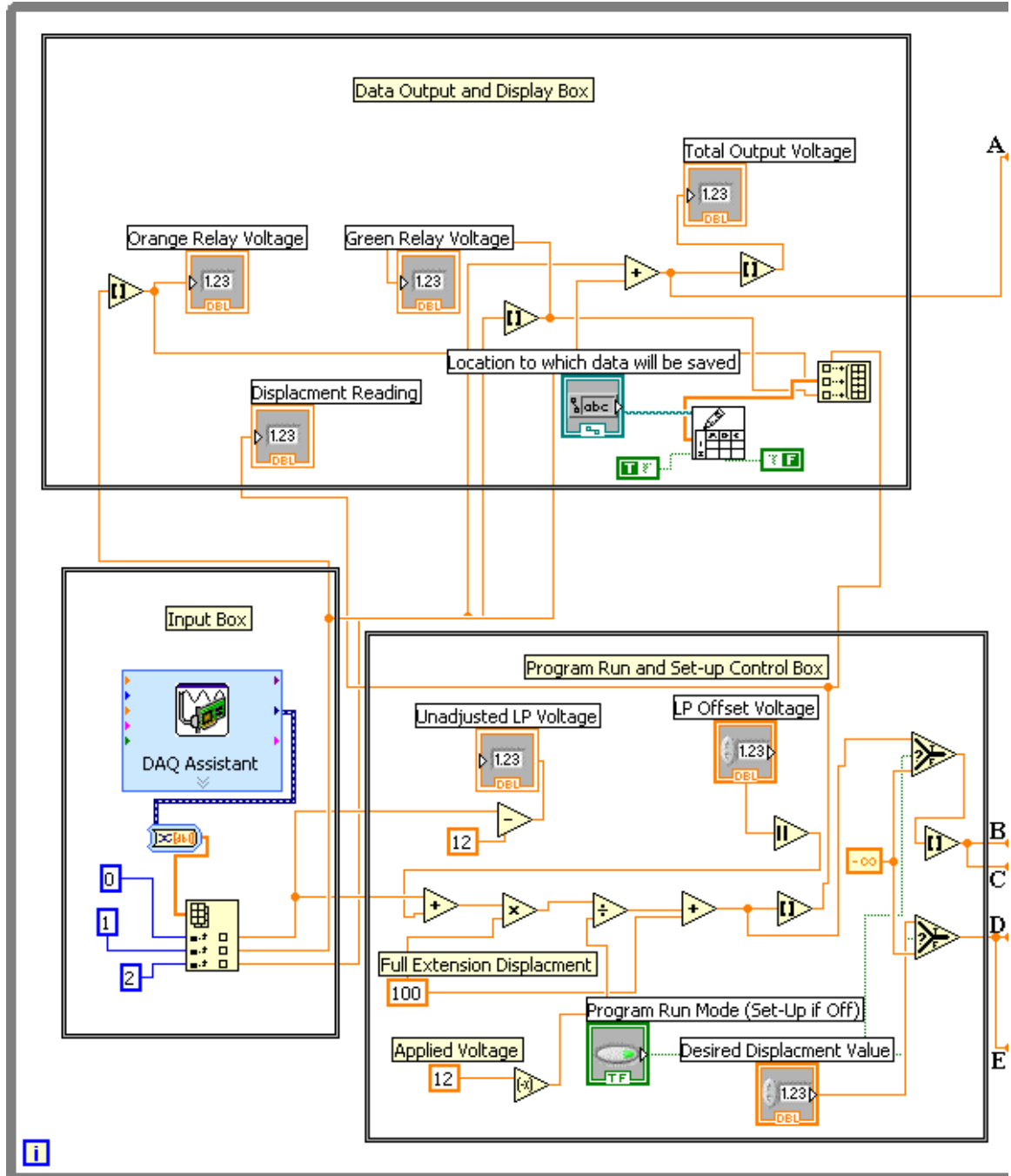


Figure 30: The first half of the control program, largely the input and data manipulation components of the program. The connections to the second half of the program are labeled A-E, along the right side of the program.

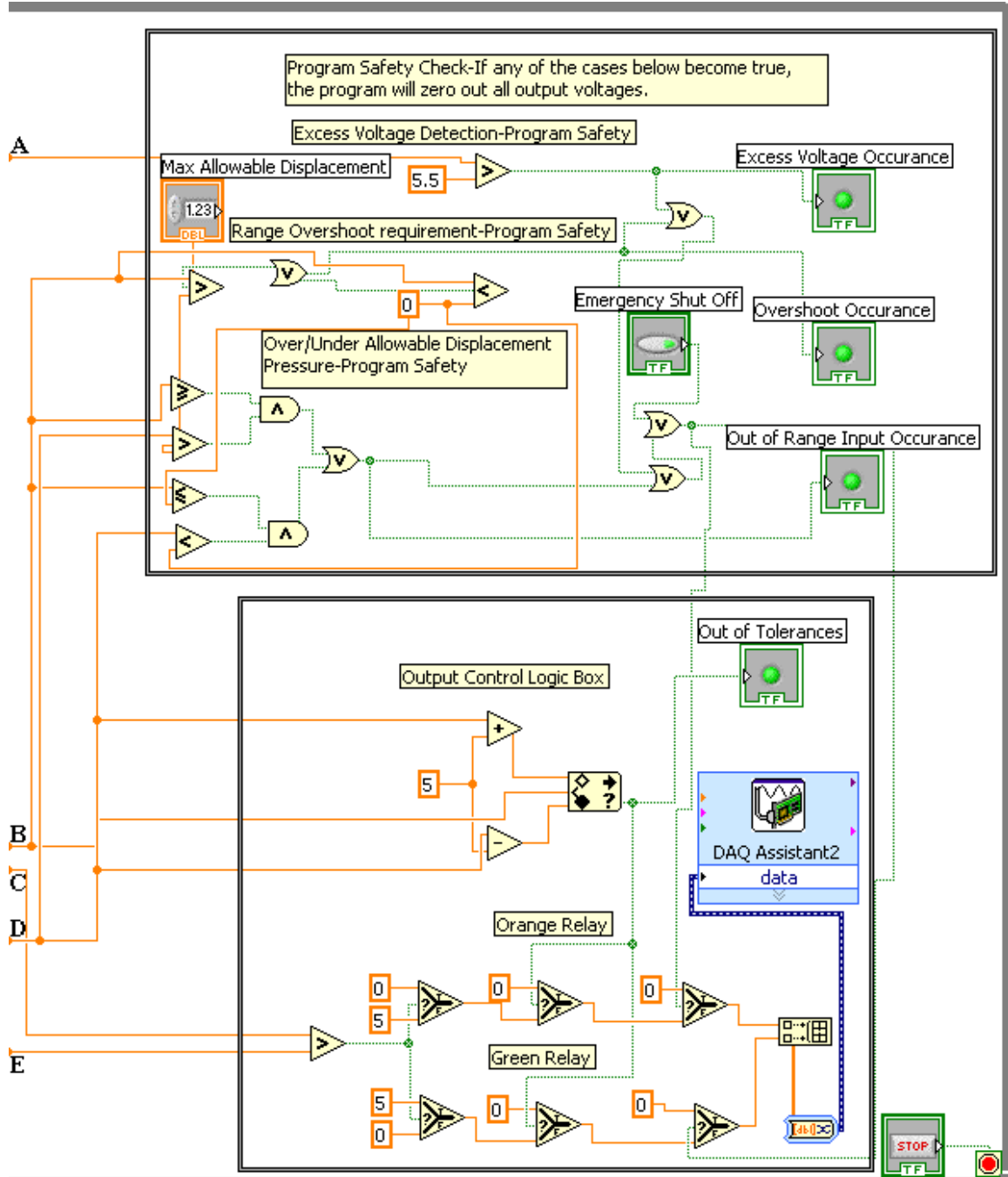


Figure 31: The second half of the program contains mostly the logic systems, safety switches and the output controls. The connections to the first half of the program can be seen on the left hand side of the program, labeled A-E.

System Testing:

As the prototype was approaching a final desired configuration, extensive testing was done on the Stage 3 Prototype to ensure proper system operation. Early tests showed a familiar yet nagging problem, overshoot. While it was expected that overshoot would be greatly reduced by the addition of the solid state relays and the new DAQ system, tests quickly showed the problem to be worse than ever. Where as the Stage 2 Prototype

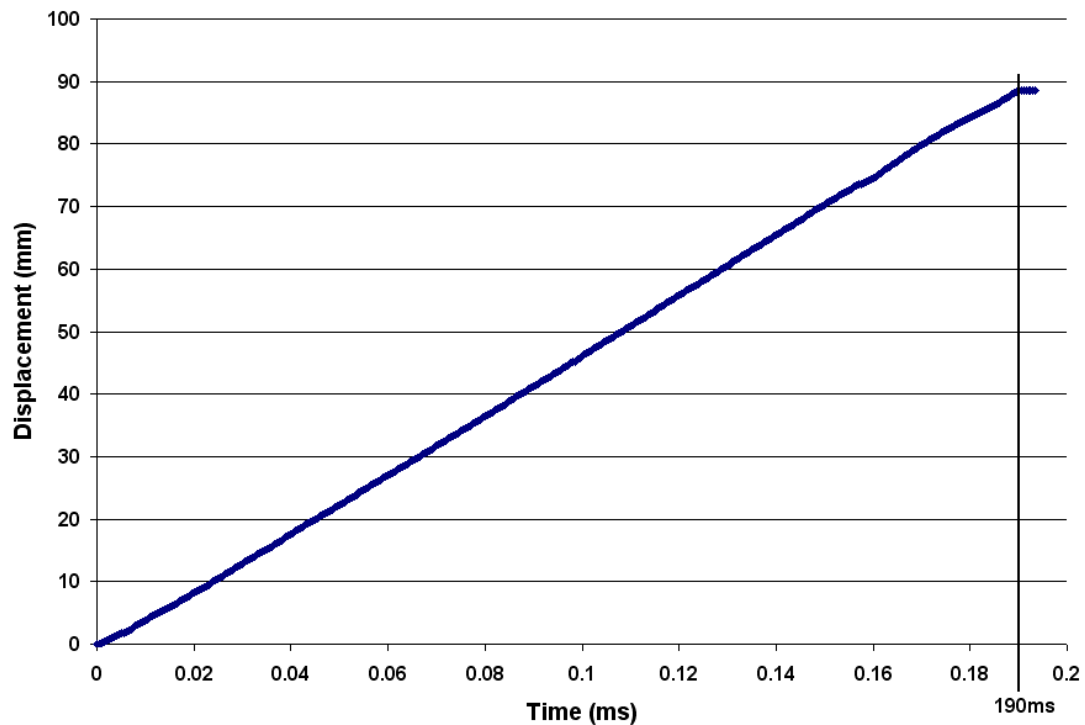


Figure 32: The Stage 3 Prototype showed excellent deployment times, deploying to the full 89mm in only 190ms.

consistently saw overshoots up to 5mm, the Stage 3 Prototype saw average overshoots of 14.3mm on tests of 24, 25 and 26mm, three times the overshoot seen in the Stage 2 Prototype [28]. These results were the complete opposite of the expected effect of the transition to the new prototype. Further analysis quickly revealed the cause of the

excessive overshoot. While the initial flap required around 580ms to fully deploy to 43mm, tests showed the Stage 3 Prototype was capable of deploying to 89mm in 190ms, as can be seen in Figure 32. For the flap to deploy that quickly showed there had to be significant decrease in resistance in the system. Examination would show the resistance in the prior system likely came from the linkages that connected the actuator to the flap. While eliminating the linkages increased the efficiency and speed of the system, it also resulted in greatly increased overshoot.

Due to the excessive overshoot, many tests were run to examine methods of mitigating the overshoot. To prevent overshoot, it was first necessary to understand what caused it. Several different tests were run to do this; the first tests examined the velocity profile of the actuator, before the full extension was reached. This was necessary so that the acceleration, constant velocity region and deceleration of the actuator could be seen. A number of these tests were run, to different extensions, before the power was released. The program utilized to run the tests was a very basic program, which simply input the displacement value and recorded the values to an output file. This allowed for very high sample rates, a sampling rate of 2000 samples/second was used and the program ran for two seconds. The simplicity was necessary to get sufficient information, but as a result, required the actuator to be controlled by creating and breaking the circuit by hand. The tests were then conducted by starting the program then touching the lead from the actuator to the battery, momentarily. This extended the actuator to a point and the data of the movement was recorded and provided detailed information of the full spectrum of the velocity of the actuator.

To get a good array of information, fifteen tests were run at a variety of extension values. One of these tests can be seen in Figure 33. As can be seen, the actuator accelerates to full velocity very quickly, within approximately 0.011s, the velocity then remains relatively steady around an average of 473mm/s, until the voltage is removed, at which point the actuator begins to decelerate. The time required to decelerate is

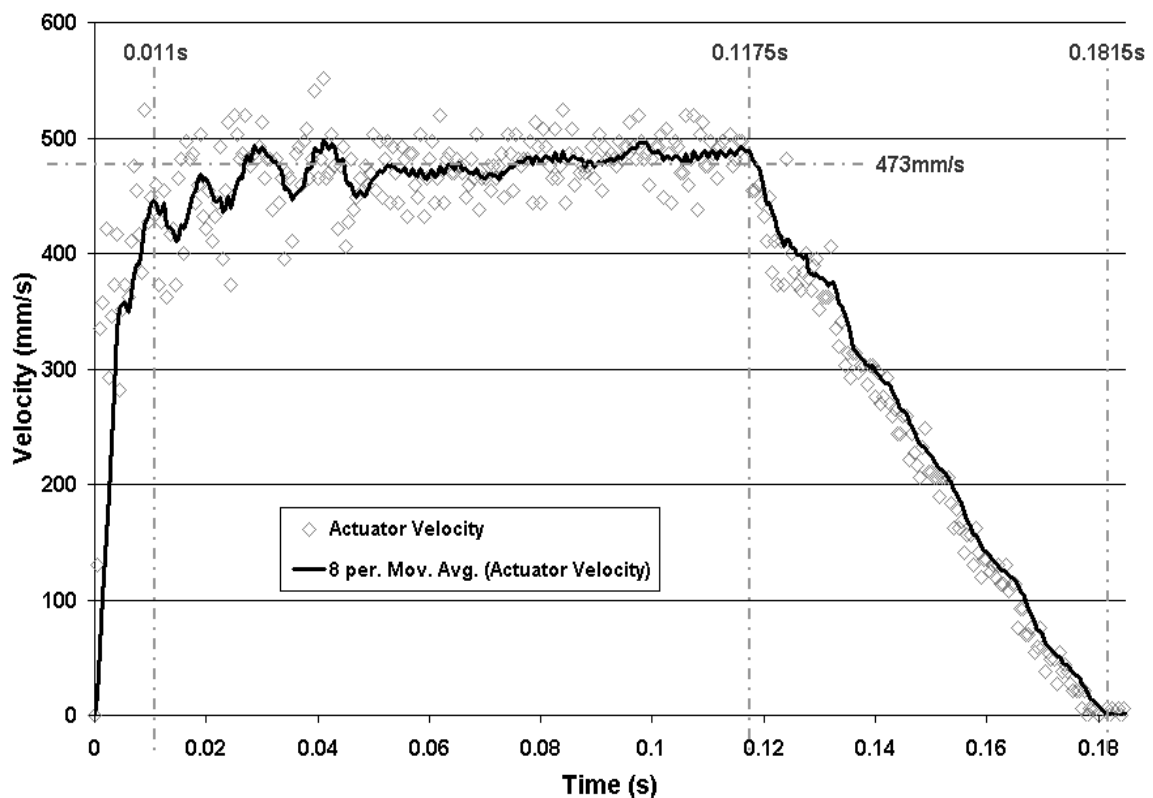


Figure 33: The actuator accelerates very quickly and attains a high maximum velocity; however the time required to decelerate is significantly longer, contributing to overshoot.

approximately 0.064s, nearly six times as long as required for acceleration. Examining the deceleration region shows it to be relatively linear. Examining only the deceleration region allows for applying a line of best fit, as seen in Figure 34, which can then be used to find the distance traveled by the actuator after the power was released. In this case, that

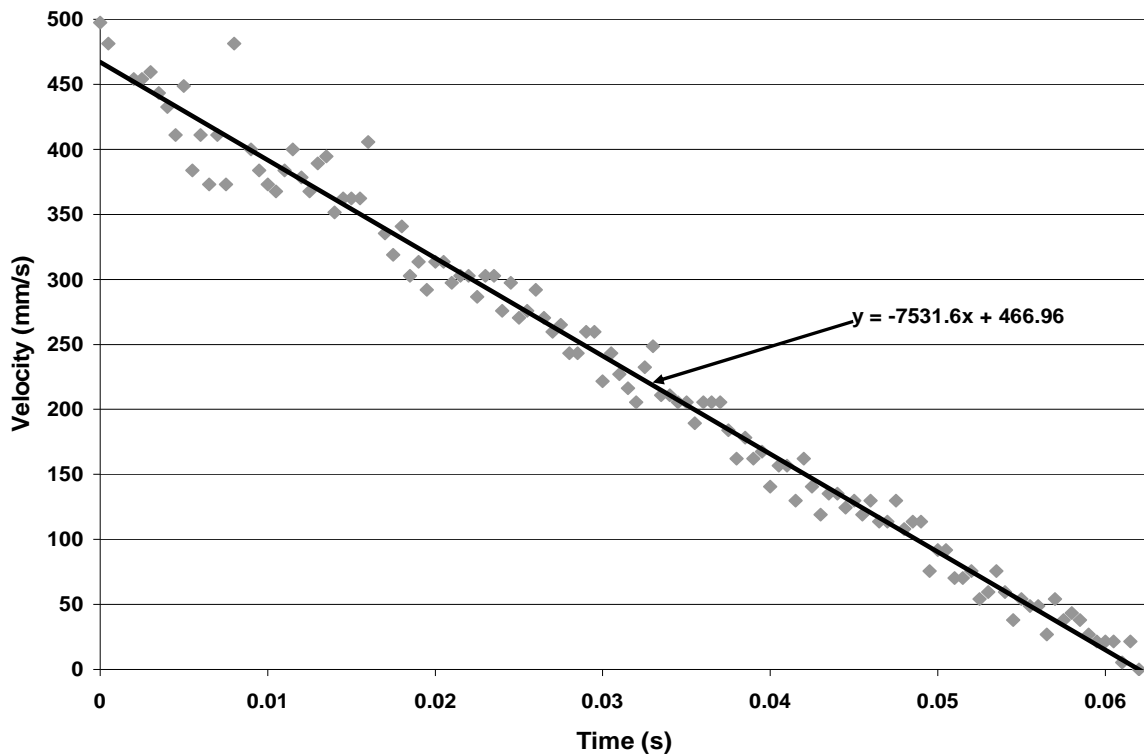


Figure 34: The slope of the deceleration region is relatively linear, which helps in predicting overshoot.

Table 4: A listing of the tests conducted to examine the maximum velocity, deceleration and overshoot of the actuator, at various actuation distances.

	Deceleration Rate (m/s ²)	Final Displacement (mm)	Maximum Average Velocity (mm/sec)	Time for Deceleration (s)	Magnitude of Deceleration Region (mm)	Actuation Distance (mm)
Test 1	7.5316	68	481	0.06386	15.36	52.64
Test 2	6.3334	55	481	0.07595	18.27	36.73
Test 3	7.1392	77	487	0.06821	16.61	60.39
Test 4	7.7584	74	487	0.06277	15.28	58.72
Test 5	6.4088	54	481	0.07505	18.05	35.95
Test 6	7.6818	74	487	0.06340	15.44	58.56
Test 7	6.566	48	470	0.07158	16.82	31.18
Test 8	7.3416	66	476	0.06484	15.43	50.57
Test 9	6.6108	10	341	0.05158	8.79	1.21
Test 10	7.1214	45	476	0.06684	15.91	29.09
Test 11	7.552	24	470	0.06224	14.63	9.37
Test 12	6.7458	54	476	0.07056	16.79	37.21
Test 13	7.7558	77	487	0.06279	15.29	61.71
Test 14	7.9998	26	470	0.05875	13.81	12.19
Test 15	7.495	25	465	0.06204	14.42	10.58
Average	7.20276	51.8	469	0.06536	15.39	36.41

distance was 14.5mm, which corresponds quite well with the previous values seen for overshoot. The test in this case was out to a distance of 68mm, so further tests were examined to find a relation between time for deceleration to occur and the magnitude of the deceleration region, the results can be seen in Table 4. Some of the results can be seen in Figure 35. As can be seen the tests kept a relatively similar slope and the average deceleration line fell nicely in the middle of the range of other values. Utilizing this information allows some degree of predictability when attempting to mitigate the effects of overshoot. By knowing it will take an average of 15mm to decelerate from maximum velocity to zero, the voltage to the actuator can be controlled in a way to begin to stop the actuator in a timely manner to prevent overshoot. For small actuation distances, this presents a significant problem though. The actuator will generally travel a minimum of

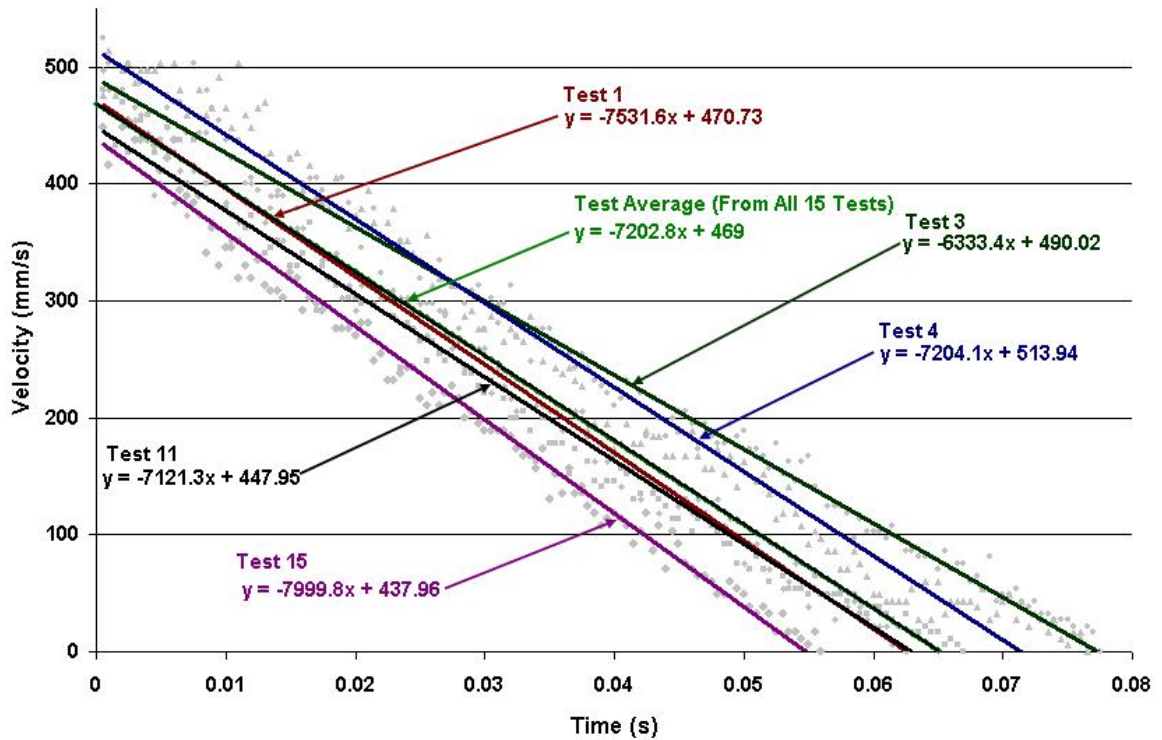


Figure 35: Deceleration rates vary only slightly between all of the tests, even allowing for varying initial velocities.

around 10mm, making small adjustments very difficult to obtain, if not impossible, with the current system.

Another important factor in mitigating the overshoot of the actuator was the sampling rate of the system. With the previous tests, the program which was used was a very simple program which was capable of achieving very high sampling rates, however, the control program built to run the prototype was significantly more complicated, which would limit the capacity of the program to achieve high sampling rates. With an average velocity of 468 mm/s, the sampling rate needed to reach at least 500 samples/sec if the program was to cleanly control the actuator and generate enough data to make any attempt to eliminate overshoot. To check this, a series of tests were run to a distance of 52mm and the points were recorded, these tests showed a severe disparity between the achievable sampling rates and the necessary rate. These tests were plotted along a graph for displacement from the previous set of tests, which had a matching final displacement and actuation distance, as seen in Figure 36. The displacement values were matched with a corresponding time marker, enabling the time between tests to be determined, the full results of these tests can be seen in Table 5. The results showed that samples were being read every 0.030s to 0.032s on average, corresponding to sampling rates between 31.6 and 33.1 samples/sec, roughly $1/15^{\text{th}}$ of the sampling rate needed to accurately control the prototype. This disparity between capable and necessary sampling rates, combined with the extension of the actuator during deceleration crippled the ability of the prototype to function properly and resulted in the severe overshoot seen.

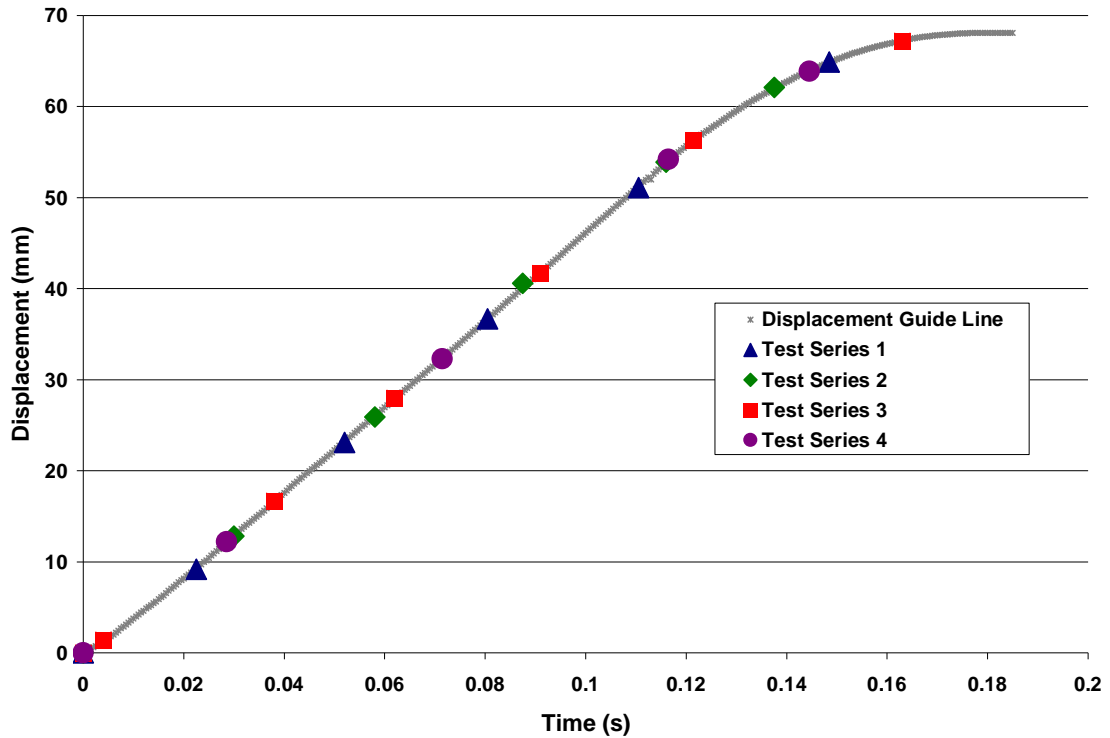


Figure 36: The slow data acquisition rate achieved by the control program and DAQ caused large gaps in the data, during extension.

Table 5: Data collected from tests examining the sampling rate of the DAQ system, during full speed actuation of the flap.

	Test Set 1			Test Set 2		
	Time (s)	Displacement (mm)	Change in Time (s)	Time (s)	Displacement (mm)	Change in Time (s)
Point 1	0	0	0	0	0	0
Point 2	0.024	9.2	0.024	0.03	12.8	0.03
Point 3	0.053	23.1	0.029	0.058	25.9	0.028
Point 4	0.081	36.7	0.028	0.0875	40.6	0.0295
Point 5	0.1115	51.1	0.0305	0.116	53.9	0.0285
Point 6	0.1485	64.9	0.037	0.1375	62.1	0.0215
	Test Set 3			Test Set 4		
Point 1	0	0	0	0	0	0
Point 2	0.004	1.4	0.004	0.0285	12.2	0.0285
Point 3	0.0385	16.7	0.0345	0.0715	32.3	0.043
Point 4	0.063	28	0.0245	0.1165	54.2	0.045
Point 5	0.092	41.7	0.029	0.1445	63.9	0.028
Point 6	0.1225	56.3	0.0305			
Point 7	0.163	67.2	0.0405			

The Stage 3 Prototype showed two serious flaws which had to be overcome before the prototype could fully function properly. However, the integration of the new components into the existing system occurred smoothly and created a better and more effective prototype. As well, moving the system into the blade section made for a prototype which could be tested in a wind tunnel, greatly expanding its usefulness. The prototype developed into a useful tool in the investigation of the transient response of a system capable of partial deployment as compared to the quasi-steady response of an on-off system design. While problems were present, progress was made throughout the course of the Stage 3 Prototype development, and the overshoot and the spacing between sampling points were reduced through extensive reworking of the control program. Also, several enhancements were conceived for improving the function of the prototype, which could then be implemented in the Stage 4 Prototype. While a great deal of work remained to be done, the Stage 3 Prototype was an important step in the process of creating a fully functioning partial deployment prototype which acted as a proof of concept design and could be tested in a wind tunnel.

Prototype-Stage 4

The Stage 4 Prototype was the culmination of a year of effort in programming, electronics and hardware. That experience resulted in a complete reexamination of the prototype. The first step in the creation of the Stage 4 Prototype was an examination of the control program, and resulted in a series of completely new control programs, each of which took a very different approach, compared to the previous programs. Next up was the hardware, mitigating the momentum of the actuator at voltage off was necessary for the actuator to properly function, resulting in the addition of a linear damper to help stop the actuator. The final examination was of the electronics, tests had shown the prototype worked much more smoothly when operating at 12V, however it was also much slower, so the program was changed with the addition of a stepped voltage method, which stepped the voltage from 24V to 12V as the actuator neared the final position, slowing the actuator, to allow more precise control. The affect of each component was individually tested, then combined to get the maximum effect. Once a capable system was developed, another goal was achieved with the incorporation of a pressure transducer, which was connected to the prototype and utilized to control the extension of the actuator. The Stage 4 Prototype was utilized to create a complete working system and incorporate all the goals set out for the prototype.

The Programs:

For the Stage 4 Prototype, two completely new and very different control programs were utilized, in attempt to increase the sampling rate of the systems. The first

program took a very different approach from all of the previous programs and utilized Math Script Nodes. Math Script Nodes allowed for the use of MatLab programming code to operate the program, this greatly simplified and cleaned up the program, as can be seen in Figure 37. The wiring was nearly eliminated, leaving only the fundamentals, however, the Math Script Nodes also take up a lot of memory and LabVIEW is not capable of operating them as quickly as their clean appearance would tend to make one believe. Tests showed the program actually operated more slowly than previous programs and utilized a great deal more memory. The overall sizes of the programs were between 0.9 and 1.3 MB and, compared to the previous programs which were no larger than 0.3 MB. It became quickly apparent that the Math Script Node based programs would not achieve the desired results and faster program operation, another program would be needed.

The next program went back to the previous concepts utilized in the Stage 3 Prototype, however, those programs didn't work as well as they needed to and had to be reinvented. With that, several major improvements were made, the complete logic structure was reanalyzed and simplified, and any unnecessary steps were eliminated. The next major change was the elimination of the DAQ Assist modules. While these modules simplified the building of the program they take up a large amount of memory and were replaced with more basic input and output modules. Several other small modifications were made, including pulling the data writing node out of the while loop, through the use of a Shift Register, which allowed the program to write the collected data after the program had been run, rather than as it was running. As can be seen in Figure 38, the

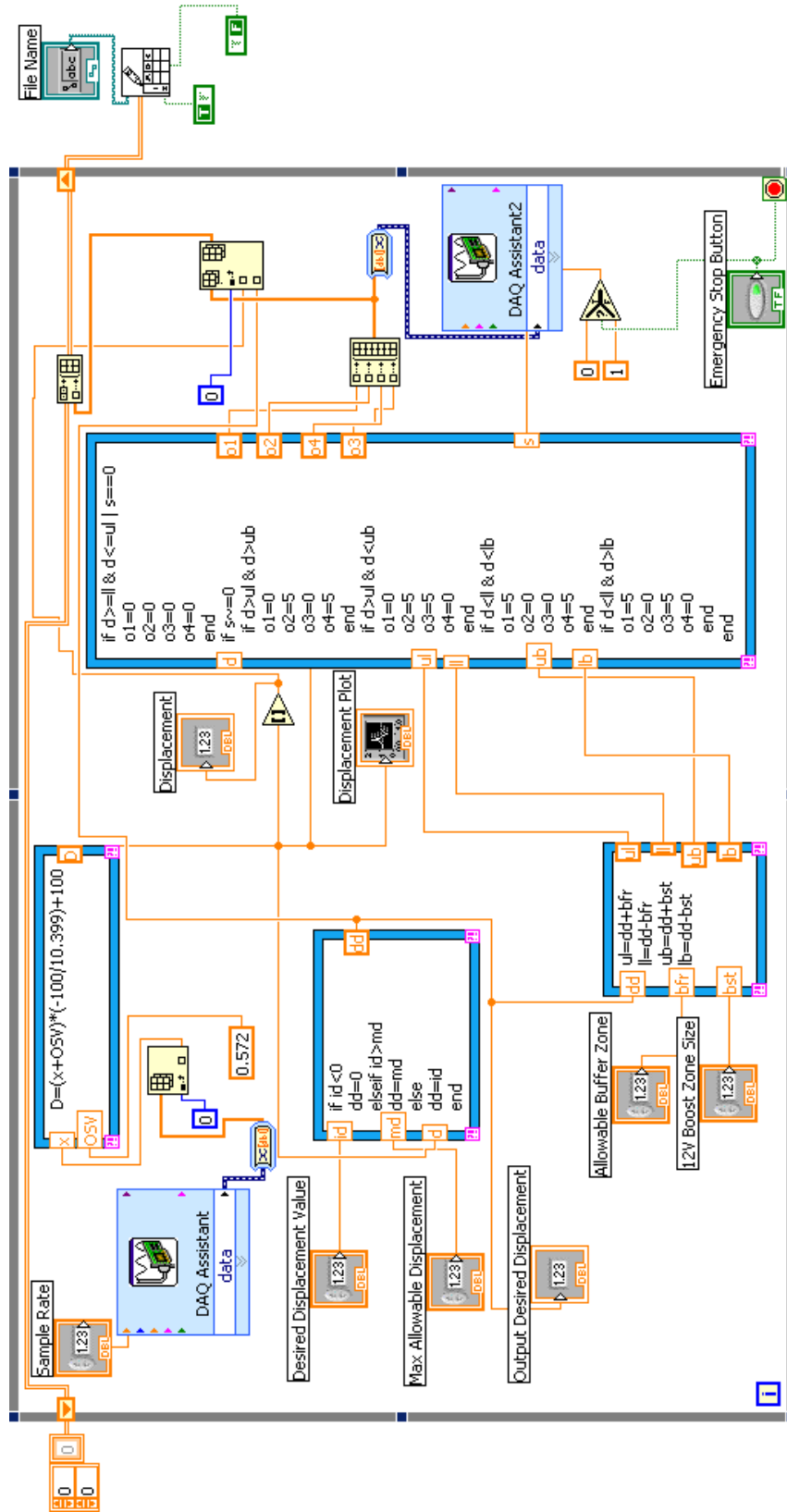


Figure 37: The use of the Math Script Node created a much cleaner, simpler and ostensibly better program, which may have been easier to understand but, in operation, proved to be even slower than previous programs.

program was massively streamlined and simplified from the earlier Stage 3 programs; the size of the new program was only 0.04 MB less than 1/30th of the size of the previous Math Script Node based programs and 1/5th the size of the smaller previous programs.

When tested results showed that, despite the greatly reduced size of the program, the overall performance of the system was relatively unaffected. Tests examining overshoot at 45mm, a distance which had shown to be problematic in previous tests, showed a consistent overshoot averaging 26.7mm. This was clearly not the desired affect of the new program. So, while the simplification of the program created a much smaller program, the program itself was clearly not performing the way it was expected to.

Inclusion of a Damper:

With the poor results from the tests using the new programs, it was clear that other steps would be required to get an effective and fully functioning prototype. Previous tests from the Stage 3 Prototype had shown the actuator carried a great deal of momentum with it at power-off, the Stage 2 Prototype had also shown that resistance in the system greatly reduced that momentum. With the results from the previous sets of tests the concept of providing some sort of resistance to the actuator was promising. Several ideas were examined, one was for a mechanical brake which would activate at power-off, however, a mechanical brake required major changes to the current prototype and added questions of reliability. Rotational dampers utilizing ferrofluid were also considered, but were generally too small to have the desired effect. Finally the decision was made to use a linear damper which could be connected, parallel to the LP and actuator.

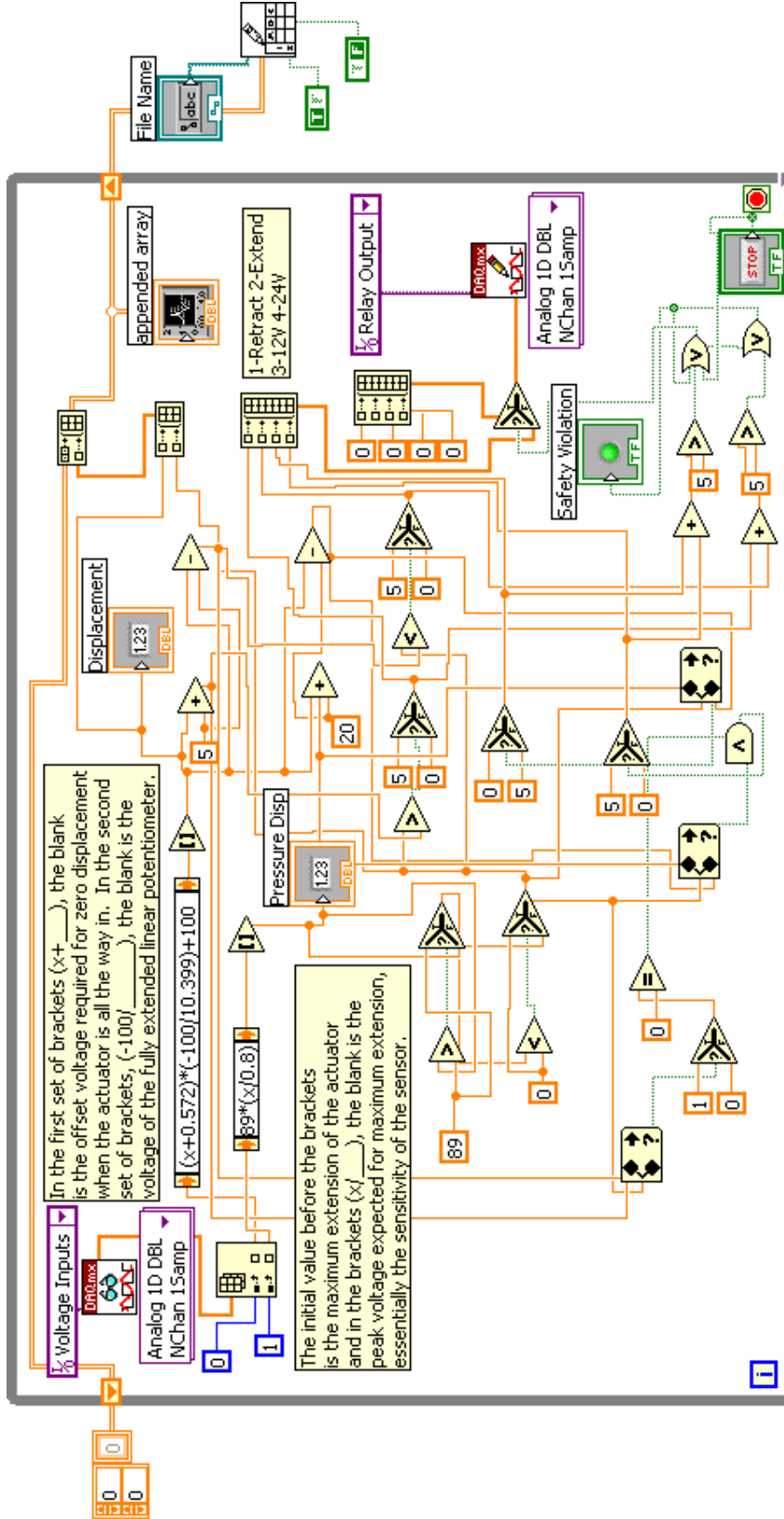


Figure 38: The logic structure of the control program was completely re-examined and re-thought, culminating in a much smaller and simpler control program than had previously been developed.

Tests quickly showed that overshoot was greatly reduced by the inclusion of the linear damper. The overshoot was tested in the same manner as the previous program testing, to a distance of 45mm, and showed an overshoot of only 8mm, a 70% reduction. One of the major factors contributing to this was the distance traveled by the actuator, after power-off, previously in the Stage 3 Prototype testing an average value of 15.39mm, by including the linear damper that was reduced to 1.27mm, a 92% reduction. This showed that the damper was doing exactly what it was intended to, however, the reduction in displacement after power-off did not make up for the full difference between the overshoot of the two sets of tests. By including the damper, the maximum velocity of the actuator was reduced as well, as a result of the added resistance the damper provided

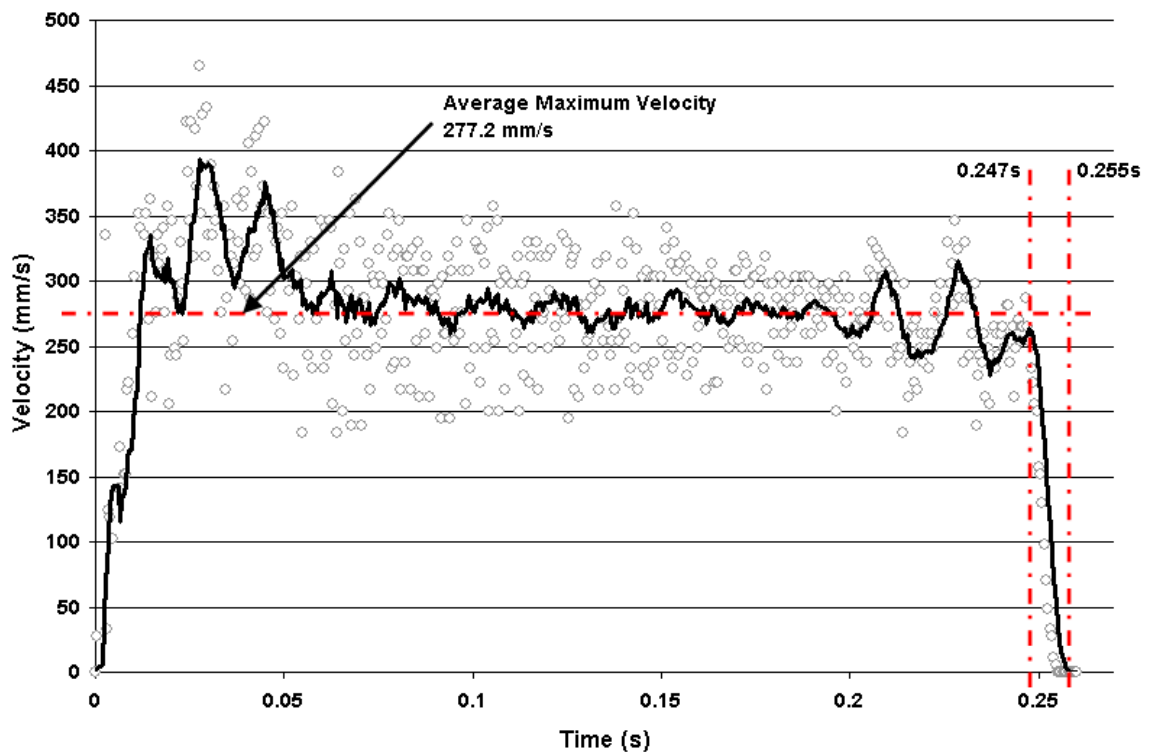


Figure 39: Tests showed a dramatic reduction in the extension of the actuator after power-off, with the inclusion of the damper. .

(Figure 39). This provided a secondary concern, the prototype had set requirements for activation time, reducing the speed of the actuator couldn't be allowed to push it activation time over 500 ms.

A test examining the time for the actuator to fully extend showed the prototype to be working well within the limits set forth in the initial design stage. As can be seen in Figure 40, the actuator remained capable of extending to a distance of 87.5mm in only

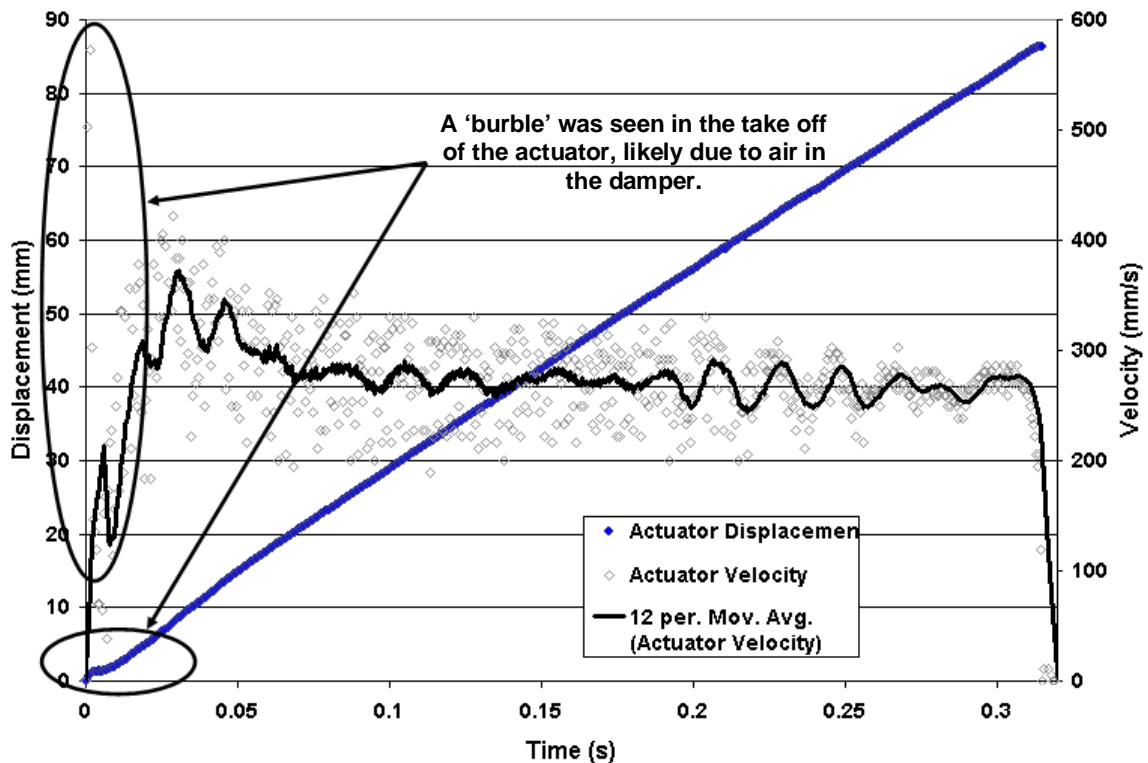


Figure 40: Tests showed a 'burble' at the onset of the test, this was likely the result of a small amount of air in the damper.

0.315s, with an average maximum velocity of 277.2 mm/s. Also seen in the test was a 'burble' at the beginning of the test. This 'burble' resulted in a large spike in the initial velocity as well as a hump in the displacement curve, before the velocity stabilized. The 'burble' was likely the effect of a small amount of air present in the damper; the

manufacturer claimed the air to be necessary in the design of the damper to prevent it from seizing. The air provides almost no damping, initially, resulting in the spike, before the damping oil provides resistance and slows the actuator. The results of these tests showed the damper to be a very effective method of reducing the stopping distance of the actuator and helping mitigate the overshoot of the system, while keeping the prototype working within the set constraints. However, for the system to function properly, further reduction in overshoot would be required.

Adding a Power Boost:

While the damper had a substantial effect on reducing overshoot, further reductions were required if the prototype was to be fully functioning prototype and could be expected to operate independently without being continuously monitored. To achieve this, a property of the actuator was utilized, the lower the voltage powering the actuator, the slower the actuator extended. The construction of the prototype allowed it to be run on either 12V or 24V and tests showed that running at 12V, while slower, provided much more consistent and dependable performance. With that in mind a series of tests were run examining the overshoot when the actuator was run at 12V. These tests showed the actuator still experienced overshoot, but, at 15.9mm it was significantly lower than the 24V tests, at 26.7mm. The results were promising, while not eliminating overshoot completely, when combined with the damper, overshoot could possibly be eliminated.

Tests were first conducted to examine the velocity and actuation time of the actuator when run at 12V with the damper. The tests quickly showed the system actuated at a much slower velocity than the 24V tests, down to an average velocity of 149.97

mm/s, from the previous velocity of 277.2mm/s, this resulted in a actuation time of 586.5ms, higher than the allowed 500ms (Figure 41). While tests showed an excessive required activation time, they also showed that the time required to stop the actuator after power-off dropped to 0.778mm, a huge improvement from both the un-damped tests and the 24V damped tests. These results were very encouraging and couldn't be completely ignored, because of the required activation time.

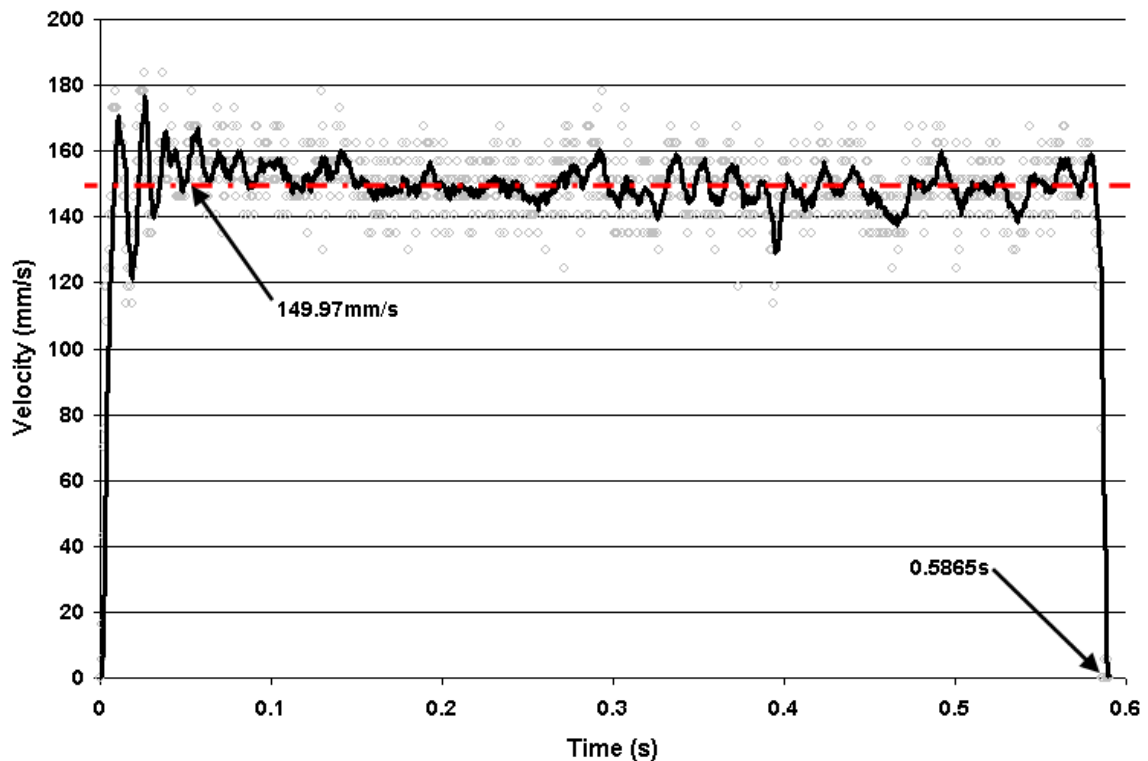


Figure 41: At 12V the actuator ran slower, allowing for more precise control of the actuator, but took longer for full activation.

To obtain the required activation time and still utilize the 12V activation accuracy, another method would be required, beyond simply running the system at 12V. The solution was a stepped voltage, taking advantage of the speed of the 24V system, when large activation distances were required, and then dropping to 12V as the actuator

approached the desired position, taking advantage of the accuracy of the 12V system.

This system would come to be known as the Boost system, boosting the voltage when needed. Tests quickly showed this to be an effective mechanism of quickly extending the actuator to the required location, yet retaining the accuracy of the 12V design, as seen in Figure 42, the actuator quickly extended to approximately 63mm, within 223ms, at which point the voltage was cut to 12V, as the actuator extended out to 85mm, during the next 151ms. This led to a full distance actuation time of 374ms, well under the 500ms limit and much quicker than the 586.5ms activation time required for full 12V activation.

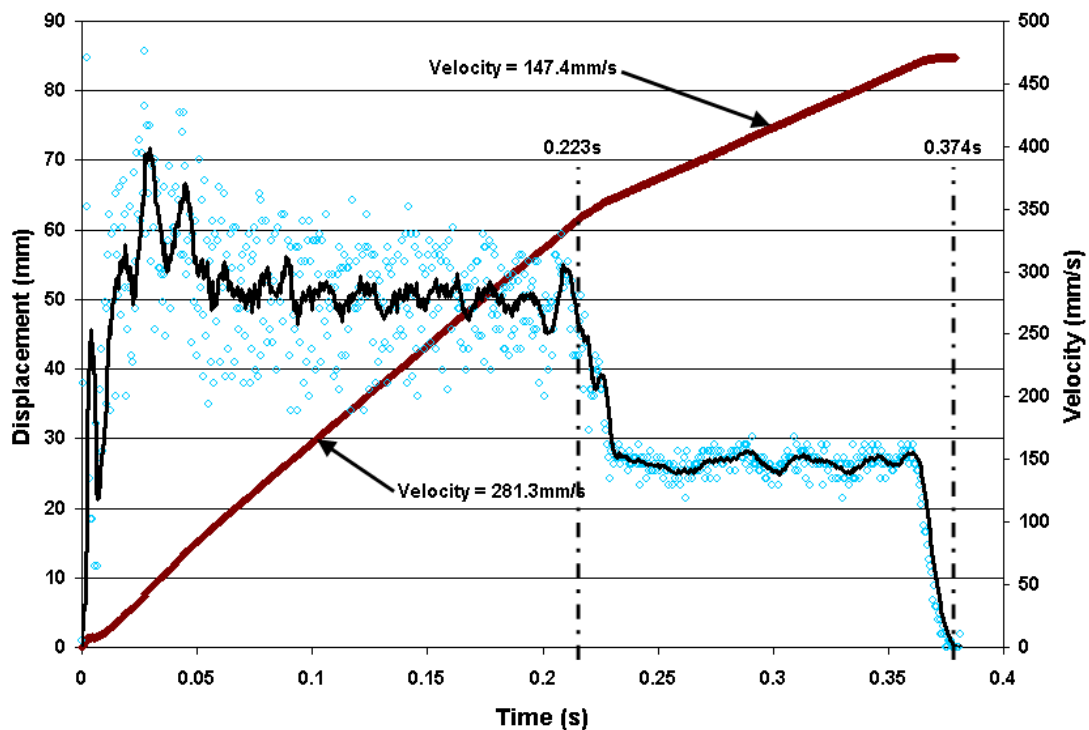


Figure 42: The Boost voltage design allowed for a stepped voltage, dropping from 24V to 12V as the actuator approached the desired location, as is demonstrated by the change in slope.

The addition of the Boost voltage significantly increased the complexity of the circuit to control it. Adding the Boost voltage required wiring three additional relays into the prototype, to switch between 12V and 24V. The addition also required extensive

rewiring, the addition of an extra semiconductor fuse block and conventional fuse block and a restructuring of the control program to control the new relays.

System Testing:

To examine the effectiveness of the new system, combining both the Boost and the damper, another series of tests were run examining overshoot. The tests were run in an identical manner to the previous tests and the results were then compared to the previous tests. Results of the tests proved the combination of the Boost voltage and damping allowed the prototype to work effectively and nearly eliminate overshoot, bringing overshoot down to an average of 3.9mm. That was significantly lower than any previous tests and allowed the prototype to operate within the normal 5mm buffer zone allowed for stopping the actuator. The full results of the four sets of tests can be seen in Table 6, the results of the tests had some degree of variation which was not seen in later tests and results were notably worse than those that would be achieved in later tests, but

Table 6: Tests were run to an actuation distance of 45 mm, with varying combinations of Boost and Damping; the closer the average test stopping distance was, to 45 mm, the better the results.

Test	NB & ND (mm)	ND (mm)	NB (mm)	Both (mm)
1	60	59	49	50
2	76	62	60	41
3	76	58	50	51
4	62	62	59	51
5	78	58	50	43
6	65	64	59	51
7	80	63	49	50
8	78	63	51	50
9	63	63	53	52
10	79	57	50	50
Test Average	71.7	60.9	53	48.9
	ND-No Damping	NB-No Boost	Both-Boost and Damping	

the results were consistent throughout the four sets of tests and backed up the effectiveness of the combination of the Boost voltage and damping mechanisms.

All the test sets utilized a 20mm boost zone and/or a 5mm buffer zone, while the results of these tests were effective, another series of tests were run examining the effect of increasing and decreasing the size of the boost and buffer zones, to allow for the most effective overshoot mitigation, while still allowing the fastest system actuation possible. Tests were run at buffer-boost ranges of 5-25mm, 5-20mm, 5-16mm, 3-20mm, 3-16mm, 3-25mm and 4-18mm, to compare the overshoot with each. Full results of the tests can be seen Table 7. These tests showed that reducing the buffer zone from 5mm to 3mm, had the most substantial effect and resulted in large increases in the overshoot distance. Also, the tests showed that increasing the size of the boost region from 16mm to 20mm

Table 7: Numerous tests were run to an activation distance of 45 mm, to examine the effect of changing the buffer zone size and the boost zone size; the closer the average final stopping distance was to 45 mm, the better the results.

Test	5-25 (mm)	5-20 (mm)	5-16 (mm)	3-20 (mm)	3-16 (mm)	3-25 (mm)	4-18 (mm)
1	46	45	48	45	45	45	46
2	46	44	47	46	46	46	47
3	43	45	47	46	46	46	46
4	43	45	46	47	46	48	46
5	43	45	46	45	47	45	46
6	43	46	46	46	47	45	48
7	45	46	47	46	47	49	46
8	45	45	42	46	46	45	46
9	45	45	42	46	46	45	47
10	46	46	42	47	46	45	46
11	45	46	47	47	46	46	46
12	46	46	46	45	45	49	48
13	46	46	47	47	46	45	46
14	46	45	46	47	46	46	46
15	43	45	47	45	47	49	47
Test Average	44.73	45.33	45.73	46.07	46.13	46.27	46.47
Test Notation: eg. (5-20) Buffer Zone Size (5)-Boost Zone Size (20)							

and finally 25mm, resulted in a smaller overshoot. An interesting result was seen when an attempt to find a middle ground set of values was tested. The optimum buffer zone was found to be 5mm while the boost region was sufficient at 20mm, tests at 3mm and 16mm, respectively showed an increase in overshoot, but was not detrimental, in an effort to keep the buffer and boost zones as small as possible, tests were run with a 4mm buffer and 18mm boost, while test results were expected to fall somewhere in the middle of the tests and provide a nice compromise between smaller zone sizes and overshoot distances, the results actually proved to be the worst of all sets of tests. As a result of these tests the zone sizes were left at 5mm for the buffer and 20mm for the boost.

While all the previous tests were run to 45mm, a distance which had been shown to provide problems for the prototype in many previous tests, it was important to ensure that the prototype worked properly and was effective in a wide variety of displacements which could be seen by the prototype. To do this a series tests were run at displacements of 30, 55, 70 and 85mm, these allowed a variety of displacements to be examined, from small to large. The results of the tests, as seen in Table 8, proved the system to work

Table 8: Tests were run to various distances throughout the activation limits of the prototype. The top value is the distance the following series of tests was run to.

Test	Test Set Activation Distance (mm)				Actuation Stopping Distance
	30	55	70	85	
1	27	56	72	82	
2	27	55	68	82	
3	27	56	68	86	
4	27	56	68	86	
5	28	56	71	86	
6	27	56	68	86	
7	27	56	72	82	
8	27	55	68	83	
9	27	56	67	83	
10	27	56	71	83	
Test Average	27.1	55.8	69.3	83.9	

effectively, regardless of the extension distance and actually showed the larger extensions to have a small degree of undershoot, rather than the overshoot that was seen at smaller extensions.

Addition of the Pressure Transducer:

A complete and functioning prototype required the inclusion of some sort of mechanism to automatically determine the wind velocity and utilize that to set the required flap extension. There are many different methods of doing this, ranging from strains on the blades to the rotational velocity of the blades; another method of doing this is to utilize air pressure. As air velocity increases, the pressure created on a surface increases, this increase in pressure can be monitored by a pressure transducer and can be interpolated to find the air velocity. Utilizing this would provide a mechanism through which the control surfaces can be activated and controlled. Before any attempt could be made to utilize pressure to control the prototype, it was necessary to have a fully functional system as any deficiency in a relatively static, human operated system, would be magnified by utilizing a rapidly changing variable such as air pressure. Once the prototype reached the appropriate level of maturity, realized with the Stage 4 Prototype, the pressure transducer was connected to the system and the control program was modified to allow the prototype to be controlled by air pressure.

Connecting the pressure transducer had been planned since the initial stages of the prototyping process and was utilized early in the Stage 1 Prototype, so the control programs had been designed to easily accommodate the pressure transducer without major modification. Once the pressure transducer operated program was run it was

immediately apparent that the prototype had achieved a degree of operational effectiveness where it could be effectively controlled by sensors, creating a complete closed loop control system, requiring no human intervention. Rapid, large and small scale pressure changes were easily handled by the prototype without error. Plots of the pressure determined displacement and actual flap displacement, shown in Figure 43, showed excellent correlation with only a small disparity, accounting for the required activation times. It can also be seen, the stepping of the actuator, following a gradually increasing pressure load and the ability to remain stable despite small variations of the pressure, due to the 5mm buffer zone.

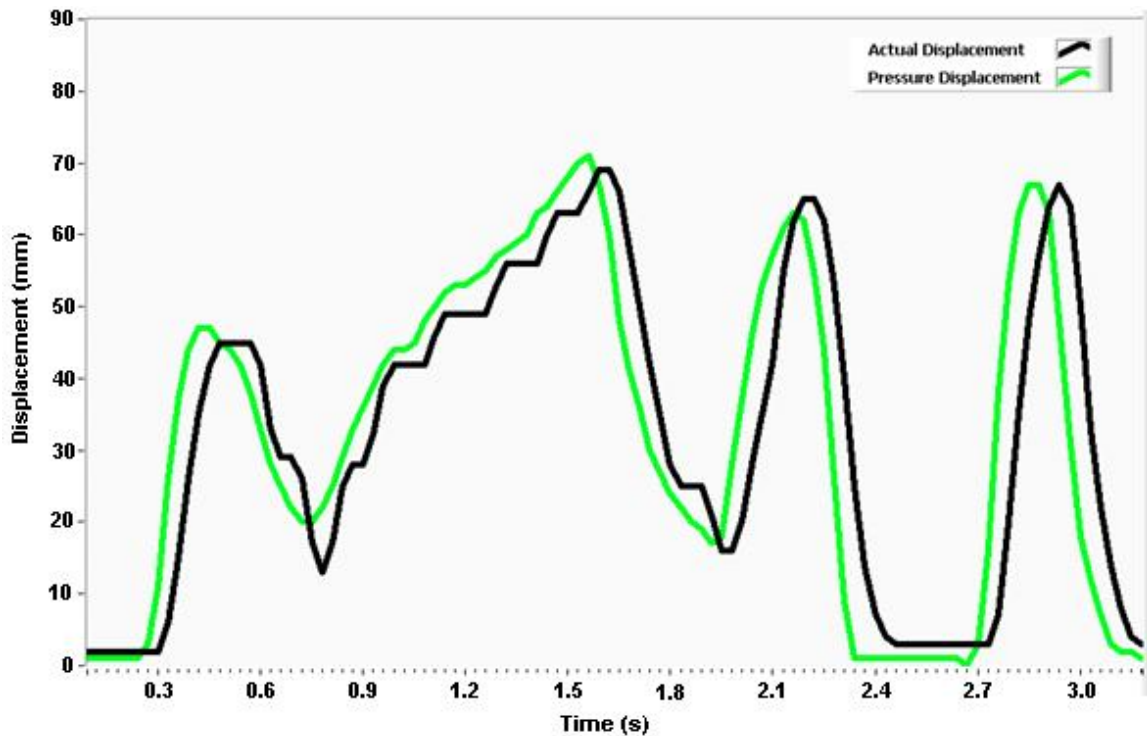


Figure 43: A plot of the pressure derived actuation distance and actuator location shows an excellent correlation between the two values.

Conclusion:

The Stage 4 Prototype successfully demonstrated the ability to create an autonomous, functioning smart structure. The prototype effectively eliminated the overshoot which had plagued the previous systems, bringing it down to a level which was acceptable and manageable. The improvements required to complete this were extensive, requiring not just upgrades to the existing programs, but a whole new approach to the function of the programs, as well, additional mechanical and electrical hardware were necessary, all which had to work together effectively to achieve the goals and meet the system requirements. The addition of the pressure sensor further improved the real world functionality of the system, enabling it to become fully autonomous. Further improvements will be required down the road, but the current system is an important tool for further research of an active control surface and its application to wind energy.

Active Control Surfaces and Prototype Conclusions and Future Work

The series of prototypes produced demonstrated the capability to utilize the Gurney flap as a load shedding mechanism from a proof of concept standpoint. The piano-hinge design provided a simple and reliable method of forming a Gurney flap; however, the design also provided some challenges, from the functional standpoint. As discussed, the affect of the flap height, mounting distance from the trailing edge and the flap mounting angle all affect the lift generation, and all come into play with the piano-hinge style flap. While a fully deployed flap will provide a tall, nearly vertical flap at a location, very near the trailing edge, a condition which is well understood, the effect of partial deployment is not currently understood. As the flap is initially activated, the mounting angle is very low, the effective location of the flap is very far forward and the effective height of the flap is very low, combined these can reliably be assumed to result in a very small lift effect from the flap, at initial deployment. High degrees of extension would be required before the flap had any significant impact on the lift created by the airfoil. Further understanding of the transient response will require the type of detailed wind tunnel testing that the prototype was designed for.

It is also necessary to examine the transitional effect of the partial flap deployment. As the wind loads on the blade change, the flap will deploy to the required extension, however, as could be seen in Figure 43, there is a lag time from when a required displacement, converted from the pressure reading, is established and when the flap reaches that point. While that lag time is minimal, no more than 374ms, the effect on the blade during that time must be understood. It will also be necessary to determine the

effect that a length of flap can have to allow for both a balance between the load shedding capability of a flap and the capacity of an actuator to safely and reliably handle the loads seen by the flap. Once that is determined it will be possible to determine the number, spacing and location of the flaps along the length of the blades. To do this will require extensive use of computational fluid dynamics and wind tunnel testing.

Additional work will be required to determine the best mechanism for controlling the system; the current prototypes utilize a pressure transducer. While pressure is a capable means of monitoring wind speed, it may not necessarily be the best option. Pressure does provide several benefits that other systems may not be capable of, or would require more extensive programming to accomplish. Pressure can be easily monitored at many locations throughout the length of the blade, allowing for point by point wind speed monitoring, allowing for not only each blade to be controlled individually, but individual flaps or sections of flaps, to be controlled by the wind at that exact location. Also, pressure is independent of the activation of the flaps, meaning that when a flap is deployed, it will not affect the pressure created by the wind velocity, whereas systems like strain or rotational velocity would be affected by the load shed by the flaps, possibly causing confusion in the necessary flap activation. While this can be compensated for through programming, it will require further investigation and testing.

The prototype itself can be advanced further as well, the current system, will functional, can be improved. The current data acquisition rate of the program, around 33 samples/second, can withstand significant improvement. Increasing the data acquisition rate to between 500 to 1000 samples/second would allow for much smoother system

operation and may allow for reducing the damping or even elimination of the damper, by predicting the momentum carried by the actuator, more accurately. This could also allow for full 24V operation. These two factors would increase the speed of activation, allowing the activation time to be reduced to near the Stage 3 Prototype numbers.

While a great deal of work is needed in developing a fully functional smart active control surface, it is also necessary to examine the integration of the Gurney flaps into the blades as well as the effects that the flaps would have on the blades and turbine as a whole. The addition of an active control surface into a wind turbine will require a great deal of modification to current blade systems. Space for the equipment would be needed, in the small confines of the trailing edge of the blades, yet the individual systems would need to be easily accessed for maintenance, repair or replacement, if necessary. Power would need to be provided down the length of the blade, made all the more complicated by the several degrees of rotation which must be accommodated. Also, the additional weight of the system must be taken into account in the design of the blade. The dynamic response of the blade, during activation of the flaps, must also be taken into account. The blade must be tested to examine for possible oscillations, fatigue and control surface reversal. Each of these effects can be detrimental to the life of the blade, having the exact opposite of the intended effect.

While a great deal of work remains, over a broad range of areas, likely well beyond what is mentioned above, the Gurney flap concept is valid and the prototype is an important step in the advancement of the idea of applying a smart active control surface to a wind turbine.

SENSORS

Introduction

Sensors are a pivotal component in a smart structure or active control surface, without them, there would be no feedback to the control program and no way of monitoring the structure. Current wind turbines utilize many sensors at the base of the



Figure 44: The base of the tower and the nacelle have many sensors, the blades, however, still have no sensors.

tower and throughout the nacelle, as seen in Figure 44; however, the blades themselves have none. The lack of sensors in the blades creates a massive hole in the working knowledge of each wind turbine, which can prove to be dangerous, with the size of modern blades. This also hampers the implementation of the active control surfaces. As a result, there are three main goals to the implementation of sensors: create a real-time source of data for use with active control surfaces, structural health monitoring and damage detection. Achieving these goals will require the addition of many sensors of several types, but will advance the

safe, long-term operation of the wind turbines and reduce the required maintenance costs, helping make wind energy a more viable alternative.

While an array of sensors will be needed to fully monitor a wind turbine blade, the primary sensor which will be examined is the strain gauge. The other sensor types are important, but their selection can be heavily influenced by the choice of strain gauge. As it will ultimately be shown, the choice of the fiber optic strain gauge as the best for wind energy will also allow for the incorporation of several other types of sensors necessary for a wind turbine blade, including temperature, pressure and acceleration. With that the focus of this paper will be on the strain gauge choice and its adaptation into wind energy.

Senor Options and Selection

When selecting a strain gauge to be used with a wind turbine blade, there are numerous and unique considerations which must be taken into account. The environment of the wind turbine blade is diverse and extreme, not to mention the difficulty associated with accessibility or the massive dimensions of the blades. With these factors, a lengthy and diverse list of requirements was assembled:

- Ø Sensors must be reliable, with an expected lifetime at least comparable to the blades themselves.
- Ø Sensors must have a safe, strain range comparable to that of fiber glass.
- Ø Sensors must be capable of being embedded in a fiber glass laminate with minimal effects of the surrounding laminate.
- Ø Sensors should take a minimal amount of effort for installation.
- Ø Sensors should require minimal maintenance.
- Ø Sensors must be capable of transmitting information over distances comparable to the size of the blades which are currently in production or will soon be in production.
- Ø Sensors must have a minimal effect from outside electrical disturbances.
- Ø Sensors and related equipment should be as cost effective as possible.
- Ø Sensors should be readily available for manufacturing and testing.

It is implausible to expect any one type of sensor to meet all these criteria, so choosing the best sensor will require examining which sensor best fits the criteria overall.

With the long list of requirements for the strain gauges, there is a long list of types of strain gauges which must be examined when choosing the best option for this case. There are commonly known strain gauges as well as many which are lesser known, but no less important:

- Ø Metal Foil
- Ø Piezoelectric (PZT)
- Ø Active Fiber Composite (AFC) and Macro Fiber Composite (MFC)
- Ø Fiber Optic
- Ø Optical

Each of these sensors has certain properties which make them ideal in various situations, but for wind turbine blades, the diverse requirements for the sensors make many of these sensors inappropriate.

The Different Sensors:

Strain is a fundamental metric which is essential in the determination of many other metrics, some of which can and some which cannot be measured by other mechanisms. A few of these include stress, temperature and pressure. The simple mechanics of strain, the ratio of a change in length to an original length, make it relatively simple to measure, as compared to many other metrics, and allow for many different methods of measurement to complement the broad set of applications. While there are numerous methods of strain measurement, ranging from mechanical measurements to changes in wavelength of reflected light, a practical selection of these methods will be discussed for their application to wind energy.

Metal Foil Strain Gauges: Metal foil strain gauges are the oldest and most common type of strain gauge. The basis behind the function of the metal foil strain gauge dates back to 1856 when Lord Kelvin reported a change in resistance in a metallic conductor, subjected to a mechanical strain. However, the concept didn't come into practical use until the 1930s [29]. The concept behind the gauges is simple, a thin, typically around 0.025mm thick, metallic element (Figure 45) is bonded to the surface of an object, when that object experiences a strain, the resulting change in the length of the element causes the electrical resistance of the element to change as well. The change in resistance is linear and can be monitored, the linear relationship allows for a simple calculation to determine strain.

There are many advantages to the use of the metal foil strain gauge, one of the primary advantages is the low cost; the long history of their use and their simple design allows the gauges to be produced easily and makes them very inexpensive.

This has also led numerous companies to produce the gauges, helping lower prices.

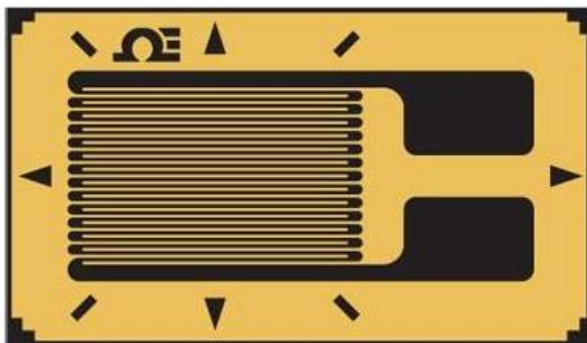


Figure 45: The metal foil strain gauge is a simple gauge and is one of the oldest and best understood mechanisms for measuring strain.

Individual gauges are readily available from numerous manufacturers, for under \$5 per gauge. The long history and simple operation has produced a great deal of understanding and information regarding the sensors, they are well understood and can be well

predicted, eliminating many of the questions involved with some other types of sensors and easing the transition from research to implementation. Another advantage of the sensors is their size. Metal foil strain gauges can be easily and inexpensively found with a surface area of less than 2mm^2 and a thickness of 0.025mm or less. With the numerous benefits provided by the metal foil strain gauges, there are also important drawbacks which must be taken into consideration.

One of the primary drawbacks of the metal foil strain gauge is signal drift. When installed over long periods of time, as required by wind energy, the resistance of the gauge will drift, requiring periodic recalibration and significantly adding to the maintenance requirements of the system. Also, the signal is electrical and must be transmitted over the long distance of the wind turbine blade. This has several drawbacks, first is the effect of outside electrical interference, the wind turbine itself is a massive power generator which can be located hundreds of feet in the open environment, dealing with electrical energy in the air. These two influences can combine to create significant noise in the signal returned from the sensors. Also, being an electrical signal, transmitted over a length of nearly 200ft with current 5.0MW wind turbine blades, signal amplification would likely be required to ensure a strong enough signal is transmitted to the data acquisition system.

Several other major concerns for any sensor system are ease of installation, survivability and blade affects. Installation of each metal foil strain gauge requires either two or three separate wires. When numerous strain measurements are desired, this leads to a relative mess of wires and numerous points where a failure could occur.

Additionally, there are two methods of mounting the sensors, both of which can cause reliability issues. The first and most common method is to utilize an epoxy or glue to bond the sensor to the desired surface. This is a relatively simple method which can be done to provide for a maximum life, but, over the long life of the wind turbine blade, can

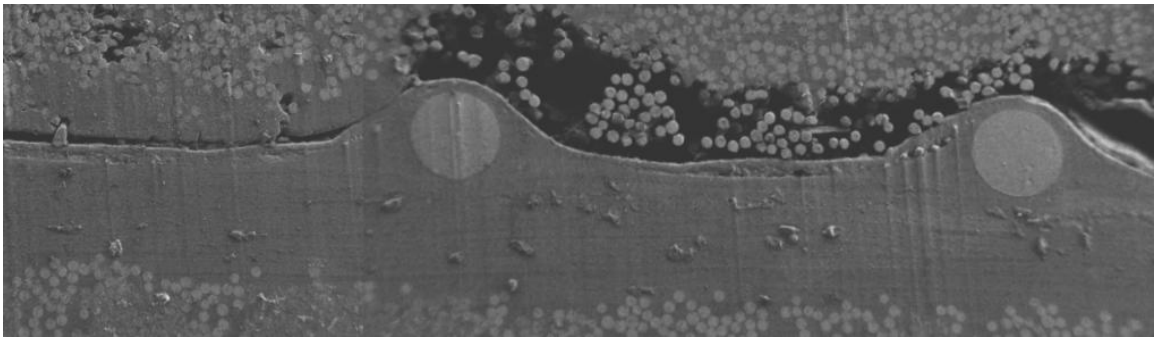


Figure 46: As seen in this SEM image, embedded metal foil strain gauges can cause localized resin rich zone and debonding.

result in premature debonding and repair, of the sensor. The other method, with the composite structure of the blade, is to embed the sensor into the laminate. While this will encase the sensor in epoxy, it does not eliminate the possibility of the sensor debonding from the surrounding matrix material, also it can result in a local matrix rich zone around the sensor (Figure 46), creating a stress concentration and increase the possibility of local delamination occurring, possibly leading to wide spread damage, initiating at the sensor.

While there are many benefits to the metal foil strain gauge, when examining the appropriate strain gauge for use with wind energy, the drawbacks are significant. The gauges must be simple to install and maintain, as well as be reliable to provide for the long life expected of a wind turbine. These are requirements which are not met by the metal foil stain gauge, which erase the initial cost benefits and render them inappropriate for this application.

Piezoelectric Strain Gauges: Piezoelectric electric materials are those, which when exposed to a stress, create a voltage, as seen in Figure 47. The voltage is generated by opposite charges created on the surface of the material; those charges generate a voltage when two electrodes are connected to the surface, opposite from one another [30]. The effect was first discovered in 1880s by the brothers Jacques and Pierre Curie while performing experiments on quartz [31]. However, the effect was not utilized for industrial sensing purposes until the 1950s [32].

There are two common types of piezoelectric sensors, the first and most common type “Lead Zirconate Titanates (PZTs) are solid solutions of lead zirconate and lead titanate, often doped with other elements to obtain specific properties[33].” The other is a Polyvinylidene Fluoride (PVDF) polymer, made of long repeating monomer chains [33]. Both types of these sensors are now made by numerous manufacturers and are readily available and understood. The sensors are extremely sensitive, much more so than most other types of sensors and are capable of sensing much lower strains. Also the sensors have a high elastic modulus, similar to that of many metals and the sensors are not affected by electrical fields, making them capable of handling harsh environmental conditions.

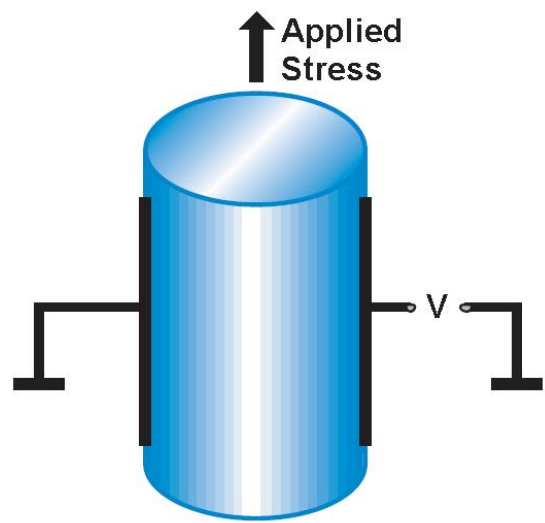


Figure 47: A stress applied to a piezoelectric material causes positive and negative charges to be created on the surface of the material.

There are several drawbacks to piezoelectric sensors, as well. While they have a very high sensitivity, they commonly also have a very limited strain range, which may not correspond well with being embedded in a fiberglass laminate. Piezoelectric strain gauges also perform very poorly in static or near static situations, when a strain is applied a voltage peak is formed, however as that strain remains, the voltage begins to decay. While dynamic situations causes peaks to be formed rapidly and prevent an opportunity for decay to occur, static situations do not allow for this, meaning during periods of relatively constant wind, the strain sensed would drop to zero, causing the deactivation of the control systems and creating control program confusion, which could potentially cause blade damage. Those factors combined with the larger size of the sensors and the multiple wires needed for each gauge make piezoelectric strain gauges inappropriate for wind energy.

Fiber Optic Strain Gauges: A unique type of strain gauge developed beginning in the 1970s is the fiber optic strain gauge. The gauges use reflected light to calculate strain. This is accomplished through the use of FBGs, which are small patterns printed into an optical fiber. The gratings reflect a specific wavelength of light. The reflected wavelength shifts slightly with an applied strain and that shift can be detected and converted to a strain value by an interrogator.

The use of light as a strain sensor creates many advantages for fiber optic strain gauges. One major advantage is the ability to multiplex; meaning hundreds of sensors can be located along one optical fiber and be simultaneously monitored. This greatly reduces the clutter of wiring individual strain gauges with the other systems discussed. In

conjunction with that, more than 60 different parameters can currently be measured by different types of FOSs [34], including many that utilize FBGs, such as temperature, pressure and vibration [35]. Combined with the ability to multiplex, this allows one system to completely monitor nearly all sensing requirements and require only one optical fiber to do so. This ability would simplify installation and decrease costs as well as the costs to install and integrate multiple data acquisition systems.

Optical fibers and sensors can also be embedded in composite laminates, as seen in Figure 48. This allows for cleaner manufacturing and provides a level of safety to the optical fibers as well as more robust damage detection. It also allows the sensors to be utilized during the manufacturing process for cure monitoring, ensuring the laminate has properly cured. This can also detect defects in the laminate that may occur during the curing process. For existing blades and repairs, the sensors can be attached to the surface of the blades, allowing for widespread use.

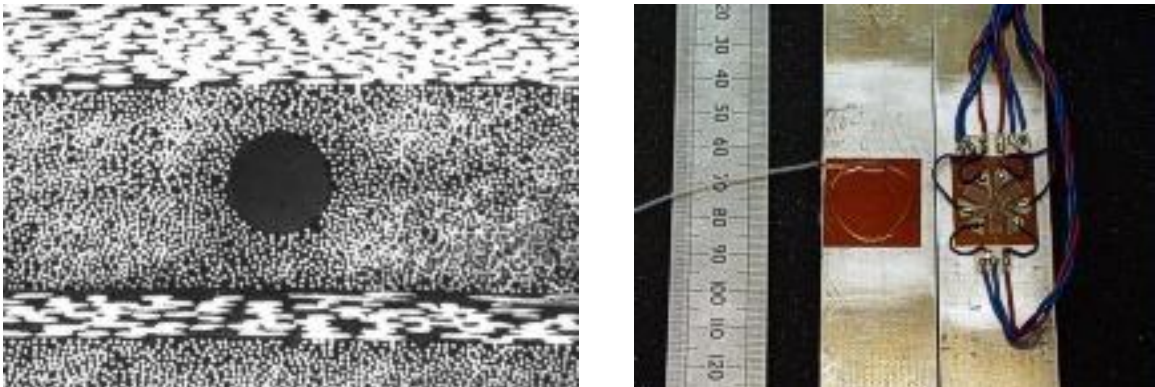


Figure 48: In the first image an embedded optical fiber is shown, as can be seen, the fibers are small enough to be embedded directly in a laminate. The second image shows two strain gauge rosettes, the one on the right utilizes fiber optics while the rosette on the left utilizes metal foil strain gauges this demonstrates an advantage of multiplexing [38].

Additionally, there is no electricity needed for the sensors making them safe from outside electrical noise or interference, so they can't be influenced by the turbine power generation or lightning strikes [36]. This adds both stability and reliability to the operation of the system. It also makes it a passive system; it cannot cause a spark or start a fire, a serious hazard for a wind turbine.

Reliability is another benefit of fiber optic strain gauges. During the course of a lifetime, wind turbine blades can experience between 10^8 and 10^9 fatigue cycles over the course of 20 to 30 years [37] and an embedded sensor must be expected to survive that lifetime. Tests are currently on going examining the life of FOSs embedded in fiber glass composites, with results showing the sensors to be capable of handling the typical, 25 year, expected life of the blades [38]. Also, the passive nature of fiber optics results in a stable sensor that has no tangible signal drift during the lifetime of the sensor. This results in a system that doesn't need to be recalibrated over time, greatly increasing the reliability of the collected data and reducing maintenance requirements [38]. As well, the multiplexing ability allows for a single optical fiber that is relied upon, rather than having possibly, hundreds of individual soldered wires that could fail.

While fiber optic strain gauges have numerous benefits, they also have several serious drawbacks. The most serious of these drawbacks is cost, the price of the gauges currently ranges from \$100 to \$900 and the price of the interrogation units commonly start around \$7,000 and can cost as much as \$50,000 for more capable systems. Some less expensive systems may exist, but prices from major manufacturers of fiber optic sensing systems are in this range. These costs are, in some cases, hundreds of times the

cost of competitive systems. However, costs are coming down as the technology evolves and becomes more main stream.

Another consideration of FOSs is their susceptibility to damage and degradation during embedment and processing. Embedded optical fibers and FBGs can often suffer corporeal degradation and in some cases even complete failure [40]. During the embedding and curing processes, sensors or the optical fiber can fail. Surviving sensors can experience a degradation of both signal transmission and return. As will be discussed later, this can be minimized by appropriate treatment of the optical fiber and the sensors, but it is a factor which must be considered.

Also, the short history of the FOS must be considered. Fiber optics were first proposed in the 1960s [40] and the first FBGs weren't created until 1978 [41], over 90 years after the piezoelectric effect was first discovered and more than 120 years after the concept behind metal foil strain gauges was first found. The history of the other gauges has created a mature technology with an extensive knowledge base, something that can't be said for FOSs.

Other Strain Gauges: There are several other classes of strain gauges which deserve mention. The first of these are active fiber and macro fiber composites. Active fiber composites (AFCs) and macro fiber composites (MFCs) are both based off of similar concepts and hold many similarities to piezoelectric strain gauges. They utilize uniaxially oriented PZT fibers sandwiched between a set of interdigitated electrodes and embedded in a polymer matrix (Figure 49). The electrodes allow the polarization of the fibers in the longitudinal direction, achieving much greater piezoelectric properties than

other monolithic piezoelectric materials [40]. By utilizing PZT fibers, an applied voltage to the electrodes will cause a strain in the fibers and likewise an applied strain will result in a voltage output. The difference between AFCs and MFCs is that AFCs utilize round

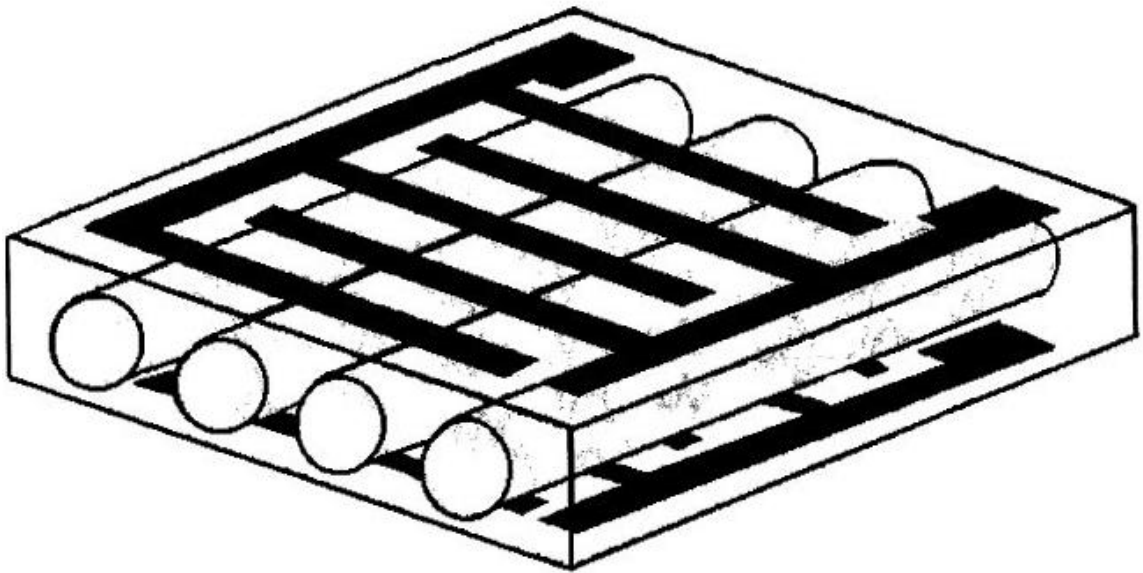


Figure 49: Active Fiber Composites (AFCs) and Macro Fiber Composites (MFCs) are made by embedding PZT fibers in a polymer matrix, layered between a set of interdigitated electrodes.

PZT fibers, whereas MFCs are made using rectangular fibers as seen in Figure 50 [41].

On top of the greater piezoelectric properties, AFCs and MFCs are also much tougher and more flexible than standard, monolithic, PZTs. While they are a relatively new technology, without a great deal of testing in industry applications, AFCs and MFCs hold a great deal of potential, including smart structures.

Another type of strain sensor is the optical sensor. Rather than being a sensor in the typical expectation, the optical sensor is more of a visual monitoring system, where an object is monitored by a camera, which outputs the images to a computer which

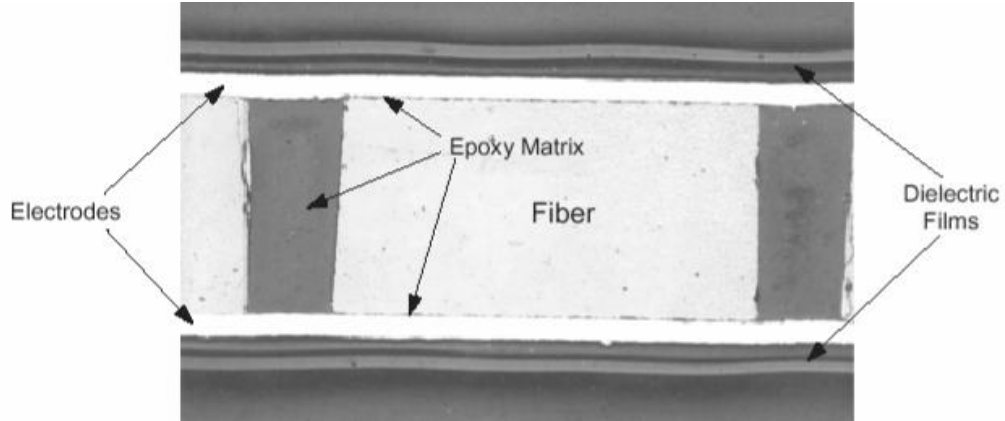


Figure 50: In this SEM image, it can be seen that MFCs utilize a rectangular PZT fiber, which is much easier to manufacture and greatly reduces the costs of MFCs, compared to AFCs.

examines the images at the subpixel level and determines strains by changes in the pixel patterns. This is a very new technology which has just begun to develop. While it holds potential in many systems which cannot, or are very difficult to sense through traditional methods, it is currently a largely laboratory based system which is very sensitive to outside effects.

Sensor Selection: Despite the issues which exist, the benefits of FOSs, combined with the ongoing and existing research, outweigh the disadvantages, making fiber optics the best sensing method for wind energy. While it is a relatively new technology, it is improving at a rapid pace. Many of the issues that currently exist are being researched and mitigated. Advances in manufacturing and system design are bringing costs down to more reasonable levels and should continue to do so. Ultimately, to revolutionize an ancient technology, like wind energy, advanced and modern technologies will be required.

The Fiber Optic Sensor and Fiber Bragg Gratings

The Fiber Bragg Grating:

Many different types of FOS exist, relying on different principles, such as intensity modulation, interferometry and refractive index changes. However the FBG is a comparatively advanced technology [44], which was first demonstrated in 1978 by Hill et al. at the Canadian Communications Research Centre [41] and commercially released in 1995 [45].

“A fiber Bragg grating is a periodic perturbation of the refractive index along the fiber length which is formed by exposure of the core to an intense optical interference pattern [41].” Light traveling down the optical fiber, when it strikes the grating, is

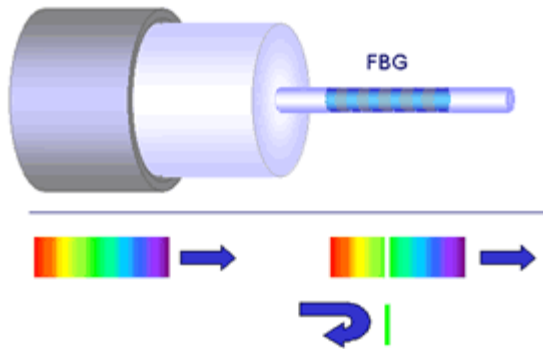


Figure 51: When light travelling down an optical fiber reaches a FBG, only a select wavelength of light is reflected back down the optical fiber.

partially reflected, as demonstrated in Figure 51. Each grating reflects only a specific wavelength, essentially acting as a selective mirror, while the rest of the light is allowed to continue down the fiber, uninterrupted. Varying the grating pattern changes the reflected wavelength. When the gratings are

exposed to a strain, be it thermal or mechanical, small shifts in the reflected wavelength result. These shifts demonstrate a change in the spatial period of the grating pattern, which can be determined and utilized for the calculation of the strain which the sensor is being exposed to.

Creating and Manufacturing the Fiber Bragg Grating:

The formation of a permanent grating in an optical fiber was first demonstrated by Hill et al. in 1978. To accomplish this, Hill and his team launched intense Argon-ion laser radiation into a germania-doped fiber. By observing the gradually increasing intensity of the returned light they were able to determine the formation of a very narrow band Bragg grating. This demonstrated a previously unknown photosensitivity of the germania-doped optical fiber [41]. These initial gratings were accomplished exposing the core of the fiber to an interference pattern created by oppositely propagating modes of 488nm or 514.5nm continuous long wave, blue-green light from an Argon-ion laser [46]. The intense laser light that the core of the fiber is subjected to carries enough energy to break the highly stable silicon-oxygen bonds of the glass [44]. This causes damage to the structure of the fiber by creating local defects in the molecular structure of the glass [47], which slightly increases its refractive index [44].

Later work by Meltz et al. determined that the gratings can “also be formed by illuminating the core from the side of the fiber with,” a two-beam interference pattern of, “coherent UV radiation that lies in the 244nm germania oxygen-vacancy defect band. This intense absorption band, which is ~35nm wide, coincides with the second harmonic of both blue-green argon-ion laser lines used in previous research [46].” This single photon ultraviolet light proved to be far more effective, leading to grating formation that was found to be orders-of-magnitude more efficient. This also allowed for changing the interference pattern and thus the grating period, by changing the incident wavelength and the angle of the beams [41].

This method, known as the transverse holographic method, seen in Figure 52, was developed in 1989 and for several years, was the best method of forming the gratings; possessing several benefits. One of the primary benefits was that the gratings could be photo-imprinted in the core without requiring the removal of the cladding of the fiber. This was possible because the cladding around the fiber is transparent to the UV light used, whereas the fiber core easily absorbs the UV light. Also the grating period could be changed much more easily than the technique used previously by Hill, making it the primary method of forming FBGs, for several years [41].

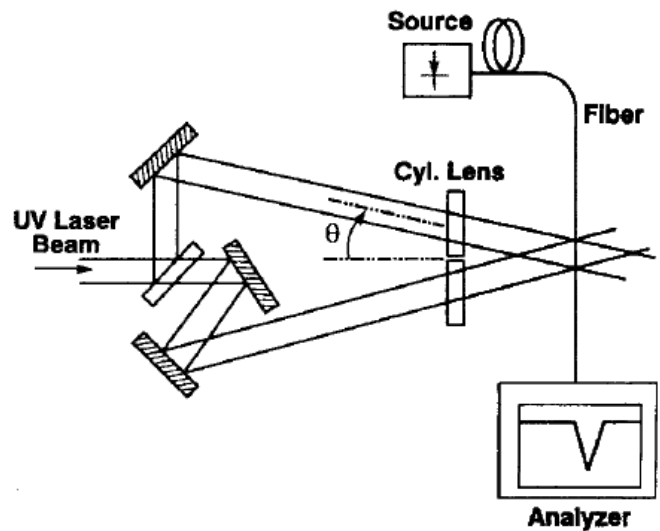


Figure 52: The holographic method utilizes two intersecting coherent beams of ultraviolet light to create an interference pattern.

In 1993 Hill et al. released their work on utilizing a phase mask to manufacture FBGs and the method quickly superseded all previous methods. A phase mask consists of a flat slab of fused silica which is transparent to UV light [41]. The surface of the phase mask is a photolithographic etched, periodic surface-relief pattern, with a square wave profile [48]. The periodic spacing of the corrugations is chosen to create a specific interference pattern where the period of the resulting index grating, photo-imprinted into the core of the fiber, is one half of the periodic spacing of the phase mask [41]. The

phase mask is brought into contact or near contact with the bare optical fiber, with the corrugations normal to the direction of the fiber, and UV light, incident normal to the phase mask, passes through and is diffracted by the corrugations, as can be seen in Figure 53, where the zero order light is suppressed to around 5% of the total light and the +1/-1

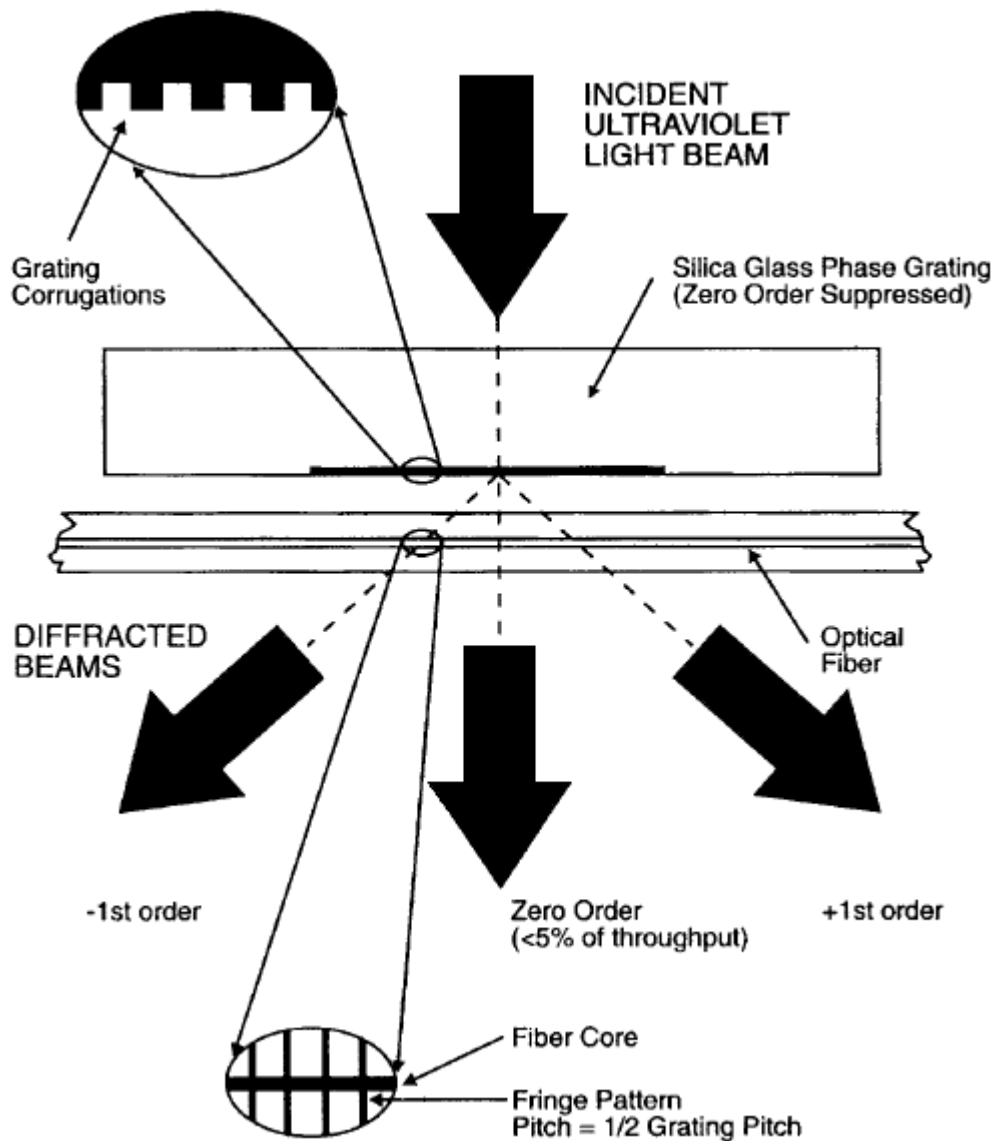


Figure 53: With a phase mask UV light passes unimpeded through a diffraction grating which suppresses the 0 order while the +/- 1 orders each contain approximately 40% of the diffracted light, creating the interference pattern.

orders each contain around 40% of the diffracted light [41]. The amplitude of the corrugations is specifically designed to suppress the zero order UV light. It was later shown that it is possible to use different wavelengths of light as well as different shapes of phase masks, besides a square wave, to produce the gratings [48].

The use of the phase mask has numerous benefits over previous methods, mainly in the vast simplification of manufacturing. The phase mask method allows for easier fiber alignment as well as reduced stability requirements for the manufacturing equipment and lower coherence requirements for the UV laser beams. As well, the phase mask allows for numerous fibers to be photo-imprinted simultaneously by situating the fibers parallel to one another, beneath the mask. The method does require that each grating period has an individual phase mask, yet the other capabilities compensate and allow for reduced manufacturing costs while yielding high performance FBGs [41].

Applying FBGs to Sensors:

As mentioned previously, the principle behind the operation of FBG based FOSs, is small, monitored shifts in the reflected wavelength. Each grating partially reflects the full spectrum of light traveling down the fiber, however all but a small range of the reflected wavelengths, interfere destructively, so as to prevent them from returning back up the fiber. This allows only a small range of constructively interfering wavelengths to return up the fiber, centered about a maximum reflected wavelength; while the rest of the spectrum is allowed to continue down the fiber uninterrupted. The maximum reflectivity of a FBG occurs at the Bragg wavelength, λ_B , given by Equation 4 [44]. Any strain that

$$\lambda_B = 2 \cdot n_{eff} \cdot \Lambda \quad 4$$

Where λ_B is the resulting Bragg wavelength, n_{eff} is the effective refractive index of the mode propagating in the fiber and Λ is the period of the imprinted Bragg grating.

is applied to the FBG will cause a small shift in the Bragg wavelength, which can be monitored. Through the stress-optic affect any applied strain will alter both the refractive index of the fiber and the FBG period, which, as can be seen from Equation 4, will change the reflected Bragg wavelength. Not only does a mechanical strain affect the fiber, though; any change in temperature will change the grating period through a thermal strain and the refractive index will be affected by the thermo-optic effect. With these two factors, the resulting total strain can be determined through monitoring the change in the maximum reflected wavelength, $\Delta\lambda_B$, by Equation 5 [44]. Commonly FBG sensors have a sensitivity to strain of $\sim 1.2 \text{ pm}/\mu\epsilon$ and of temperature in the range of ~ 10 to $\sim 30 \text{ pm}/^\circ\text{C}$ [49].

$$\Delta\lambda_B = \lambda_B(1 - \rho_\alpha) \cdot \Delta\epsilon + \lambda_B \cdot (\alpha + \xi) \cdot \Delta T \quad 5$$

Where $\Delta\lambda_B$ is the maximum reflected wavelength; ρ_α , α and ξ are the photo-elastic, thermal expansion and thermo-optic coefficients of the optical fiber; $\Delta\epsilon$ is the change in mechanical strain applied to the fiber and ΔT is the change in temperature, to which the fiber is exposed.

Because of the sensitivity to temperature, it is often necessary for the system to utilize some means of temperature compensation. To do this, many sensors utilize two FBGs, one which is bonded to the surface to monitor strain and another which is free to monitor temperature, by monitoring both sensors simultaneously, the system is able to compensate for any changes in temperature. Utilizing Equation 5 then allows for the determination of any mechanical strain applied to the FBG strain sensor.

Interrogation Methods:

While a FBG sensor is a valuable tool, an interrogation system must be utilized to garner the data which the sensors are providing. The interrogation unit monitors the returned light from the sensors and monitors the Bragg wavelength for changes, which can be converted into strains. To do this there are two different types of systems, time-division multiplexing and wavelength-division multiplexing. These units operate on very different principals and each has their own benefits and drawbacks.

Time-Division Multiplexing: A time-division multiplexing (TDM) system utilizes a simple, pulsed, broad band light source in conjunction with low reflectivity gratings, sometimes less than 5% [40], each of which is written with the same grating period [50]. The light reflected by each sensor will progressively take longer to return to the interrogator as the sensors extend further down the optical fiber, away from the interrogator. By monitoring the time required to acquire the returned signal, the

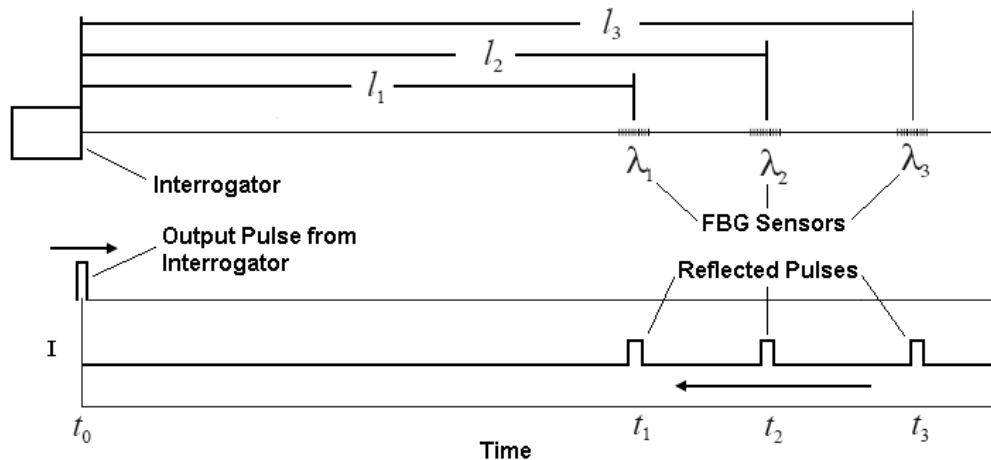


Figure 54: With a TDM interrogator, signals are differentiated by signal return time, the further away from the interrogator a FBG is located, the more time is required for the signal from the sensor to return.

interrogator is capable of determining which sensor is being monitored, as demonstrated in Figure 54. The returned signals are passed through a system of passive sloped filters, which determine the wavelength of the light returned from each sensor [44].

There are many advantages to the use of the TDM interrogator. TDM systems utilize a broadband light source which is significantly less expensive and less complicated than the tuned laser utilized by some wavelength-division multiplexing systems [44]. Also, by utilizing one single FBG period, manufacturing is simplified and costs are further reduced [50]. TDM interrogators are solid state systems, meaning there are no moving parts, improving the long term reliability of the system and making it capable of operating in harsh environments that wavelength-division multiplexing systems cannot handle. TDM systems are capable of handling more than 100 sensors along a single optical fiber and can achieve sampling rates over 1kHz, depending only on the processing speeds [44]. The units themselves can be much smaller than wavelength-division multiplexing interrogators and some systems can operate on low current, 12V power source [50].

While there are numerous advantages to using a TDM interrogator, there are also several disadvantages. One of the main disadvantages is that a minimum of one meter is required between each individual sensor so that sufficient time is allowed between the return of the signals from each sensor. Another concern is cross-talk, cross-talk can result from two different sources, multiple reflections and spectral shadowing. Cross-talk is interference between two returned signals that can be detrimental to the reliability of the returned signal [40]. TDM systems also require faster signal processing to accurately

monitor the signals from all sensors [50]. While there are several problems that come with TDM interrogation systems, current technology has, for the most part, cured the problems, making TDM an effective and reliable method of interrogating FBG sensors.

Wavelength-Division Multiplexing: The most common interrogation method, currently used is wavelength-division multiplexing (WDM). With WDM systems, there are several methods of operation; they can utilize a broadband light source with a spectrometer or a tunable swept-wavelength light source with photodiode detectors [44]. Most systems now operate using a fast sweeping laser light source [40]. With WDM interrogation, each FBG must have a different grating period to operate. As the swept light source passes through the range of wavelengths, the wavelength of the light passing



Figure 55: With a WDM interrogator each FBG reflects only its individual Bragg Wavelength, by monitoring that wavelength, the interrogator is capable of differentiating the individual FBGs.

down the optical fiber is always known. When the wavelength passing down the optical fiber coincides with the Bragg wavelength of FBG, the light is reflected back up the fiber, to photodetectors [44] (Figure 55). To operate, each sensor must have a window of wavelengths around it, within which it is capable of experiencing strains, without overlapping other FBGs, the typical window for this is around 8.9nm, with an operational

wavelength range of 50 to 100nm, this allows for around 5 to 12 sensors per channel [40, 50]

The WDM interrogation has some unique benefits and shares others with TDM interrogation. WDM interrogation is capable of achieving higher levels of accuracy than TDM and is also more sensitive to small changes in strains. Another big advantage of WDM interrogation is that the sensors can be located as close to one another as they can be connected to the optical fiber, eliminating any spacing concern and increasing the flexibility of their use [44]. As long as appropriate ranges are given to each FBG, there is also no concern of cross-talk between the sensors [40]. While the number of sensors that can be multiplexed along one optical fiber is smaller than that of TDM interrogation, the technology is improving and increasing the number of sensors that can be simultaneously monitored. The sampling rate of WDM is also much lower than TDM, but several hundred samples per second is easily achievable and some systems are capable of achieving much higher rates than that, with proper processors [44].

WDM interrogation has numerous benefits for certain situations, but there are also numerous drawbacks, which must be considered. One of the major drawbacks is the size and sensitivity of the system; many systems are around the size of a desktop computer, whereas a TDM interrogator can be as small as a VHS tape. The tuned swept-wavelength laser source is a delicate piece of equipment which is sensitive to more harsh environments where vibrations are to be expected [44]. The WDM interrogator itself also, generally requires a higher current, AC power source, as compared to a TDM interrogator. The use of a tuned swept-wavelength light source greatly increases the price

of the interrogator as well, as it is a much more complicated component than the broadband light source used with TDM [50]. The few WDM systems using a broadband light source, require a series of complicated filters, which increase the price and complexity of the interrogator [44]. Manufacturing FBGs with numerous Bragg wavelengths, increases the costs of manufacturing the sensors, as well, further increasing the costs of a WDM interrogation system [50].

Interrogation Conclusion: With the advantages and disadvantages of the different interrogation methods considered, the use of TDM interrogation is the best method for wind energy. One major factor in this is the rugged, solid-state nature of the interrogator. With wind energy, the interrogator will be exposed to harsh environments, yet be expected to remain operational for many years. The major drawback of TDM, which hasn't been cured with advanced technology, is the distance required between sensors, with the massive size of a wind turbine blade, the sensor spacing essentially becomes a non-issue. As well, many more sensors can safely be located along a single optical fiber, allowing for a less expensive interrogator, which is less expensive than a WDM interrogator to begin with. The use of the same sensor throughout the blade also allows for easier manufacturing. With all of these factors considered, TDM interrogation is the best option for wind energy.

Considerations of Embedded FBG Based Strain Gauges

When embedding an optical fiber in a composite laminate, there are several effects which must be taken into consideration. Once embedded, it is not reasonable to attempt to remove, repair or otherwise modify the optical fiber or related sensors, as a result, there is a high degree of reliability necessary, or the embedded sensors are wasted. While studies have shown the sensors to exhibit a high degree of reliability, once in use, concerns still remain about the survivability of the sensors during the embedding process (Figure 56) and laminate curing stages. Concerns of sensor survivability include the mechanical survival of the optical fiber as well as any optical degradation of the fiber due



Figure 56: Damage to the optical fiber during handling and manufacturing is a major concern in the survivability of FOSs.

to the heat of the curing process. Secondly, an embedded optical fiber, while very small in diameter, around $125\mu\text{m}$, still has a significant impact on the laminate. Including the fiber in the laminate creates a stress concentration in the laminate; it disrupts the location of the fibers, causing a resin rich region and can ultimately comprise both the static and fatigue strengths of the laminate. These are important factors and the degree to which they affect the long-term reliability and stability of a wind turbine, must be understood before FOSs are embedded in blades.

Reliability of Embedded FBGs

There are two main mechanisms by which FBGs fail when embedded in a composite laminate. The first method is by mechanical failure, where the fiber is exposed to excessive static or fatigue loadings during manufacturing or operation and fails or is exposed to environmental conditions which erode the mechanical properties of the fiber, ultimately leading to mechanical failure. The second mechanism is optical degradation of the optical fiber and or the FBG. The heat and pressure which the fiber and the FBGs are exposed to, during the curing process, can have a detrimental impact on the signal strength of optical fiber and the reflectivity of the FBGs, hurting their sensing abilities and their signal reliability.

Mechanical Failure:

An unflawed optical fiber is a brittle material and behaves completely elastically up to failure; as well, it is very strong in tension, with a tensile strength between 600-700ksi. Unfortunately, that strength is compromised by any flaws from the manufacturing processes, handling or environmental effects. Flaws can also stem from the coating and stripping processes as well as by the photo-imprinting process. These effects can severely affect the strength of the fibers and, in some cases, make them incapable of handling even minor loadings. To sort out these severely compromised fibers, many manufacturers pretest any FBG to ensure that it is capable of handling expected loads, typically fibers are expected to handle a minimum of between 50 ksi to 200 ksi [51]. Proper manufacturing techniques can allow much higher strength fibers.

The formation of FBGs is accomplished by causing damage to the molecular structure of the optical fiber and the manufacturing process used to form the FBGs can result in excessive damage to the fiber. The more energy a fiber is exposed to the more damage that can be caused to the fiber. As well, the type of energy can further compromise the fiber strength. It has been shown that FBGs can be formed with a continuous, low-power, doubled Argon laser, which can be used to create micro-cracks and defects in the fiber core, changing the refractive index of the fiber, without compromising the strength of the fiber. However, using a low frequency, high-powered pulsed laser can be used to create a much thermodynamically stable gratings, but does so at the cost of weakening the fiber [47].

Optical fibers are covered in a protective coating, designed to protect them from flaws during handling as well as from environmental effects. The formation of FBGs requires the stripping of that silicone coating, which is applied over the fiber cladding

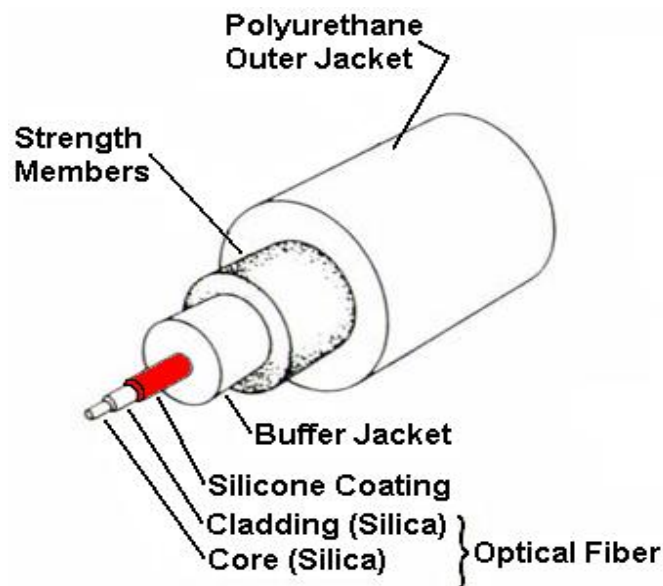


Figure 57: The general construction of an optical fiber includes a silicone coating which is applied over the top of a silica cladding.

(Figure 57), the stripping and recoating processes used to accomplish this can also have a significant impact on fiber strength. Tests conducted by D.H. Kang, et al. showed that the use of a hot sulfuric acid bath decreased the strength of the fibers by about 51%, where as using mechanical strippers lowered the strength of the fibers by an additional 7.5%. When the sulfuric acid stripped fiber was recoated it had only a minor effect, improving the strength of the fiber by only about 2% [52], within statistical variations; the results of the tests can be seen in Figure 58. Shown, as well, is the effect of the creation of the FBG in the fiber core. The formation of the FBG within the stripped fiber

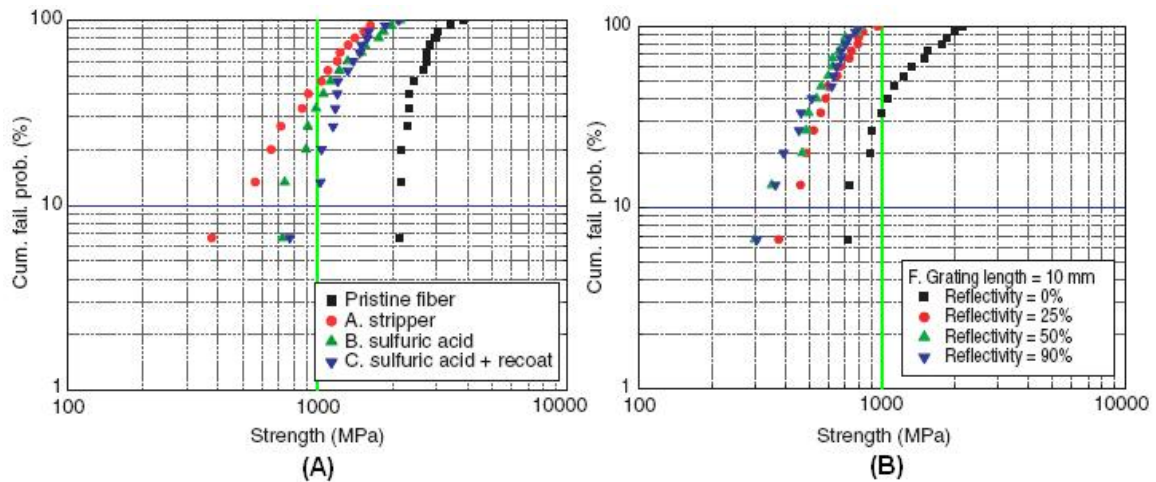


Figure 58: (A) Stripping of the coating, covering the fiber core and cladding can reduce the mean strength of the fiber by over 50%. (B) Once stripped, the creation of the FBG further reduces the strength of the fiber, the mean value can be reduced by as much as 56%.

reduces the overall strength of the fiber by, approximately, an additional 55% [52]. Over time, environmental effects can cause the coating to flake away, exposing the fiber to the elements, which can quickly begin to form flaws and degrade the mechanical properties of the fiber. Another concern is the coating becoming permeable to OH⁻ ions which can etch the glass [47]. Some coatings can help provide for

a longer life for the fiber, but cause as much as 75% reduction of the initial fiber strength [47]. While manufacturing can have a major effect on the long-term survivability of FBG based FOSs, proper manufacturing techniques, used by most reputable FBG manufacturers, maintain much of the initial strength of the optical fibers.

Failure of the fiber during embedment is also a common problem. Attempts to manufacture a laminate, with optical fibers included with the fibers, of the composite, have shown the optical fibers to fail easily when high tensile loads are used [39]. Also, handling of the fibers during manufacturing makes the fibers susceptible to failure. The points at which the fibers enter and exit the laminate must also be monitored and handled with care to prevent failure. The use of arc-fusion splicing to connect FOSs and the optical fibers creates connections which are very weak to transverse stresses [39]. Combined, these manufacturing techniques and processes cause numerous points at which damage may be caused to the optical fibers and, or the FOSs. To help prevent this, covering the fibers with an adhesive film can provide a level of protection for the fiber optics. As well the use fiber optics manufactured with FBGs in them eliminates the need for splicing the fibers and eliminates another weak point [39], however, it would likely cause a dramatic price increase in the manufacturing of the fiber optics. In general, one of the primary methods of protecting the fiber optics is simple care and caution.

Optical Degradation:

The other concern is optical degradation of the optical fiber and the FBGs, when they are embedded in a composite laminate. FBGs are formed by creating molecular defects in the core of the optical fiber; however, these defects are thermodynamically

unstable and semi-reversible. This means that any increase in molecular energy, such as heat and time, can cause a return to a more stable structure [47]. During the curing process of a laminate, the fiber optics will be exposed to high temperatures; these temperatures can cause the degradation of the FBG. There are two theories about the formation of the FBG, each of which provides a separate explanation of what results in the optical degradation of the FBG.

Color Center Model: The first method, is known as the color-center model; “a color-center model, based on the bleaching of the 244nm absorption band and the creation of other absorption bands, has been proposed to account for the UV-induced index changes through the Kramers–Kronig relationship [53] (Equation 6).” In the color-center model, electrons are trapped in defects or wrong-bonds, “UV light is assumed to photoionize some bleachable defects of the germanosilicate glass: the wrong bonds. Electrons released from these defects are free to move through the glass matrix and be retrapped at other defect sites [55].” The electrons get retrapped at new defects where the

$$\Delta n(\lambda') = \frac{1}{2\pi^2} \text{PP} \cdot \int_0^{\infty} \frac{\Delta\alpha(\lambda)}{1 - \left(\frac{\lambda}{\lambda'}\right)^2} d\lambda \quad 6$$

Where $\Delta n(\lambda')$ is the detected refractive index change, $\Delta\alpha(\lambda)$ is the photoinduced change in absorption, λ' is the wavelength at which the refractive index change was calculated at and PP is the Cauchy Principal Part [55, 56].

defects are more polarizable, due to “the fact that their electronic transitions peak at longer wavelength(s) or have stronger transitions [55].”

Thermal reversibility then stems from the demarcation energy of the newly created defects [53]. The defects and corresponding electrons reside at a distribution of energy levels or trap states. The demarcation energy is the energy required to release the electrons from the trap states. An increase in energy can achieve levels of demarcation energy, which, once reached, releases the electrons residing at the corresponding trap states. Electrons residing at lower demarcation energies will more easily return to their original states [53]. An increase in energy due to an increase in temperature can result the release of trapped electrons and the thermal reversibility of photo-imprinted gratings.

Densification Model: The second description is the densification model; the densification model is based from the differential form of the Lorentz-Lorenz relationship (Equation 7). As can be seen from this relationship, a change in the volume and, or refractivity of the glass would result in a related change in the refractive index of the fiber [55]. What this says is that the change in the refractive index of the fiber results from a localized compaction of the glass, a change in the local volume, resulting in a UV-

$$\frac{\Delta n}{n} = \frac{(n^2 + 2)(n^2 - 1)}{6n} \left(\frac{V}{\Delta V} \frac{\Delta R}{R} - 1 \right) \frac{\Delta V}{V} \quad 7$$

Where n is the refractive index, V is the glass volume and R is the refractivity.

induced index. The mechanics behind the model are not yet fully understood, but research has been conducted to provide support for the model [53].

Many studies conducted into densification were summarized by Douay et al. [55]. One study found an increase in tension on the core of an optical fiber, during the photo-

imprinting process. The tension was suggested to result from the structural densification of the glass core, into a more compact form. Transmission electron microscopy has also provided evidence of core glass densification, resulting from photo-imprinting, however, the results did not provide evidence to the degree of densification. Another study has “suggested that densification in germanosilicate fibers is due to the collapse of the higher-order ring structure into one comprising only two or three rings [55].”

In the case of densification, thermal reversibility results from a thermally induced stress relaxation [55]. A series of activation energies are required to reorganize the glass matrix back to its original state. Similar to the color-centered model, the densifications occur at different energy levels and once the corresponding energy levels are achieved, the glass matrix will reorganize to its original state [53]. As mentioned, the mechanics of the formation of Bragg gratings is not yet fully understood and research has shown that they are likely formed by a combination of the two methods [54].

Power-Law and Log-Time Models: To predict the optical degradation of FBGs, in non-hydrogen loaded fibers, Erdogan et al. [56] proposed the power-law model to predict the reflectivity of a FBG, for a given time and temperature (Equation 8). In this

$$\eta = \frac{1}{1 + A \left(\frac{t}{t_1} \right)^\alpha} \quad 8$$

Where η is the normalized reflectivity, A and α are functions of temperature and material specific constants solved by Equations 9 and 10 and, t is the time the fiber is exposed to the applied temperature and t_1 allowed to be 1 minute.

$$A = A_o \cdot e^{aT} \quad 9$$

Where A is a function for application to Equation 8, A_o and a are material specific constants derived from curve fitting for individual types of fibers and T is the Temperature which the fiber is being exposed to.

$$\alpha = \frac{T}{T_o} \quad 10$$

Where α is a function for application to Equation 8, T_o is a material specific constant derived from curve fitting for individual types of fibers and T is the Temperature which the fiber is being exposed to.

equation the factors A (Equation 9) and α (Equation 10), are functions of the material constants a , A_o and T_o , which are all parameters derived by testing individual fiber types and creating curve fits based on the power-law equations and the collected data points [56]. This has shown FBGs to degrade in a predictable manner, with time and temperature, showing an initial rapid decrease in grating reflectivity, which transitioned to a much slower, more gradual decrease over time [56]. An excellent correlation between the power-law and experimental results was seen (Figure 59).

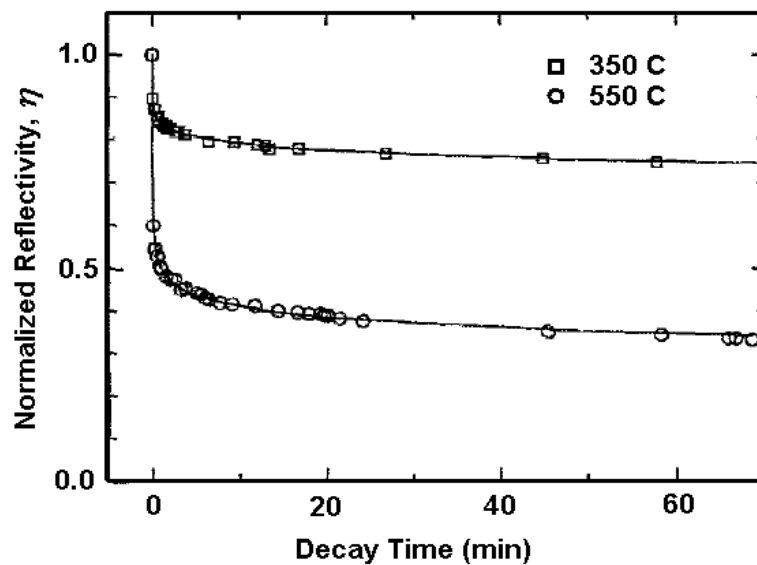


Figure 59: The power-law correlation developed by Edrogan et al. to describe the optical decay of FBGs, written in non-hydrogen loaded fibers.

While excellent results were shown for non-hydrogen loaded fibers, the results began to break down when hydrogen loaded fibers were examined. Hydrogen loaded fibers exhibit greatly increased photosensitivity, making them essential in some applications; however, gratings written in hydrogen loaded fibers do not exhibit the stability shown by non-hydrogen loaded fibers. They are believed to have more electrons residing at lower energy states and as a result, decay more rapidly [53]. The power-law model could be used to provide some estimate of decay, but the possibility existed to generate a better correlation. To correct for the affect of hydrogen loading, a new model was developed by Baker et al. in 1997, known as the log-time model (Equation 11). In the model, similar to the power-law model, τ , given by Equation 12, K, E_a , R and A are parameters

$$\eta = 1 - K \cdot \log\left(\frac{t}{\tau}\right) \quad 11$$

Where η is the normalized reflectivity, τ is a function of material specific constants and the exposure temperature, t is the time the fiber is exposed to the given temperature and K is a material specific constant.

$$\tau = A \cdot e^{\frac{E_a}{RT}} \quad 12$$

Where τ is a function for application to Equation 11; A, E_a and R are material specific constants derived from curve fitting for individual types of fibers and T is the temperature which the fiber is exposed to.

derived by testing individual fiber types and creating curve fits based on the power-law equations and the collected data points [53]. With this model a much better correlation can be developed for optical decay of hydrogen loaded fibers (Figure 60).

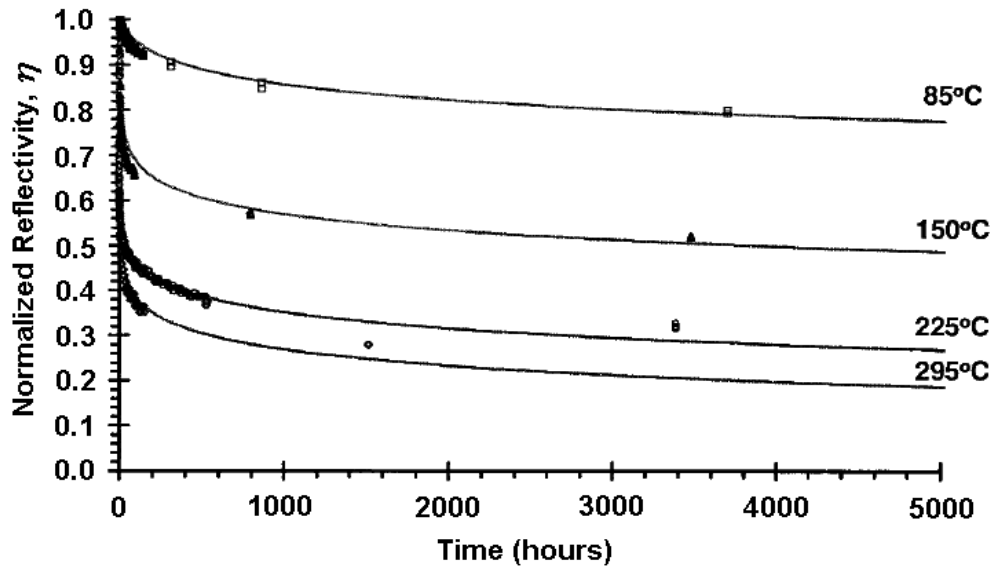


Figure 60: The log-time model accomplishes a much better correlation, compared to the power-law model, with experimental data for hydrogen loaded fibers.

Fiber Annealing: By being able to predict how the reflectivity of a FBG will degrade at a given temperature and time and the relative stability realized after the initial drop in reflectivity, it becomes possible to manufacture gratings which will be extremely stable, even at high operating temperatures. This is accomplished by initially, overwriting the gratings, creating stronger contrasts in the in the fringes refractive index, then annealing the grating at an elevated temperature [47, 53]. This removes the unstable portion of the UV-induced index, accelerating the aging process forward to a point where it becomes thermally stable over the operational lifetime of the FBG [53]. Once annealed, the FBG becomes stable at any temperature below the annealing temperature, however, temperatures above the annealing temperature may still result in the optical degradation of the grating and care must be taken when selecting FBGs for use in high temperatures [51].

The previous models, allow for a way to determine the parameters needed to accomplish the proper annealing process for the expected operating lifetime and maximum temperature which a FBG will be exposed to, allowing for the production of stable and reliable FBGs. The power-law model gives Equation 13, which depends on

$$t_2 = e^{a \cdot T_o \cdot \left[\left(\frac{T_1}{T_2} \right)^{-1} \right]} \cdot t_1 \left(\frac{T_1}{T_2} \right) \quad 13$$

Where t_2 is the required annealing time to achieve the desired stability, T_1 is the expected maximum operating temperature for the grating, t_1 is the desired life expectancy of the grating, T_2 is the temperature at which the grating will be annealed and the parameters a and T_o , are same material specific constants used in Equations 8 and 9.

the same material specific constants a and T_o as used in Equations 8 and 9 and are, again, specific to the doping which the fiber has been subjected to [53]. Using the log-time model gives Equation 14, where the τ_1 and τ_2 values stem back to Equation 12, where τ will be solved to find τ_1 and τ_2 with the respective T_1 and T_2 values and then utilized in Equation 14 [53].

$$t_2 = t_1 \left(\frac{\tau_2}{\tau_1} \right) \quad 14$$

Where t_2 is the required annealing time to achieve the desired stability, t_1 is the desired life expectancy of the grating and the τ_1 and τ_2 values are solved with Equation 12, where τ will be solved to find τ_1 and τ_2 with the respective T_1 and T_2 values, where T_1 is the expected maximum operating temperature of the grating and T_2 is the annealing temperature.

By annealing the gratings, a great deal of thermal stability is achieved, generally it can be expected that a properly annealed grating will experience less than 0.3% degradation over the course of 25 years. By selecting a grating which has been annealed

for operation at temperatures greater than those experienced during the curing process of a laminate, there should be little concern of thermally induced optical degradation of the grating during the process. Most sensors are annealed to be safe at temperatures up to 400°C and should be within safe tolerances at curing temperatures [51]. Selection of the sensors used will be important, to achieve a stable and reliable system, especially if the gratings are in hydrogen loaded fibers.

Effects of Embedded Optical Fibers on Laminates

The effects of embedding optical fibers in a laminate are not limited simply to the fiber optics; the laminate itself suffers non-trivial consequences as well. While a typical optical fiber is of a very small diameter, usually around $125\mu\text{m}$ and generally between $100\mu\text{m}$ and $200\mu\text{m}$, they are approximately the same diameter as a common ply thickness and much larger than the surrounding fibers, which typically range from $5\mu\text{m}$ to $10\mu\text{m}$ [57]. When embedded, the optical fiber causes a large resin pocket to form, surrounding it (Figure 61). The resulting pocket will generally take an “eye” shape and depending on



Figure 61: Embedding an optical fiber in a laminate results in a large resin pocket surrounding the optical fiber, which can compromise the strength of the laminate.

the orientation of the optical fiber and the surrounding plies, the resulting pocket can be equal to the height of the optical fiber, the length of the pocket can be approximately 8 times the diameter of the optical fiber and the surrounding plies can be

affected, up to 3-4 times the diameter of optical fiber [57]. The pocket formed creates a stress concentration at the location of the optical fiber which has an impact on both the static and fatigue strengths of the laminate. The degree to which the strengths are affected will be shown to depend, to a great degree, on the orientation of the loading and the direction of the surrounding plies, with respect to the direction of the optical fiber, the thickness of the laminate and the protective coating on the fiber [58].

Effect on Static Strength:

Numerous studies have been conducted examining the effect of embedded fiber optics on the static strength of laminates. This paper will address two of these studies, one conducted by E.J. Friebele et al. in 1999 and another by Jose Silva et al in 2005.

E.J. Friebele et al.-1999 [58]: The study conducted by Freibebe et al., was performed for the Naval Research Laboratory to examine the application of FOSs to spacecraft. Much work was done, including an examination of the effects of embedded fiber optics, on the tensile and compressive strengths of a laminate, under static loading. Tests were conducted examining both unidirectional and quasi-isotropic lay-ups in longitudinal and transverse directions. The individual lay-ups and fiber orientations,

Table 9: The tests conducted by Freibebe et al. were as shown, the fiber orientation represents each individual test conducted, the previous columns describe the method of the test.

Lay-up	Test Format	Test Direction	Fiber Orientations Tested
[0] ₁₆	Tension	Longitudinal	None/0/90/45
[90] ₁₆	Tension	Transverse	None/0
[0/45/-45/90] _{s2}	Tension	Longitudinal	None/0/90/45
[0/45/-45/90] _{s2}	Tension	Transverse	0/90
[0] ₃₂	Compression	Longitudinal	None/0/90
[90] ₃₂	Compression	Transverse	None/90
[0/45/-45/90] _{s4}	Compression	Longitudinal	None/0/90/45

tested, are shown in Table 9. The tests examined a full spectrum of fiber orientations, lay-ups and loading directions, giving an excellent perspective on the effects of embedding fiber optics, including the affect of fiber orientation with respect to the surrounding plies.

The results of the experiment showed that, in the tensile tests, the unidirectional laminates with an embedded optical fiber, parallel to the surrounding plies had a minimal effect on the tensile strength of the laminate, only about 7%. However, in the longitudinal tests, when the optical fiber was embedded at an angle to the surrounding plies, there was up to a 19% drop in the tensile strength of the laminate, there was little difference between the optical fibers embedded at 90° and 45°. The transverse tests actually showed a minimal increase in the tensile strength, however the poor properties of composite material to transverse loadings is likely a more important factor in the increase, than the optical fiber itself. Quasi-isotropic laminates were degraded by up to 16% by optical fibers embedded transverse to the surrounding plies, but only slightly in when embedded parallel to the surrounding fibers.

In compression the results were much more erratic and inconsistent than those seen in the tensile tests. In the unidirectional tests, the results showed the laminates to exhibit a strength decrease of up to 11%, with an embedded optical fiber and fiber orientation had a minimal effect on the results. The transverse tests were similar to the tensile tests, showing a small but insignificant increase in strength. The quasi-isotropic materials, however, showed no consistency, with data scattered widely, above and below the strength of the control specimens. The results of tests can be seen in Table 10.

The experiment showed that proper orientation of the optical fiber, to the surrounding plies, is essential in maintaining the integrity of the laminate. When the optical fibers were oriented parallel there was little degradation of the mechanical properties of the laminate, regardless of the laminate and testing method. Orienting the optical fiber transversely to the surrounding plies, regardless of the angle, could be expected to compromise the strength of the laminate by up to nearly 20% in all longitudinal tests. Stiffness varied slightly, in all cases and was generally within the limits of statistical variability. It is also suggested that the thickness of the laminate plays a significant role on the degradation of the laminate, the thicker the laminate, the less significant the impact of the embedded optical fibers, this is even more significant with the quasi-isotropic materials. This plays critical importance with wind turbine blades which are very thick laminates, further reducing the effects on the blade.

Table 10: The results of the experiment showed that optical fiber orientation, with respect to the surrounding plies, has a significant effect on the degradation of a laminate.

Tension	Longitudinal /Transverse	Fiber Orientation	Modulus (GPa)	Standard Deviation	Strength (MPa)	Standard Deviation
[0] ₁₆	Longitudinal	90	425.00	3.00	872.00	26.00
[0] ₁₆	Longitudinal	0	441.00	13.00	1002.00	35.00
[0] ₁₆	Longitudinal	None	437.00	6.00	1072.00	28.00
[0] ₁₆	Longitudinal	45	439.00	4.00	876.00	29.00
[90] ₁₆	Transverse	0	5.82	0.07	21.28	3.38
[90] ₁₆	Transverse	None	5.80	0.14	17.61	5.28
Compression						
[0] ₃₂	Longitudinal	None	441.00	25.00	285.00	33.00
[0] ₃₂	Longitudinal	0	426.00	18.00	254.00	35.00
[0] ₃₂	Longitudinal	90	463.00	11.00	257.00	33.00
[90] ₃₂	Transverse	None	6.00	0.07	84.30	17.80
[90] ₃₂	Transverse	90	5.83	0.04	106.00	3.40
[0/45/-45/90] _{s4}	Longitudinal	None	131.00	4.00	123.00	2.00
[0/45/-45/90] _{s4}	Longitudinal	0	127.00	7.00	177.00	8.00
[0/45/-45/90] _{s4}	Longitudinal	90	132.00	9.00	129.00	N/A
[0/45/-45/90] _{s4}	Longitudinal	45	129.00	7.00	119.00	7.00

Jose Silva et al.-2005 [59]: The study conducted by Silva et al. examined the impact of embedded optical fibers in laminates which were loaded in three point bending. The tests utilized a Seal Texipreg HS 110 REC carbon fiber prepreg with an epoxy matrix and a volume fraction of 32%. The laminates were each assembled from 18 plies:

$$\emptyset [0]_{18}$$

$$\emptyset [0_2/90_2/0_2/90_2/0_2]_s$$

The laminates were assembled with optical fibers situated in three different ways; without an optical fiber, as control specimens, with a fiber centered in the laminate and with a fiber located between the third and fourth plies. By examining the specimens in three point bending, shear stresses were introduced into the investigation, which had not been previously examined and, as a result, developed another consideration when examining the effect of embedded FOSs. It must be noted, all tests were performed with the optical fibers in a direction parallel to that of the surrounding plies.

The results of the tests showed there to be little effect on the static strength of the laminates in three point bending. The centered specimens showed the best results, each achieving a slight increase of 3 to 6% in the strength of the specimens, when compared to

Table 11: Three point bending tests showed there to be little variation of both the stiffness and the modulus of rupture of the specimens with and without embedded optical fibers.

Lay-Up	Fiber Location	Stiffness (GPa)	Standard Deviation	Modulus of Rupture (MPa)	Standard Deviation
$[0]_{18}$	None	96.9	10.8	1340.5	115.7
$[0]_{18}$	Center	99.0	1.7	1384.0	35.5
$[0]_{18}$	3/4 Plies	94.8	7.4	1259.0	26.5
$[0_2/90_2/0_2/90_2/0_2]_s$	None	71.9	2.8	1045.9	7.5
$[0_2/90_2/0_2/90_2/0_2]_s$	Center	73.2	4.5	1107.5	29.6
$[0_2/90_2/0_2/90_2/0_2]_s$	3/4 Plies	71.4	2.6	1019.7	22.7

the control tests. The off center specimens showed only a minor loss of 3 to 6% of the total strength of the specimens. The trends of the stiffness results closely matched those of the modulus of rupture, with a slightly smaller magnitude. The full results of the tests can be seen in Table 11. In general the effect of the embedded optical fibers could be considered minimal and within statistical variation.

Effects on Fatigue Strength:

While it is useful to understand the affect embedded fibers have on the static strength of a laminate, wind turbines are not static structures, to the contrary, wind turbines experience extreme fatigue loadings during their lifetime. As a result it is essential to understand how the laminates will be affected by these high fatigue loadings when embedded with optical fibers. To this end, a great deal of work has been done. Several studies will be discussed here.

Surgeon and Wevers 1999 and 2001 [60, 61]: The first study by Surgeon and Wevers was conducted in 1999 and was a broad examination of the mechanical properties of laminates with embedded optical fibers. A significant portion of the work was devoted to fatigue loading. The lay-ups which they examined were a Vicotex carbon/epoxy prepreg and were assembled with a lay-up of $[0/45/-45/90]_s$. The optical fibers were located at four different locations among five sets of test specimens, along with a control specimen, for reference:

- Ø A-No embedded optical fibers
- Ø B-Two optical fibers in the 90 direction, one embedded at each 0/45 interface

- Ø C-Two optical fibers in the 90 direction, one embedded at each 45/-45 interface
- Ø D-Two optical fibers in the 90 direction, one embedded at each -45/90 interface
- Ø E- One optical fiber located at the 90/90 interface, in the 90 direction

All optical fibers were run in the 90 direction as it had been shown, previously, to be the worst case scenario. They ran tests at 50, 65 and 80% of the tested ultimate strength of the laminates; this was equivalent to 350, 450 and 550MPa, respectively. The tests were performed with at a stress ratio of $R=0.1$ and were run at 5 Hz. Each test was run until failure or 10^6 cycles.

Tests conducted at 350MPa showed a 100% survival rate for all specimens.

When the maximum loading was increased to 450MPa the type A and E specimens all survived to 10^6 cycles, however, the rest of the specimens had much lower survival rates, with only three of the other 12 specimens surviving to 10^6 cycles. The most significant effect was seen with the type B and D sets, where the specimens failed at an average of 254,364 and 304,385 cycles

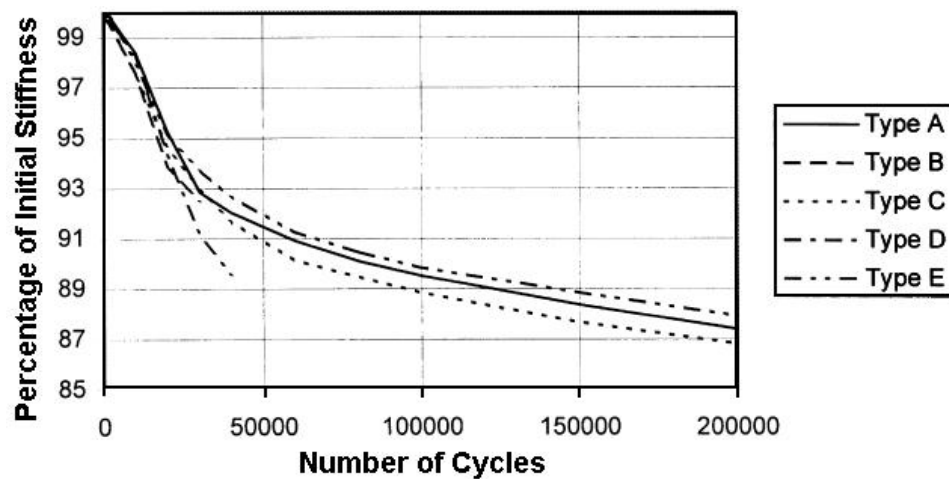


Figure 62: The decrease in stiffness of the specimens tested at 450 MPa was substantial, more than a 10% decrease before 200k cycles.

respectively. A substantial decrease in stiffness was also seen (Figure 62), with all specimens experiencing over a 10% decrease in stiffness, before 200k cycles. When the loading was increased to 550MPa, all the specimens failed before 10^6 cycles were reached, again sets B and D exhibited early failure, however, set E failed, on average,

Table 12: The cycles to failure for the different sets of specimens revealed a stark contrast in the life expectancies of laminates with embedded optical fibers, depending on the direction of the surrounding plies.

Test Set	350 MPa	450 MPa	550 MPa
A	1,000,000	1,000,000	215,205
	1,000,000	1,000,000	4,635
	1,000,000	1,000,000	17,065
	1,000,000	1,000,000	87,850
B	1,000,000	487,455	12,000
	1,000,000	30,000	22,960
	1,000,000	200,000	935
	1,000,000	300,000	6,590
C	1,000,000	1,000,000	11,500
	1,000,000	18,228	1,750
	1,000,000	1,000,000	141,950
	1,000,000	776,035	17,060
D	1,000,000	47,275	3,740
	1,000,000	123,175	5,372
	1,000,000	47,090	6,165
	1,000,000	1,000,000	72,250
E	1,000,000	1,000,000	2,710
	1,000,000	1,000,000	2,380
	1,000,000	1,000,000	67,740
	1,000,000	1,000,000	415

prior to the specimens of set D. Stiffness results were sparse due to the early failure of the specimens; however, a severe decrease was seen in all sets, before 50k cycles. The full results of the tests can be seen in Table 12.

The low cycles to failure experienced by the B set specimens is caused by the distortion of the 0-plyes surrounding the fiber. Damage initiates in the 90 and 45 plies and cracks begin to form and as the cracks continue to form they begin to interact and

eventually form a delamination. The delamination then decreases the stiffness of the plies and their load carrying capacity. As a result the loadings are transferred to the 0-ply which are already being distorted by the presence of the optical fibers and as a result, will fail prematurely. The D specimens likely fail early due to their natural susceptibility to delamination. As discussed before, damage and delamination will typically initiate in the 45 and 90 plies, by locating an optical fiber at the location, resin rich zone is formed and the discontinuity accelerates crack growth and passes the loading to the 0-ply which, as a result fail prematurely.

The study showed a significant impact on the long-term reliability of a composite laminate with embedded optical fibers, when exposed to high levels of fatigue loading. While the effect was significant, the degradation can be magnified by improper location of the optical fiber within the laminate. Disrupting the 0-ply or locating an optical fiber in the damage prone -45/90 interfaces can severely hurt the fatigue life of the laminate, while locating a fiber in the 90/90 or -45/45 interfaces provided a much more reliable specimen.

The second study conducted in 2001, stemmed from the results of the 1999 study and aimed to verify the mechanics behind the premature failures which were seen. The study utilized the same test specimen sets used previously and the specimens were all tested at the 450MPa loading, which had provided the most useable information. In the study, tests were interrupted at 100, 1k, 10k, 25k, 50k and 100k cycles and were examined with a radiograph to check for cracks in the 90s. Through this, it was possible to monitor the evolution of the damage in the specimens and compare it to the results

obtained in the prior study. To do this, the number of cracks was counted as well as their size, enabling an idea of the resulting total length of all the cracks and the area of delamination that was occurring in the specimens.

As was expected, the results showed the D set to rapidly begin forming cracks in the 90s and continue to form many more cracks than the other specimens (Figure 63). Even more significant was the growth rate of the cracks and the resulting delaminations, they initiated much earlier than the other specimens and continued to grow much quicker than the other specimens. This validated the previous belief that an optical fiber located

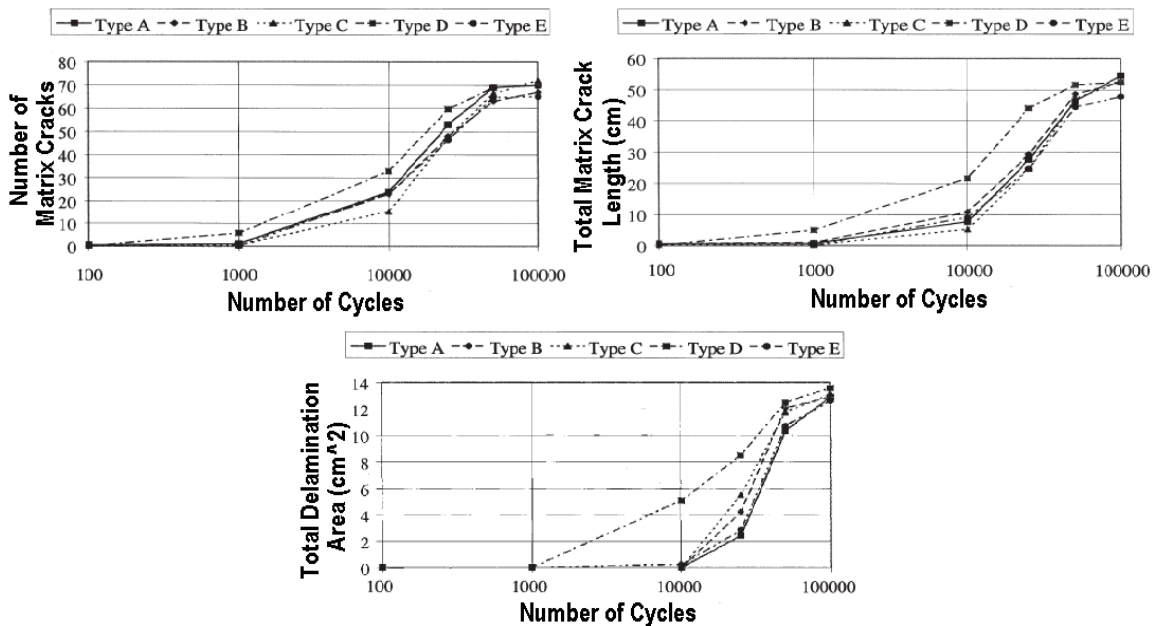


Figure 63: The second set of experiments conducted by Surgeon and Wever showed rapid crack growth in the D set of specimens, validating the damage initiation caused by locating an optical fiber at the -45/90 interface.

at the -45/90 initiated early damage formation, resulting in premature failure. The results did not show an accelerated crack growth in the B specimens, however. This result was expected, since the crack growth was not the issue, with the set B specimens, but the

reliance on the distorted 0-ply to carry the load. The 0-ply was weakened by the presence of the optical fibers, leading them to premature failure.

Jose Silva et al.-2005 [59]: As well as examining the static strength of laminates in three point bending Silva et al. also examined the laminates in fatigue. The tests were conducted using ASTM D790 standards, with a stress ratio of $R=0.1$ at 6 Hz for a maximum of 500k cycles. The loadings used were 75 and 90% of the ultimate strength of the laminates, the laminates were the same as those used in the static tests, shown above in Table 11.

The results of the tests showed some interesting results, where as, in the static tests, there was little affect from having embedded optical fibers, the fatigue tests showed much more evident, premature failure for specimens with the fiber optics. Also, where the specimens with optical fibers located at their center showed better performance, previously, in fatigue, those specimens failed much earlier than the off-center laminates. At the 75% loading, there was little decrease in stiffness. The higher loading, 90%, revealed a significant decrease in stiffness and resulted in some failures at low numbers of cycles, for most all specimens.

The unidirectional laminates generally exhibited a more steady set of results, all of the specimens without optical fibers, survived. The off-center laminate had two premature failures, both of which occurred before 100k cycles, however the rest of the specimens survived for 500k cycles without a major decrease in stiffness. The laminates with centered optical fibers all failed prior to 80k cycles and most failed before 20k cycles, presenting a stark contrast to the other specimens. For the quasi-isotropic

specimens the results were somewhat more scattered, with several of the control specimens failing prior to 100k cycles, but the majority of the specimens surviving the length of the test. The off-centered specimens, once again, generally survived the length of the test, with one exception, which failed almost immediately. The centered specimens showed an even more significant failure, with each specimen failing prior to 7000 cycles.

The premature failure of the centered laminates was an unexpected result, the prior static work had shown a slight increase in properties and the location of the optical fiber in the quasi-isotropic specimens, transverse to the surrounding plies, led to the expectation that the off-center specimens would fail prematurely. The severity of the difference in the results was surprising as well. While the reason for the early failure was believed to be the presence of large shear stresses at the center of the specimen, the reasoning is not yet fully understood. It must also be noted that the tests were conducted with a relatively limited number of samples, typically three specimens per laminate, and to a low number of cycles, yet, the results provide an important piece of information which must be taken into consideration with future work.

Effects of Embedded Fiber Optics Conclusion:

From this it can be determined that embedding optical fibers in composite laminates does have an effect on the reliability of the laminate. Some critical factors must be taken note of, to help mitigate the effects of the embedded sensors. Running optical fibers transverse to the surrounding plies will dramatically affect the strength and longevity of the laminate. Optical fibers, run transversely to the load carrying plies,

should be kept away from the load carrying plies. The thicker the laminate the less of an affect the embedded optical fibers will have. The type of loading should be taken into consideration as well, if there are going to be bending loads placed on the laminate, the fibers should be kept away from the center of the laminate. This is far from a full definition of the effects of embedded optical fibers, but provides a starting point for future work and a basis for understanding the effects.

When applied to wind turbine blades, this work shows several important factors, due to the thickness of the laminates used; the effects of embedded sensors would likely be greatly reduced. As a result of the thickness, the sensors would likely be located far from the center of the laminate, helping prevent the results seen in the three point bending tests. The loadings applied to a blade in service make three point bending a valuable examination for wind turbines, as well as fatigue testing; however, compressive fatigue loading should be examined as well. Current results show that there would likely be little effect from embedding FOSs in a wind turbine blade, but a great deal more examination must be conducted before this can be verified.

Sensors Conclusion

While FOSs utilizing FBGs were determined to be the optimal type of sensor for use in wind energy, the technology has not yet achieved the same level of maturity as other systems currently available. As a result, there is a great deal of work which remains to be done before large scale use and production can begin. The research which has been conducted here does lead to numerous conclusions.

Despite any drawbacks of the sensors, FBG based strain gauges are the best choice for wind energy for numerous reasons. The multiplexing ability afforded by FBGs allows for the simplest installation and interrogation of any available strain gauge. The small size allows for embedding the sensors with as minimal of an impact on the laminate as possible. The durability of the sensors and their resistance to electrical interference enable their use in wind turbine blades without concern of interference from the power generation unit or atmospheric influences. The stability of the sensors allow for long lifetimes without needing recalibration or servicing. Overall, the sensors allow for the simplest, cleanest, most reliable, low maintenance and robust system of any sensors available today. As well, the use of FBG sensors allows for the addition of numerous other types of sensors, including pressure, temperature and acceleration, which may prove to be necessary.

Interrogation of the sensors can be best accomplished through a TDM interrogator. TDM interrogation allows for a less expensive system, which is easier to manufacture and maintain and provides the best long-term reliability. The small size of the interrogator and being a solid state system allows for use in the harsh environments

that may be experienced during a lifetime of use in a wind turbine. The main drawback of a TDM system, the need to keep individual sensors one meter apart, is virtually nullified by the immense size of a wind turbine and if sensors must be located near to one another, methods of fiber routing can compensate for the mounting distance. The large number of sensors which can be handled, the rugged nature of the interrogator, the increased system reliability and reduced price, make TDM interrogation the best interrogation method for use with wind energy.

Embedded optical fibers in composite laminates can have a severe negative impact on the laminate and as a result, the manufacturing process becomes essential to providing a stable and reliable wind turbine, with embedded FOSs. Attention must be given when an optical fiber is located in a laminate, to the surrounding plies, whenever possible the optical fiber should be located where it is parallel to the surrounding plies and optical fibers should never be located where they run transverse to adjacent, load carrying plies. The effect of the thickness of a laminate on the resulting degradation of a laminate with embedded optical fibers lends to a further reduction in the impact of embedding optical fibers in the laminates of wind turbine blades, which are generally, very thick laminates utilizing thick plies. While embedding the optical fibers in a laminate, can have a negative impact on the laminate, proper care and attention to the orientation of the optical fiber can greatly reduce the impact and preserve the majority of the original strength of the laminate.

While a great deal of information has been garnered and many conclusions can be made as a result, even more work remains to be done. The work falls into several main

categories; system selection, effects of embedding on the optical properties of optical fibers and FBGs and the effect of embedded optical fibers on the strength and survivability of the laminate.

While FBG strain gauges, utilizing TDM interrogation has been determined to be the best system for wind energy, work still remains on system selection, interrogators and sensors must be chosen, which will provide the best long-term stability and reliability as well as provide the highest level of survivability. Finding the appropriate system and manufacturers is a non-trivial step in the development of a complete, operational system. The choice of a manufacturer that utilizes improper annealing of the FBGs, uses damaging manufacturing techniques, utilizes certain dopants to ease manufacturing or doesn't properly test the mechanical properties of the optical fibers and FBGs could result in a system which fails prematurely or provides for poor operational results, compromising the integrity of the entire system. Also, methods must be determined for the efficient transmission of data between the blades, hub and nacelle of the wind turbine, as well as provide power to the interrogator. Proper and safe manufacturing techniques must also be developed, to prevent damage to the fiber optics during the manufacturing process.

Research has shown the degradation of optical properties of FBGs, when exposed to heat, can be negated by annealing the grating during manufacturing. Despite this, embedded optical fibers have demonstrated a decrease in transmission, when embedded in a composite laminate; the causes of this degradation must be understood and steps

must be taken to eliminate the effect, providing for stable optical fibers and FBGs, before optical fibers and FBGs can begin being, reliably, embedded in laminates.

To this point, much of the work conducted, examining the effects of embedding optical fibers in composite laminates, has been quite limited in its scope and has been conducted for only limited numbers of specimens, loading conditions and limited materials and lay-ups, this small volume of information must be resolved before a well developed understanding of the effect of embedding FBGs has, both on the laminate and the FBG and optical fiber. Fiberglass has been relatively ignored by most of the research which has been conducted so far, the research has largely examined carbon fiber, large scale tests examining fiberglass in both static and fatigue loadings will provide valuable information. Fatigue tests need to be conducted examining not just tension/tension conditions, but tension/compression as well. Different loading conditions should be examined as well; the three point bending tests performed by Silva et al. provided interesting insight into the effects of other loading besides the standard tension and compression tests. While unidirectional laminates can provide a great deal of information; manufactured structures are not unidirectional, extensive work must be done looking into various quasi-isotropic laminates. With this work a data base of information can begin to develop, allowing for safe and reliable embedment of optical fibers in laminates.

Fiber Optic strain gauges provide an exciting opportunity for the future of monitoring composite structures, not only in wind turbines, but in many fields. The opportunity for in situ monitoring of the blades allows for a numerous possibilities and

can garner a great deal of information. Real time load monitoring and the lifecycle data base that can be provided, are true benefits that can be realized. Before this can safely occur a great deal of work is left to be done. For wind energy, the use of FBG strain gauges with TDM interrogation is the best system, for monitoring the blades. The integration of these systems into the wind turbine will be an essential step into the development of a complete, functional smart system.

CONCLUSIONS AND FUTURE WORK

Conclusions

The purpose of this paper is to be a base level examination of the feasibility of utilizing smart structures for use in wind turbine blades. The basis of the conclusion of this paper is that applying smart structures to the design of future wind turbine designs is not only possible, but will prove to be essential in the continued growth of wind generated power. The impact that is desired from this paper and the results of the work which has been conducted during the course of the last year and a half are as follows.

Active Control Surfaces:

- Ø The Gurney flap is an effective method of altering the lift created by an airfoil and can be used to rapidly reduce the lift on an airfoil.
- Ø The simplicity of the Gurney flap makes it an excellent choice for use with wind turbine blades.
- Ø A piano-hinge style Gurney provides the simplest type of Gurney flap, the simple design, utilizing a minimum of moving parts, lends to the most reliable, yet effective system.

The Prototype:

- Ø It is possible to construct an operational prototype, utilizing basic and readily available components and operating systems.

- Ø A control program was designed which allows for full and robust control of the prototype.
- Ø The prototype operates within the set restrictions and operates at a high level of accuracy and with precision.
- Ø The prototype is capable of functioning independently, without dependence on any human intervention.
- Ø The prototype can be easily adapted to different input sensors, to allow for the examination of different methods of control.
- Ø The prototype is ready for and capable of transportation and wind tunnel testing.

Sensors:

- Ø Fiber Bragg Grating based fiber optic strain gauges are the best type of gauge for use with wind energy.
- Ø Time-Division Multiplexing is the best method of interrogation, for use with wind energy.
- Ø Proper annealing processes and mechanical strength testing of optical fibers and FBGs, before embedment, should eliminate many concerns of optical degradation or mechanical failure during manufacturing and curing processes.
- Ø Proper optical fiber orientation within a composite laminate will help to mitigate the effect of embedded optical fibers within a composite laminate; however, it is not possible to completely eliminate the effects.

Ø The primary contributions to the degradation of a laminate with embedded optical fibers is the orientation of the optical fiber, with the surrounding plies, the thickness of the laminate, the coatings applied to the fiber, the location of the optical fibers within the laminate and the loading direction.

A great deal of information has been garnered, researched and organized throughout the course of this thesis; yet this work only lays the groundwork for future work to be done, as a result the work that is left to be done and, in some cases, is being performed already, is great and the contribution to the direction of the future work may be the most significant accomplishment of this thesis.

Future Work

Throughout the sections a great deal of discussion was made regarding the future work that is left to be done and the contributions made to the future work is one of the most important roles, which this thesis will play. Within the full breadth of the work that has been done here, a significant amount of work remains to be done.

Active Control Surfaces:

- Ø While it is believed that the Gurney flap will have the same effects when applied to the suction side of a blade, as it does when on the pressure side, there has been little examination to ensure this to be true. Computational Fluid Dynamics (CFD), Finite Element Modeling (FEM) or wind tunnel testing should be utilized to ensure the desired lift reduction.
- Ø The partial deployment ability of the later prototypes was an important goal and step in the prototype development, but the transient response of partial deployment must be fully understood, especially when viewed with the piano-hinge style prototype. The angle of the flap, height of the flap and mounting distance from the trailing edge all have an influence on the generated or dissipated lift and the combination of the effects is not understood. Again, CFD or FEM could provide important insight.
- Ø An investigation should be conducted to examine the behavior of the blade during the time between when a gust loading is detected and when the flap reaches full extension.

- Ø The effects of a deployed flap must be examined. When a flap is deployed certain torsional loads will be applied to the blades, the magnitude of the torsional load needs to be investigated as well as the effects on the blade. Work must also be done to ensure there are no detrimental harmonics of the blade that result from a deployed flap or the deployment of the flap.
- Ø Methods must be developed to allow for the integration of the Gurney flaps with the existing load control mechanisms. The active control surfaces are not meant to act alone, but in concert with pitch control systems. These two techniques must be designed to function together to provide for the best protection of the blades while yet maximize the efficiency of the turbine and maximize power output.
- Ø Steps must be taken to examine the incorporation of the systems with both existing and new blade constructions. As well, the distribution, size and numbers of the flaps will need to be selected to allow for the maximum effect through the use of the least possible number of flaps.

The Prototype:

- Ø The current operating system and control program are achieving data acquisition rates in the range of 25 to 35 samples/second. This low data acquisition rate greatly affects the ability to control flap deployment. For clean operation the control program should achieve a minimum of 500 samples/second. Steps need to be taken to increase the data acquisition rate.

- Ø Currently a hydraulic damper and stepped voltage are used to help eliminate overshoot. While effective, both of these negatively influence the time required to fully deploy the flap. Methods of eliminating overshoot must be developed which do not affect the activation time of the of the flap, this may be through PID controllers, rotational dampers, mechanical brakes or through logic control systems that may be possible to develop with increased data acquisition rates.
- Ø The control system should be reexamined, including the operating system, to determine if LabVIEW is the best program for the needs of the prototype. As well mathematical analysis of the control system should be considered, to ensure the best control and interrogation strategies are being implemented.
- Ø Different mechanisms should be examined for controlling flap deployment, current operation utilizes a pressure transducer which is monitored and determines the flap deployment. The system currently requires high pressures to fully deploy the flap, even with increased sensitivity and lowered pressure requirements for full deployment, the sensor may be unreasonable for wind tunnel testing. A better examination of the pressures that could be expected will need to be conducted to select a more appropriate sensor. Other sensing methods should be examined for their ability to control the flap deployment, as well.
- Ø The current system is such that it would be difficult to break down and reassemble without time and a deep understanding of the function of the

prototype. This can be cured by the addition of connectors and plugs which would simplify the process and eliminate the possibility of incorrect connections which could cause damage to the prototype.

- Ø Wind tunnel testing should be conducted to determine the effectiveness of the prototype and ensure that the prototype functions as desired and has the desired effect on the lift generated by the airfoil.

Sensors:

- Ø A selection process will need to be conducted to determine a manufacturer of sensors and interrogators which can meet the requirements of embedded optical fibers and sensors for wind turbines. The requirements are not trivial and must be met to achieve a stable and reliable system.
- Ø Methods will need to be devised to allow for the transfer of information between the blades, the hub and the nacelle of the wind turbine.
- Ø Manufacturing techniques will need to be assessed and developed to allow for embedding optical fibers without damaging the fibers and not compromise the laminate, yet keep manufacturing costs low.
- Ø An examination of the optical reliability of embedded fiber optics and FBGs, during the curing process will need to be conducted to ensure there is not excessive signal loss in the embedded fiber optics or a drop in reflectivity in the FBGs and if there is, steps will need to be taken to eliminate the losses.
- Ø The tests regarding the effects of embedded fiber optics on the host laminates, to this point, have been relatively limited in scope, from several

points of view. To this point most work has been done examining only carbon fiber, very little work has been done examining fiber glass, a large scale investigation will need to be conducted examining fiber glass laminates with embedded optical fibers.

- Ø Test so far have been relatively limited in size, much larger examinations will need to be conducted to develop a broad, reliable database of information.
- Ø Tests need to be conducted examining fatigue, not only in tension/tension, but tension/compression as well.
- Ø Different tests, besides simple tension and compression tests, should be conducted to examine multiple loadings which will be encountered during the operation of a wind turbine.

While the work that remains is great, it is not insurmountable and once accomplished, a technology will be available which can be a major asset to wind energy. The effort will be broad and will require many steps and will likely generate many more theses, but an important groundwork is laid out here and should be used as a spring pad to take on the future work.

Closing Remarks

The future of this project will only be determined as the future steps in the development process are completed; however, the information presented in this thesis shows there to be no reason why smart structures should not be an effective mechanism for the development and advancement of wind energy. This work gives direction for the future work to be conducted, as well as a starting point for the many different subjects which will need to be covered in more detail. As well, the prototype will allow for wind tunnel testing and verification of the transient response of the system, presenting an opportunity previously unavailable, as, to this point, no other system has been able to accomplish partial deployment. The opportunities that are afforded by the results of this thesis are bountiful and will provide a valuable well of information and future works, leading to the betterment and advancement of wind energy.

Wind energy will fill an important role in the continued drive to find clean, renewable energy sources. For wind energy to fill this role will require a great deal of research and innovation to aid the development of ever more reliable, efficient and more productive wind turbines. Smart structures will be an important technology in this goal. Since their conception in 200 B.C., windmills and turbines have continuously been an asset to humanity and have continuously evolved, to contribute ever more. The early wind turbines produced in the early to mid 1980s were highly inefficient systems which were built for their capacity and the resulting subsidies, diminishing their potential. Eventually an evolution occurred and new turbines were produced which allowed wind energy to enter the main stream. Yet another evolution will be required to take wind

energy to the next level and become a major contributor to national and worldwide power generation. To accomplish this evolution, this ancient technology will require cutting edge technology and smart structures can help.

REFERENCES CITED

- [1] Department of Energy Table 10.1 Renewable Energy Production and Consumption by Primary Energy Source, 1949-2006. United States Department of Energy. 03/12/2008. <www.eia.doe.gov/emeu/aer/pdf/aer.pdf>
- [2] Mark Rumsey. "Wind Turbine Technology." 11/28/2007
- [3] Simone Kaiser and Michael Fröhlingsdorf. "The Dangers of Wind Power." Spiegel Online, August 24, 2007.
- [4] Summary of Wind Turbine Accident data to November 30th 2007. David Craig Caithness Windfarm Information Forum. 03/19/2008
<<http://www.caithnesswindfarms.co.uk/>>
- [5] Structural Testing Of The North Wind 250 Composite Rotor Joint Clint (Jito) Coleman, Walt Musial and Hal Link 8/8/1994
- [6] McFarland, D Michael and Srinivasan, A.V. Smart Structures Analysis and Design. Cambridge University Press, 2001.
- [7] What is Wind? The British Wind Energy Association. 03/24/2008
<<http://www.bwea.com/edu/wind.html>>
- [8] Dodge, Darrel M. Illustrated History of Wind Power Development. Darrell Dodge and TelosNet Web Development. 03/22/2008
<<http://www.telosnet.com/wind/index.html>>
- [9] A Wind Energy Pioneer: Charles F. Brush. The Danish Wind Energy Association. 03/19/2008 <<http://www.windpower.org/en/pictures/brush.htm>>
- [10] History of Wind Energy U.S. Department of Energy. 03/24/2008
<http://www1.eere.energy.gov/windandhydro/wind_history.html>
- [11] Guey-Lee, Louise. Wind Energy Developments: Incentives in Selected Countries. 03/18/2008, United States Department of Energy.
<http://www.eia.doe.gov/cneaf/solar.renewables/rea_issues/windart.html>
- [12] U.S. Department of Energy. "Wind Energy Today." May 2007.
- [13] Airfoil. Merriam-Webster's Online Dictionary 03/26/2008 <<http://www.merriam-webster.com/dictionary/airfoil>>
- [14] Power Control of Wind Turbine Blades. Danish Wind Industry Association. 03/20/2008 <<http://www.windpower.org/en/tour/wtrb/powerreg.htm>>

- [15] United States Department of Energy. "Renewable Energy Annual 1996 Energy Information Administration." March 1997.
- [16] Thresher, R. W. et al. "Wind technology development: Large and small turbines." NREL, December 1994.
- [17] "NWTC AWT-26 Research and Retrofit Project Summary of AWT-26/27 Turbine Research and Development." NREL, October 1998.
- [18] "AOC 15/50 Wind Turbine Generator." Atlantic Orient Canada Inc., 2003.
- [19] Zaparka, Edward F. "Aircraft and Control Thereof." United States Patent Office, United States Patent 1893065, January 1, 1935.
- [20] Howard, Keith. "The Gurney Flap." Motorsport Magazine, September 2000.
- [21] Richie Ginther. American GP. 12/13/2007
<<http://www.ddavid.com/formula1/ginther.htm>>
- [22] Liebeck, Robert H Design of Subsonic Airfoils for High Lift, Journal of Aircraft September 1978
- [23] Nakafuhi, D.T. et al. "Active Load Control for Airfoils using Microtabs." Journal of Solar Energy Engineering 123.4, November 2001.
- [24] Jang, Cory S. et al. "Numerical Investigation of an Airfoil with a Gurney Flap." Aircraft Design 1.2, June 1998.
- [25] Jeffery, David et al. "Some Aspects of the Aerodynamics of Gurney Flaps on a Double-Element Wing." Journal of Fluids Engineering, March 2001.
- [26] Wang, J.J., et al. "Gurney Flap-Lift Enhancement, Mechanisms and Applications." Progress in Aerospace Sciences 44.1, January 2008.
- [27] Carlson, Jonathan et al. "Smart Wing Structure." May 2007.
- [28] Cairns et al. "Design and Feasibility of Active Control Surfaces on Wind Turbine Blade Systems." AAIA, December 2007.
- [29] The Strain Gauge. Omega. 09/11/2007
<<http://www.omega.com/literature/transactions/volume3/strain.html>>

- [30] Theory-Piezoelectrical Effect-Inverse Piezoelectrical effect. Piezosystem Jena Product Catalog. 06/09/2008 <http://www.piezojena.com/en/products__services/download/manuals/site__350/>
- [31] Piezoelectricity: Overview. eFunda. 06/10/2008
<http://www.efunda.com/Materials/piezo/general_info/gen_info_index.cfm>
- [32] Basics | Piezoelectric Sensors. Piezocryst Advanced Sensorics. 06/10/2008
<http://www.piezocryst.com/piezoelectric_sensors.php>
- [33] Sirohi, Jayant and Chopra, Inderjit. "Fundamental Understanding of Piezoelectric Strain Sensors." Journal of Intelligent Material Systems and Structures 11, April 2000.
- [34] Fiber Optic Sensors. Gavea Sensors. 09/20/2007
<http://www.gaveasensors.com/eng/empresa_tecnologia_bragg.html>
- [35] Fuhr, Peter. "Measuring with Light Part 2: Fiber-Optic Sensing—From Theory to Practice." Sensors Weekly, May 2000.
- [36] Rademakers, L.W.M.M. et al. "Fiber Optic Blade Monitoring." European Wind Energy Conference, November 2004.
- [37] Mandell, J.F. et al. "Fatigue of Fiberglass Wind Turbine Blade Materials." Montana State University, August 1992.
- [38] Fiber Bragg Gratings. Smart Fibres. 08/09/2008
<http://www.smartfibres.com/Fiber_Bragg_Grating.htm>
- [39] Kang, D.H. et al. "The Embedment of Fiber Bragg Grating Sensors into Filament Wound Pressure Tanks Considering Multiplexing." NDT&E International, July 2006.
- [40] "Optical Fiber Sensors Guide-Fundamentals & Applications." Micron Optics.
- [41] Hill, Kenneth O. et al. "Fiber Bragg Grating Technology Fundamentals and Overview." Journal of Lightwave Technology, August 1997.
- [42] Barbezat, Michel et al. "Integrated Active Fiber Composite Elements: Characterization for Acoustic Emission and Acousto-ultrasonics." Journal Of Intelligent Material Systems And Structures 18, May 2007.
- [43] Sodano, Henry A. "Macro-Fiber Composites for Sensing, Actuation and Power Generation." July 28, 2003.

- [44] Doyle, Crispin. "Fibre Bragg Grating Sensors-An Introduction to Bragg Gratings and Interrogation Techniques." Smart Fibres Ltd., 2003.
- [45] "Licensing Fiber Bragg Gratings." Communications Research Centre Canada, June 2005.
- [46] Meltz, et al. "Formation of Bragg gratings in optical fibers by a transverse holographic method." Optics Letters, August 1, 1989.
- [47] Lefebvre, P. et al. "Reliability characterization of fiber Bragg grating." Optical Society of America, 2006.
- [48] Hill, K. O. et al. "Bragg gratings fabricated in monomode photosensitive optical fiber by UV exposure through a phase mask." American Institute of Physics, 1993.
- [49] Micron Optics-Fiber Optic Sensors. Micron Optics. 06/24/2008
<<http://www.micronoptics.com/sensors.htm>>.
- [50] Bogue, Robert. "UK Start-up Poised to Take the Fibre Optic Sensor Market by Storm." Sensor Review 25.1, 2005.
- [51] Mendez, Alexis. Email communication between James Blockey, Tom Graver and Alexis Mendez PhD of Micron Optics, 12/13/07.
- [52] Kang, D.H. et al. "Mechanical Strength Characteristics of Fiber Bragg Gratings Considering Fabrication Process and Reflectivity." Journal of Intelligent Materials Systems and Structures 18, April 2007.
- [53] Baker, Stephen R et al. "Thermal Decay of Fiber Bragg Gratings Written in Boron and Germanium Codoped Silica Fiber." Journal of Lightwave Technology, August 1997
- [54] Leconte, Bruno, et al. "Analysis Of Color-Center-Related Contribution to Bragg Grating Formation in Ge:SiO₂ Fiber Based on a Local Kramers-Kronig Transformation of Excess Loss Spectra." Applied Optics, August 1997.
- [55] Douay, M. et al. "Densification Involved in the UV-Based Photosensitivity of Silica Glasses and Optical Fibers." Journal of Lightwave Technology, August 1997.
- [56] Erdogan, T. et al. "Decay of Ultraviolet-Induced Fiber Bragg Gratings." Applied Physics, July 1994.

- [57] Shivakumar, Kunigal and Bhargava, Anil “Failure Mechanics of a Composite Laminate Embedded with a Fiber Optic Sensor.” Journal of Composite Materials, March 2004.
- [58] Friebele, C G. “Optical Fiber Sensors for Spacecraft Applications.” Smart Materials and Structures, August 1999.
- [59] Silva, Jose M.A. et al. “Mechanical Characterization of Composites with Embedded Optical Fibers.” Journal of Composite Materials, 2005.
- [60] Surgeon, M. and Wevers, M. “Static and Dynamic Testing of a Quasi-Isotropic Composite with Embedded Optical Fibres.” Composites Part A: Applied Science and Manufacturing, April 1999.
- [61] Surgeon, M. and Wevers, M. “The Influence of Embedded Optical Fibres on the Fatigue Damage Progress in Quasi-Isotropic CFRP Laminates.” Journal of Composite Materials, 2001.

APPENDICIES

APPENDIX A

EXPANDED HISTORY AND BACKGROUND DISCUSSION

Early History

As the sun heats the earth, it heats different regions at different rates; land for example heats more quickly than water does. The differing rate at which the earth is heated by the sun causes a pressure gradient in the atmosphere. Air which is heated more rapidly rises, this rising of hot air causes a drop in pressure, which then draws in cold air, resulting in wind [7]. This movement of air provides an incredible source of energy, one that has been garnered and utilized for thousands of years.

The first recorded use of wind energy dates back to around 5000 B.C., on the Nile River, where wind was used to propel sail boats [10]. However, the use of wind to power mills developed first in China around 200 B.C., for pumping water. By the 6th century A.D., in Persia, wind energy had begun to be utilized for pumping water and grinding grain, as well [8]. Early mills were of a vertical axis design, about which sails woven of reed or wood, were mounted, similar to the replica seen in Figure 64. The design of the vertical axis mills meant that they were only able to utilize half the air that came at them and as a result were very inefficient.

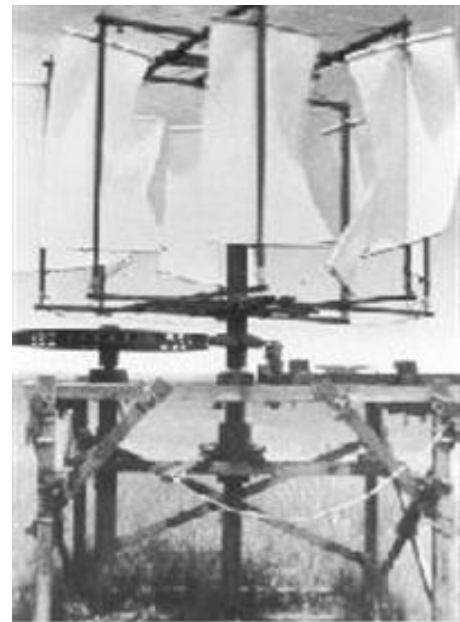


Figure 64: A replica of an early Persian, vertical style, windmill.

In the 13th century the use of wind power made its way to Europe. However, the European mills used a much different design than those of Persia and China; they utilized

a horizontal axis of rotation (Figure 65), similar to most modern wind turbines. The evolution to this style of mill is a mystery, but may have been linked to the horizontal axis style of water wheels that were used; it also resulted in much higher levels of efficiency [8]. These mills continued to evolve over the course of hundreds of years to produce ever more efficient systems. The uses for these mills continued to evolve as



Figure 65: Dutch windmills, typical of later European style windmills with more advanced blade designs.

well, expanding to include timber mills, irrigation and processing spices and tobacco. However, with the invention and spread of the steam engine, in the 19th century, the use of these mills began to decline [8].

In the remote areas, such as the western U.S., the use of wind mills continued to grow, largely after the introduction of the Halladay mill in 1854 [8]. These early mills utilized wooden blades attached to a rim, with a trailing fin to align the mill to the wind. Later, the mills were greatly improved with the introduction of steel blades, which could be shaped better and were lighter weight. These mills were generally small systems, with

a diameter around 3 feet and were used primarily for water pumping [8]. The use of these systems continued well into the 20th century.

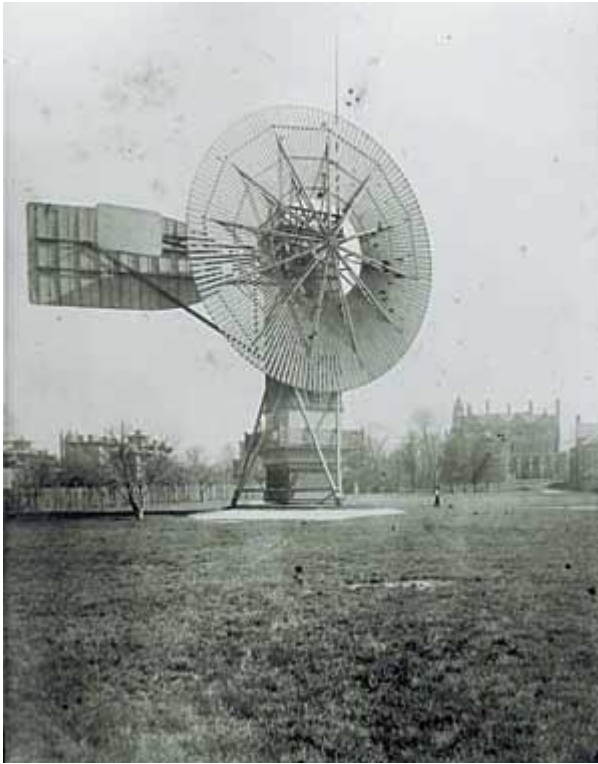


Figure 66: The Brush wind turbine was the first to use wind energy for the generation of electrical power. © the Charles F. Brush Special Collection.

In 1887, Charles Brush began building what would be the first electricity generating wind turbine (Figure 66). His was a massive device, with a rotor diameter of 50 ft and capable of generating 12 kW [9]. His wind turbine was also the first to use a step-up gear box, increasing the rotational speed of the output shaft. It operated for 20 years, charging batteries in his basement. However the design had several limitations in electricity production, namely, his turbine used many blades, which

rotated relatively slowly, resulting in a very inefficient system. This was overcome by Dane Poul La Cour in 1891, a trained meteorologist in Denmark. La Cour's design utilized a four blade, high speed rotor design which proved to be highly effective and practical [9].

With the limited power grid in the early 20th century and the vast remote expanses of the U.S., wind turbines provided a necessary source of energy in many locations. In

the 1920s, with the development of the airplane and the accompanying advancements in airfoil design, much advancement was made in the design of the blades used on wind turbines, increasing their efficiency [8]. However, in the 1930s, the federal government began the Rural Electrification Administration, which developed the power grid in many remote locations [10]. The development of the power grid led to a decline in the use of wind turbines, which were replaced by coal and steam powered generators. Despite this, the rise in efficiency combined with the size and remoteness of many communities in the Midwest and Western U.S., Europe and Australia meant that the use of wind turbines for power generation would remain critical [8]. A trend of rising and falling use of wind power continued for much of the 20th century, largely following expansion of the power grid, the power requirements and the cost of fossil fuels.

Modern Developments

20 years ago, in the United States and around the world, renewable energy was a minor factor in the total production of energy. The price of oil had subsided and stabilized and there was little competition, for oil, in the world market. However the oil crisis of the 70s had not gone unnoticed. While the crisis had eased, it had shown a volatility in the oil market which couldn't be ignored [10, 11]. That combined with the growing concern for pollution and

clean air began to push the search for 'green,' renewable energy sources. For most of human history renewable sources were the only sources of energy. Wind, water and biomass were essential to human survival for thousands of years, until the use of fossil fuels became wide spread (Figure



Figure 67: The 1300 MW Seminole Generating Station, a coal-fired power station, located in Florida, approximately 50 miles from Jacksonville. Courtesy Seminole Electric Cooperative.

67). For many years fossil fuels were the cheapest source of energy and the environmental impact caused by the use of fossil fuels was not yet understood. In the 70s and 80s, that all began to change and the resulting push for renewable energy resulted in many of the ancient sources of energy being examined once again.

The production of energy from wind didn't register until 1983 and at that time levels were less than one-one thousandth of a percent of the total renewable energy

production [1], which itself made up only a small portion of the total energy production of the United States (Figure 68). However, government legislation and incentives had begun to make wind energy and the construction of new wind turbines, a more enticing

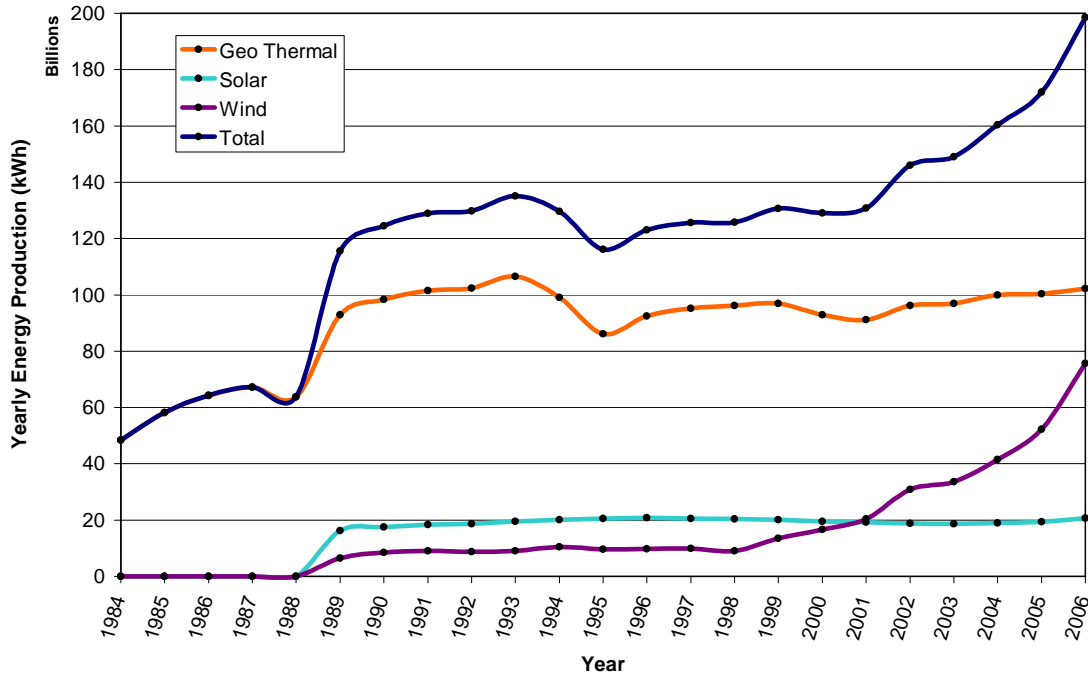


Figure 68: The yearly production of renewable energy in the United States between 1984 and 2006.

opportunity. This started in 1978 with the passage of the Public Utility Regulatory Policies Act, which guaranteed the electricity produced would be bought by the utilities, creating a market for wind generated electricity. When combined with tax credits that, in some cases, covered over 50% of the cost of the investment, wind became a viable option for generating electricity, giving rise to the industry [11].

By the mid 1980s several problems arose, that negatively impacted the wind energy industry. Key among these was a sustained period of low oil and natural gas costs and related technological advancements and the expiration of some contracts and

incentives. While technological advancements were occurring in wind energy the rate at which the field was advancing was much slower than initially expected. Early on, large scale wind turbines were often very inefficient mechanisms, achieving capacity factors which were sometimes as low as 5-10% [11]. These early designs were built largely to take advantage of government incentives which benefited capacity over productivity. This kept the cost of wind energy high, near \$0.80/kWh in 1980 [12], making wind a very expensive and impractical source of electricity.

In the early 1990s many steps were taken to reestablish wind as a viable source



Figure 69: During the 1990s government funded research into wind energy increased, providing an important key in the advancement and resulting expansion of wind generated electricity [2].

for the generation of electricity. This included a vast array of tax credits which were established, that focused on electrical generation, rather than capacity. Property taxes were reduced for land used for wind energy, reducing the burden of running a wind farm. Government subsidized loans were provided for the development of wind farms, keeping interest rates low, easing some of the costs of developing a wind farm. Also key was an increased amount of money provided by the government for research (Figure 69).

The government assistance and technological advancements helped spread the use of wind energy. In many cases the overall growth of wind power was plagued by the design of early wind turbines, which were being removed as fast as new mechanisms could be built. The new generation of wind turbines rapidly increased in size, output and efficiency and in the late 1990s the overall power produced by wind began to grow rapidly. The trend has continued ever since, now the cost of wind power has dropped to around \$0.04/kWh [12], making it a much more practical source of electricity. While the growth has been rapid, much work remains. The Advanced Energy Initiative, launched by President George W. Bush in 2006, pushes for the nation to draw on wind for 20% of all electrical generation, more than 20 times the current production [12].

APPENDIX B

UTILIZED PROTOTYPE COMPONENTS

Components Used During Prototyping

The development of the prototype utilized numerous different components, for numerous purposes. The information about the major individual parts, their purposes and their manufacturer information is presented in Table 13. Many other common pieces were used, such as wiring and connectors and are not included in this table.

Table 13: A listing of all the major components used in the construction and testing of the prototype throughout the development process.

Component	Manufacturer	Series	Item Number	Stages Used	Purpose
Linear Actuator	Ultra Motion	Bug	2-A.4-DC92_24-4-2NO-ST4/4	1-4	The actuator was utilized to extend and retract the flap.
http://www.ultramotion.com/products/bug.php					
Batteries	Interstate	Cycle-Tron	YB7-A	1-4	To power the prototype and sensors.
http://www.interstatebatteries.com					
Batteries	Bikemaster	Platinum	12V7B-B	4	Gel cell batteries, which replaced the YB7-A batteries to allow the prototype to be carried onto an airplane.
http://www.powersportrider.com/cgi-bin/zcatjpg					
Battery Charger	Battery Tender		022-0165-DL-WH	4	Two bank battery charger to completely charge both batteries simultaneously.
http://batterytender.com/product_info.php?products_id=55&osCsid=a7583b8874fc79e7f31e289148be4cd3					
DPDT Contact Relays	ELK Products		ELK-924	1-2	To change the direction of motion of the actuator; used on the Stage 1 and 2 Prototypes.
http://www.smarthome.com/7277.html					

Table 13 Continued

SPST Solid State Relays	Crydom		D1D12	3-4	To take the place of the contact relays on the Stage 3 and 4 Prototypes.
http://www.crydom.com/home.htm					
Linear Potentiometer	Celesco	CLP	CLP-100	2-4	To monitor the displacement of the actuator.
http://www.celesco.com/linearpot/					
LVDT	Omega	LD620	LD621-50	2	To monitor the displacement of the actuator.
http://www.omega.com/pptst/LD620.html					
Linear Damper	ACE Control	HB	HB-15-150-AA-P	4	To absorb some of the momentum of the actuator, at power off.
http://www.acecontrols.com/					
Semiconductor Fuse Box	Ferraz Shawmut	Ultrasafe	USM1	3-4	Fuse holder for semiconductor fuse.
http://us.ferrazshawmut.com/					
Semiconductor Fuse Box	Ferraz Shawmut	Ultrasafe	USM2	4	Double fuse holder for semiconductor fuses.
http://us.ferrazshawmut.com/					
Semiconductor Fuses	Ferraz Shawmut	A60Q	A60Q12-2	3-4	To protect the solid state relays from overloading.
http://us.ferrazshawmut.com/					
Pressure Transducer	Omega	PX209	PX209-015G5V	1	Monitoring air pressure for operating the control program.
http://www.omega.com/pptst/PX209_PX219.html					
Pressure Transducer	Omega	PX309	PX309-015G5V	4	Monitoring air pressure for operating the control program.
http://www.omega.com/pptst/PX309.html					

Table 13 Continued

DAQ Chassis	National Instruments		SCXI-1000DC	1-2	Battery powered DAQ chassis for use with LabVIEW 6. Used with Stage 1 and 2 Prototypes.
This component is now out of date and has been replaced by the USB-6229 below.					
DAQ Cards	National Instruments		SCXI-1200 SCXI-1302	1-2	Cards used with SCXI-1000DC chassis, allowing for output voltages.
These components are now out of date and have been replaced by the USB-6229 below.					
DAQ Unit	National Instruments	USB M	USB-6229	3-4	DAQ system for Stage 3 and 4 Prototypes, utilizing a USB connection and allowing more output channels.
http://sine.ni.com/nips/cds/view/p/lang/en/nid/203094					
Sprinkler Control Valve	Rain Bird		100 DV	1	For controlling air release for virtual flap.
http://www.rainbird.com/parts/valves_electric.htm					
AC Variable Power Source	Aloe Scientific	Powerstat	116-1	1	Power source for control valve.
Aloe Scientific no longer exists, any generic AC power controller will be sufficient.					

APPENDIX C

CONTROL PROGRAMS DETAIL

Because of its icon based nature, LabVIEW is a difficult program to explain and it is even more difficult to attempt to follow the work of another programmer. Many different programming styles and methods are possible and each person will have their own, making it yet more difficult. As the prototyping portion of this project is very heavily LabVIEW based, additional explanation of the programs to try and provide assistance with understanding the function of the programs, this will not explain, fully, each program, as that is not possible, but will hopefully help shed some light on them.

The Virtual Flap Control Program

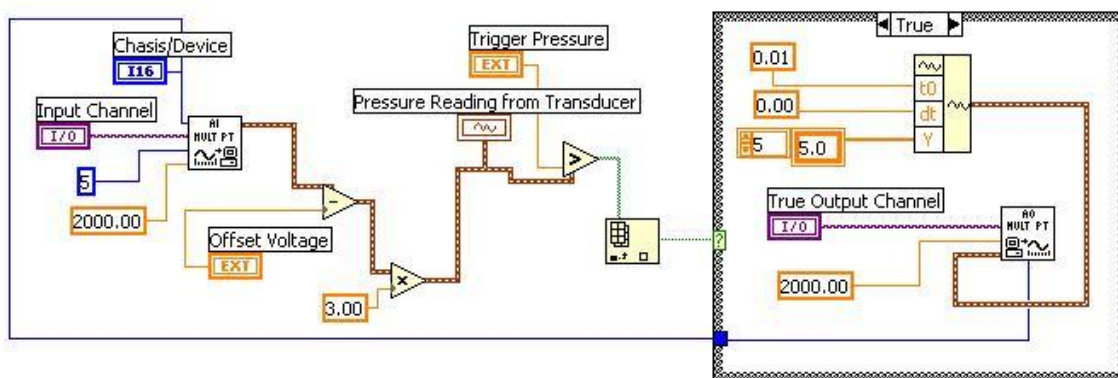


Figure 70: The complete virtual flap control program.

Shown in Figure 70 is the complete program, which is divided into three main components, the data input, data manipulation and logic and the output controls. The data input (Figure 71) controlled the voltage signal coming from the pressure transducer, which was then converted to a pressure by the data manipulation and logic portion of the program (Figure 72), where the pressure value was compared to an allowable pressure, input by the user. If the allowable pressure was exceeded by the signal from the pressure transducer a true signal was sent to the logic boxes (Figure 73), the output portion of the

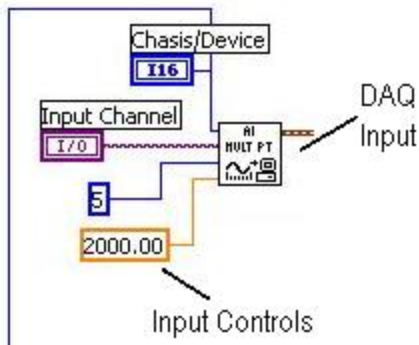


Figure 71: The input control.

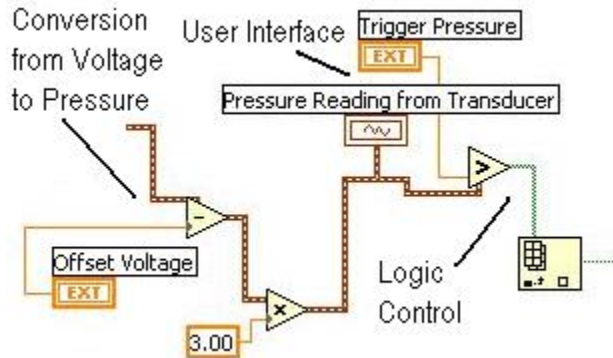


Figure 72: The output control and pressure logic.

program sent 5V to activate the relay, if false, 0V was sent to the relay, which closed it. With a 0V output the Y values were changed from 5 to 0. The values of t_0 and dt were found to be inconsequential to the operation of the program and could be left at 0. The program was very simple with only one output and one input. The program was built in LabVIEW 6.

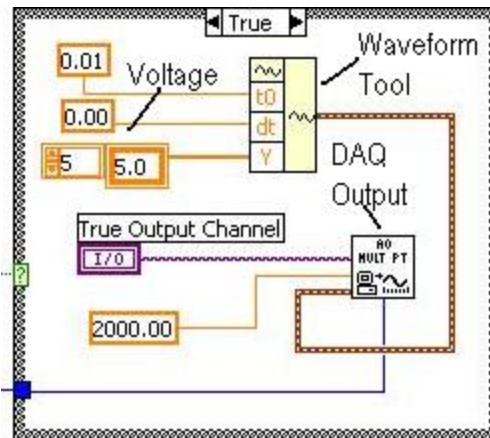


Figure 73: The output control.

The Stage 1 Prototype

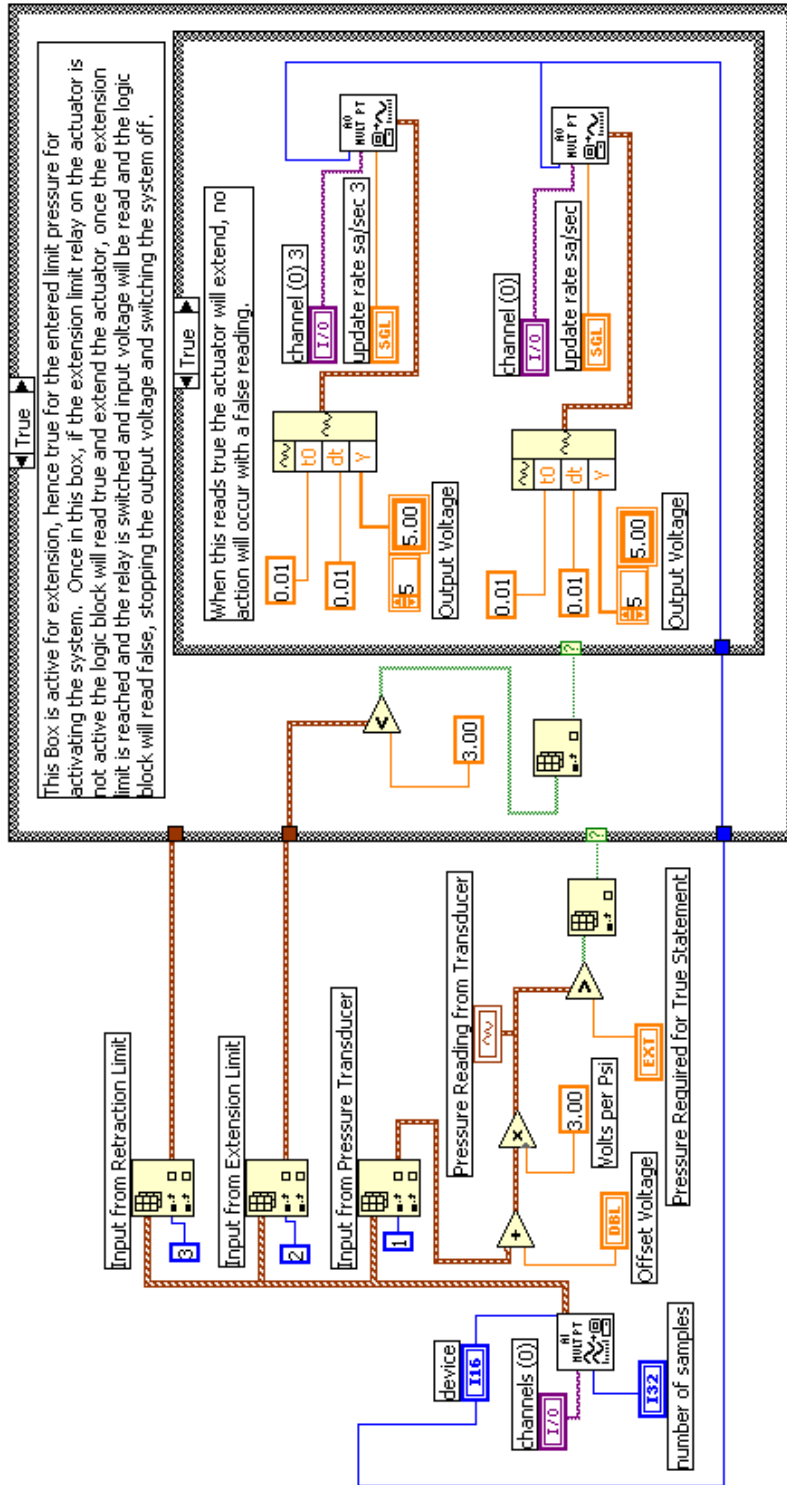


Figure 74: The complete Stage 1 Prototype control program.

While still a relatively simple program, the control program for the Stage 1 Prototype (Figure 74) was significantly more complex than that of the virtual flap. The program was built with a on-off structure. Three separate inputs were monitored (Figure 75), the input voltage from the pressure transducer as well as voltages from the magnetic switches, used for the limits of motion. No data manipulation of the voltages from the switches was needed as they were monitored only for a voltage being present or not. The pressure input utilized the same data manipulation and logic as before, for the virtual flap (Figure 76). The logic box structures and output controls (Figure 77) were where the program increased dramatically in complexity. Four different conditions were possible:

- ∅ Actuator Extension-A true-true condition where the pressure exceeded the set tolerance and the actuator had not yet reached the extension limit, 5V output to both relays.
- ∅ Actuator Stop Extension-A true-false condition where the pressure exceeds the set tolerance, but the actuator has reached the extension limit, 0V output to both relays.
- ∅ Actuator Retraction-A false-true condition where the pressure is below the set tolerance, but the actuator is not at the retraction limit. 5V is sent to the retraction relay and 0 V is sent to the other.
- ∅ Actuator Stop Retraction-A false-false condition where the pressure is below the set tolerance and the actuator is at the retraction limit. 0V is sent to both relays.

This allowed the actuator to extend once a sufficient pressure level was reached, but shut the power to the relays off once the actuator was fully extended, once the pressure dropped below the logic system controlled the voltage to retract the flap, until the magnetic switch at the fully retracted point was flipped, shutting off the voltage. The program was built in LabVIEW 6.

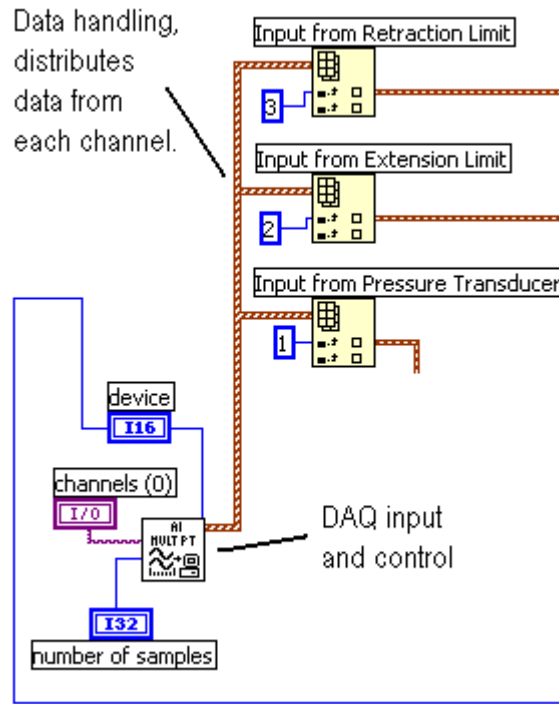


Figure 75: The input control.

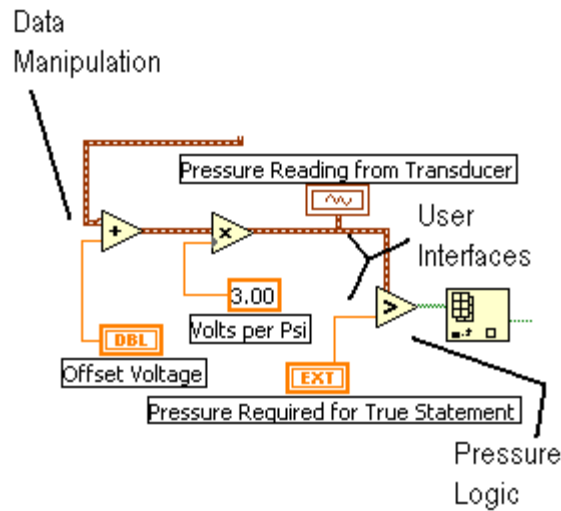


Figure 76: The data manipulation and logic section.

The Stage 2 and Stage 3 Prototypes

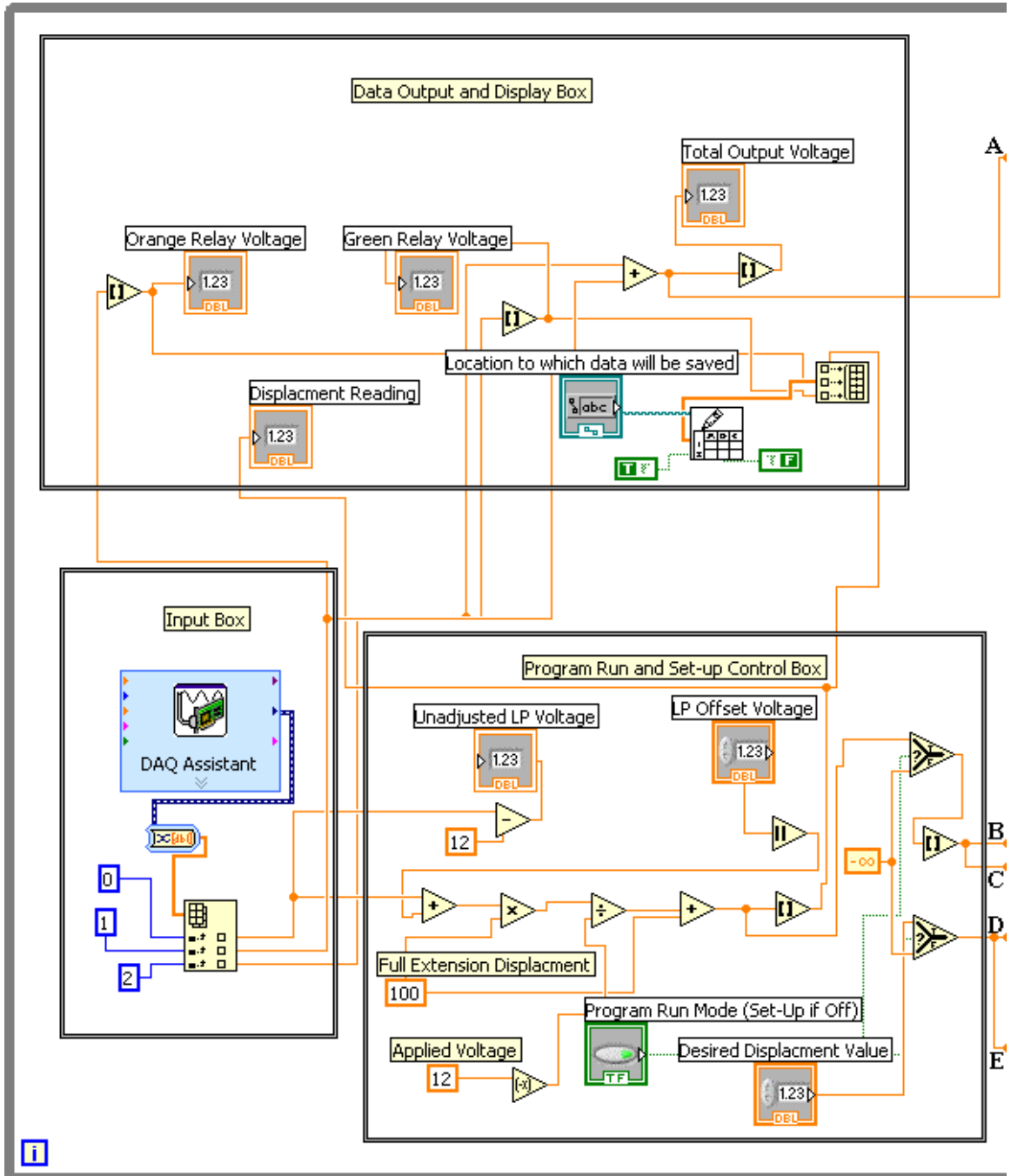


Figure 78: The first half of the Stage 2 and 3 Prototype control program. The connections to the second half of the program can be seen on the right hand side of the program, labeled A-E.

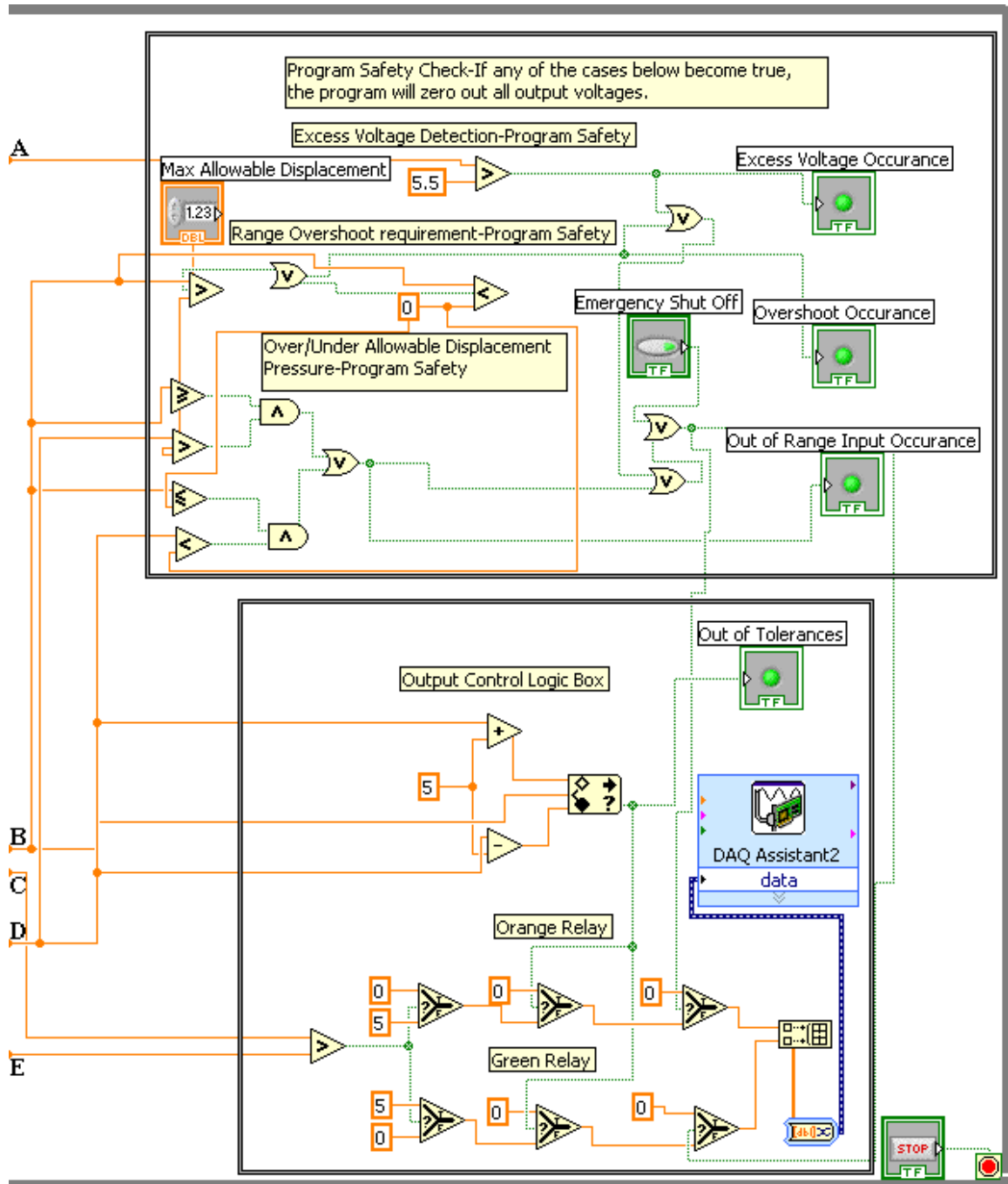


Figure 79: The second half of the Stage 2 and 3 Prototype control program. The connections to the first half of the program can be seen on the left hand side of the program, labeled A-E.

The Stage 2 and Stage 3 Prototype control programs were designed with the same premise, allowing them to be described together. The operation of the program moved from the on-off design of the previous program to a partial deployment design, adding to the complexity. One of the first changes made was to move the program (Figures 78 and 79) inside of a while loop, the grey box going around the entire program. With the while loop, the program cycled continuously until it was stopped, or while the stop button was false. This allowed for faster cycling and a higher data acquisition rate. In addition to the input, data manipulation and output sections, two additional sections were added into the program; data to file output and safety controls. The program was moved to LabVIEW 8 and as such utilized the DAQ Assist modules to construct the inputs and outputs (Figure 80).

The partial deployment required the addition of an extensometer, the LP that was chosen required signal manipulation, which added to the complexity of that section (Figure 81). As well, the logic boxes were eliminated and replaced by logic switches, which were cleaner, simpler and streamlined the program, a buffer zone was created around the desired displacement to help stabilize the system (Figure 82). The data output box was included so that a full range of data could be examined to monitor the performance of the system and control program (Figure 83). The safety switches were needed to prevent a short circuit which the solid state relays were very sensitive to and were designed to zero the output voltage if a short scenario occurred (Figure 84). The size of the file was detrimental to its cycling speed and slow sampling rates resulted. The program needed to be simplified to achieve better performance.

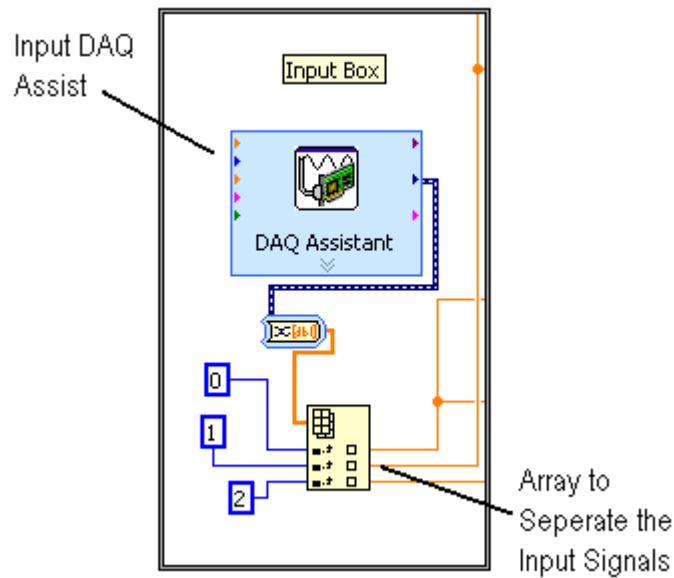


Figure 80: The input controls, utilizing the DAQ Assist.

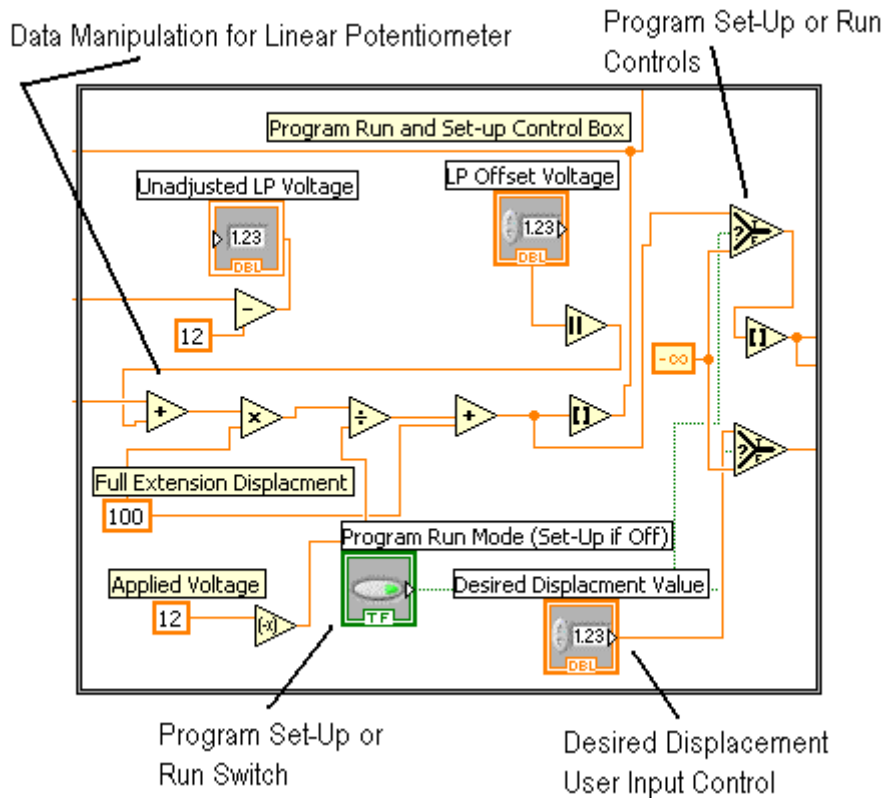


Figure 81: The data manipulation module and user controls.

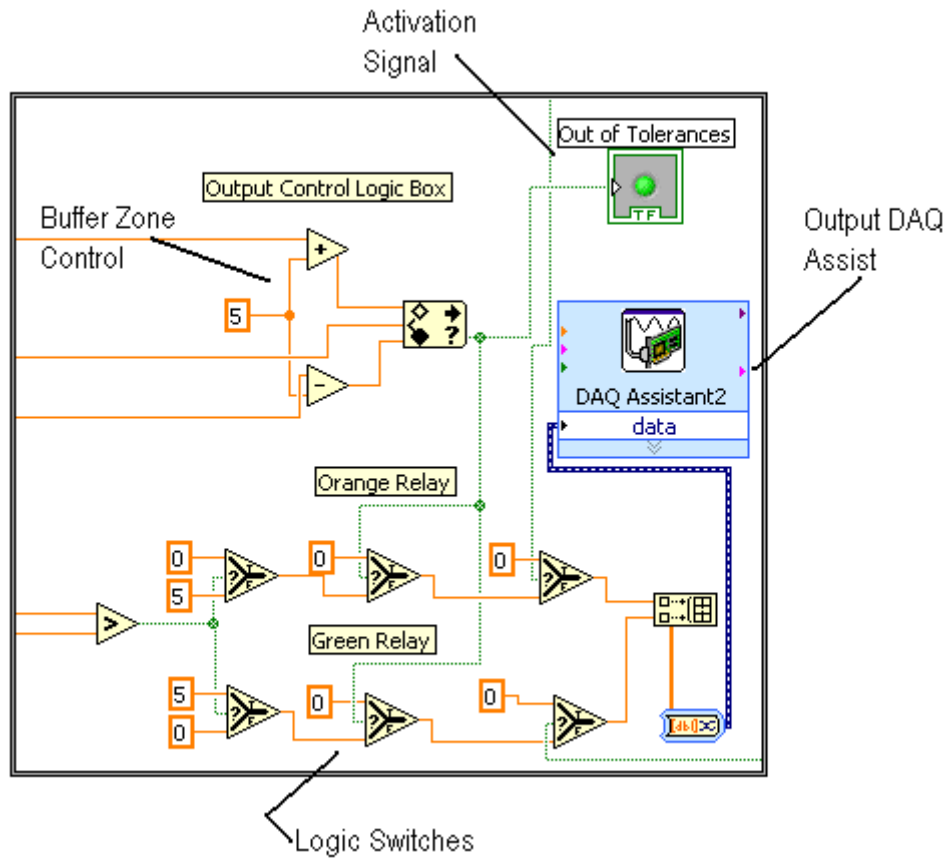


Figure 82: Output control and logic box, utilizing logic switches.

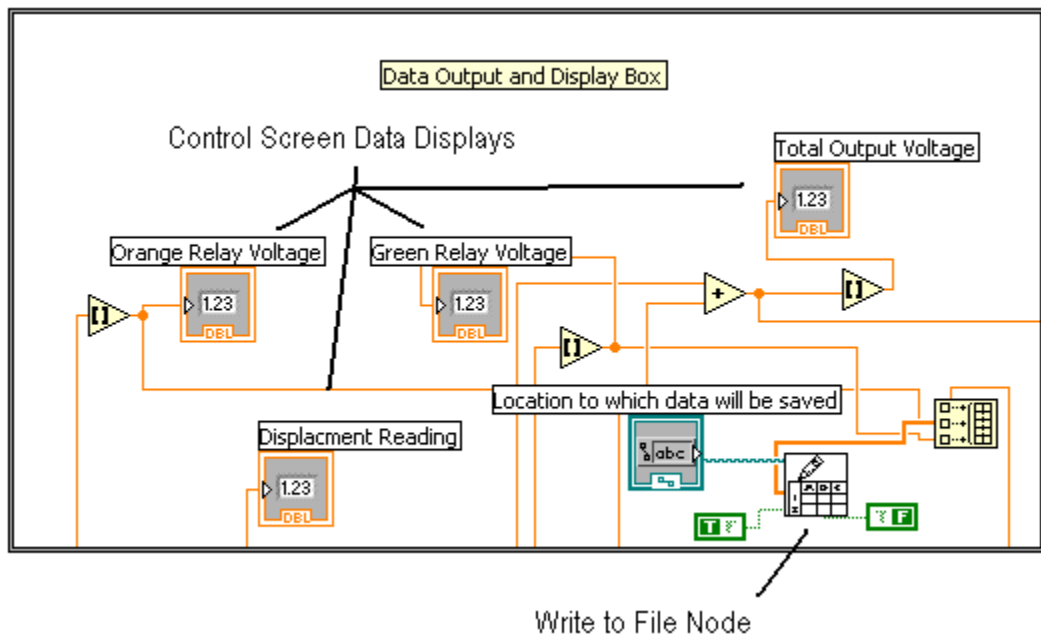


Figure 83: Data write to file output box and control screen display box.

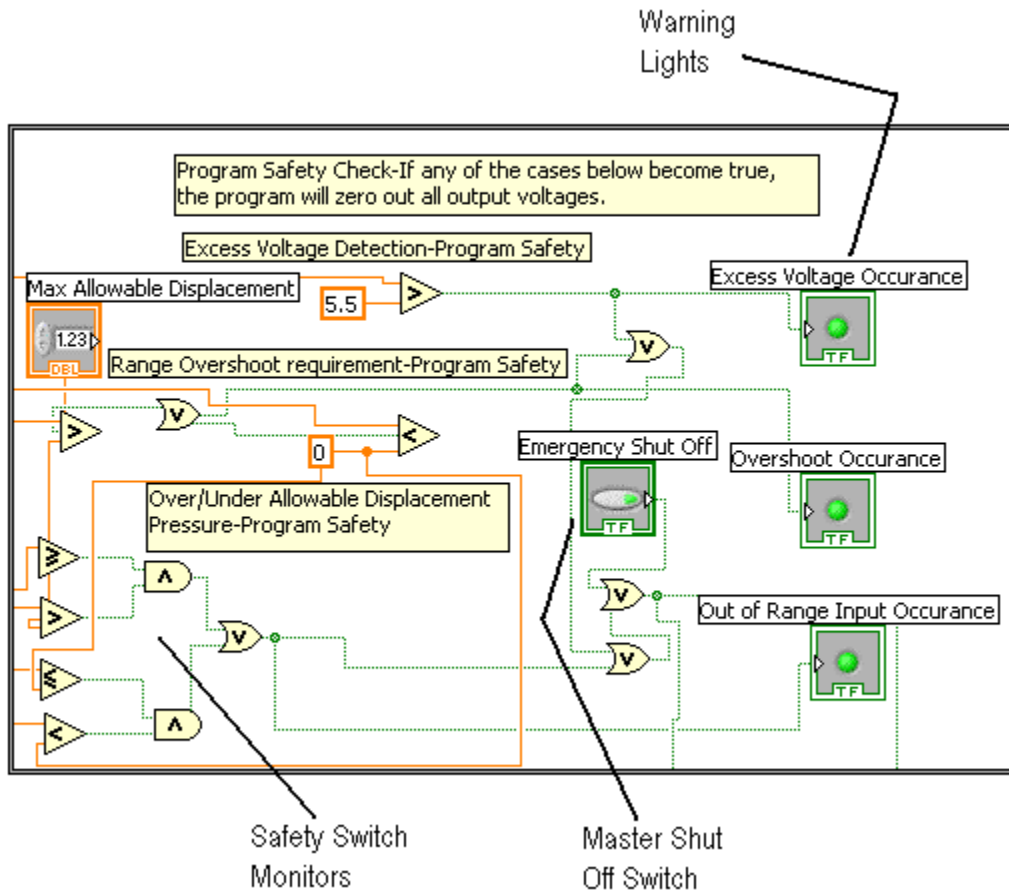


Figure 84: Program safety switches and display box.

Stage 4 Prototype-Math Script Based

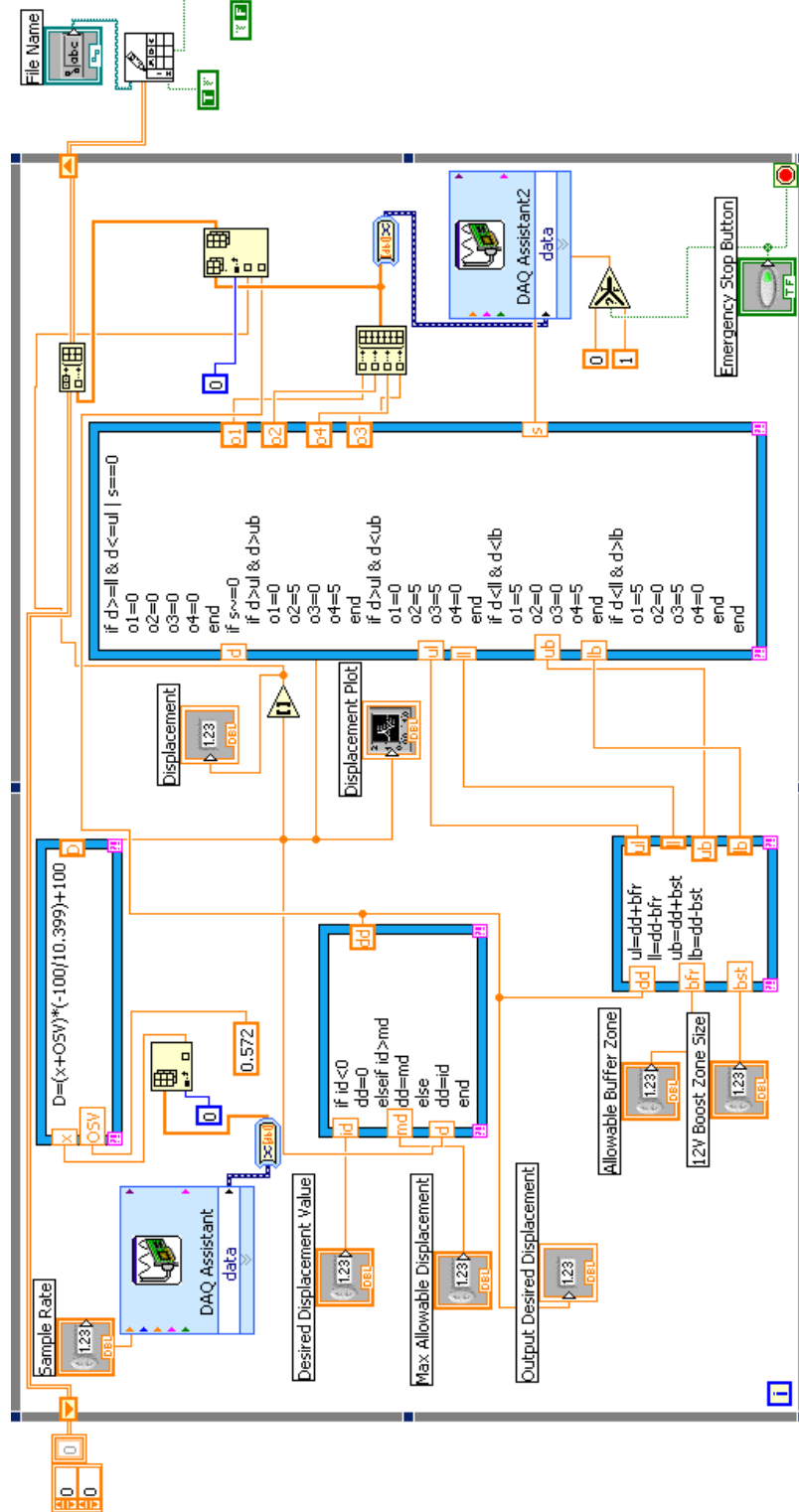


Figure 85: The complete Stage 4 Prototype Math Script based program.

The first Stage 4 Prototype program (Figure 85) which was assembled was very different from all previous programs; utilizing a more conventional MatLab based programming code for most of the program, located in Math Script boxes (Figures 86). The program was also the first to utilize the boost voltage; switching the voltage to the actuator from 24V to 12V as the actuator approached the desired displacement. This required the addition of three more relays which had to be controlled, on two outputs, for a total of four output channels (Figure 87). The write data to file component of the program was moved outside of the while loop by adding a shift register (Figure 88), this allowed the data to be written after the program was run rather than with each loop, this reduced the cycling time. The safety switches were found to be, generally, unnecessary and with appropriate measures taken to protect the relays, the switches were unnecessary and were eliminated to condense the program further. The general operation of the program was about the same, just formatted differently to attempt better operation.

In operation the program proved to be no faster than the previous programs, due in part to the amount of memory consumed by each Math Script box, they were found to consume large amounts of memory causing the files to be larger than that of the previous program. The boost proved to be an asset, helping to reduce overshoot and improving the system accuracy. The program worked flawlessly, as far as operation and protecting the relays, but it was not the solution to accelerating the control program performance.

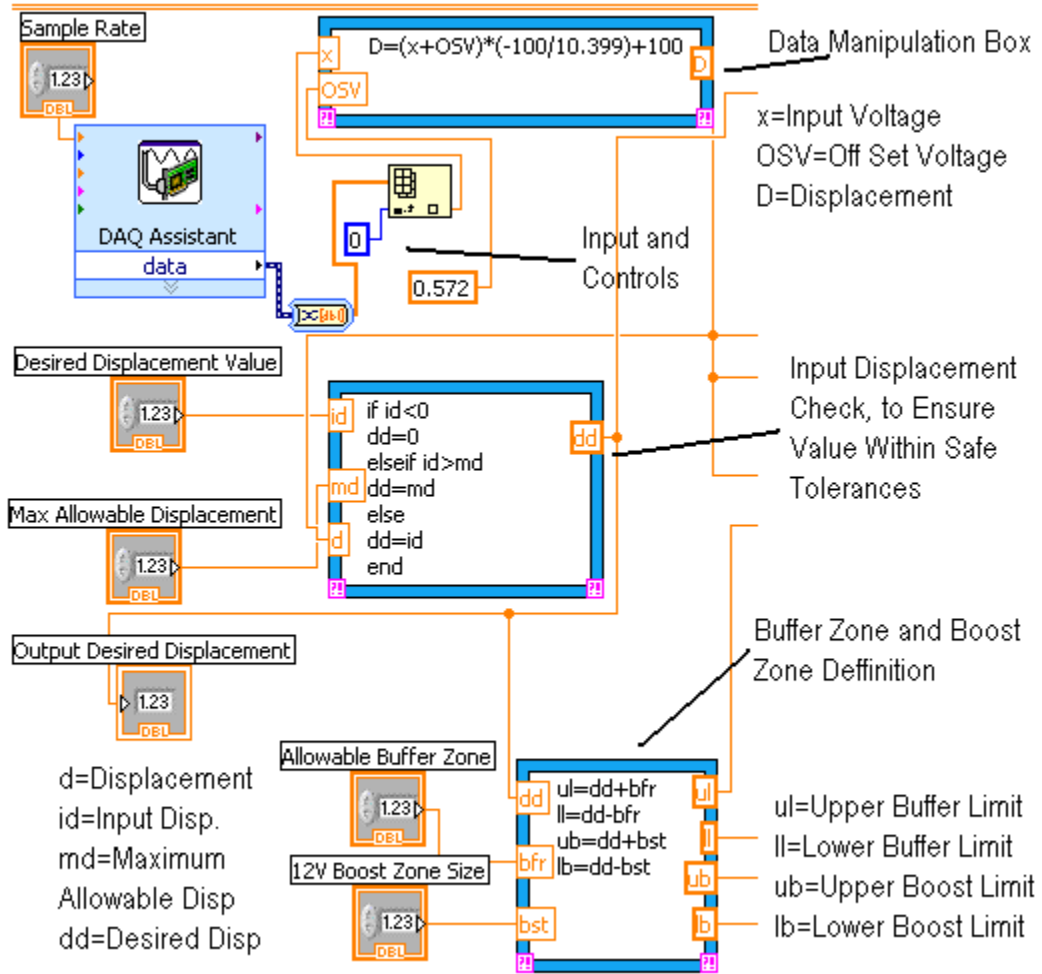


Figure 86: The input and data manipulation of the Math Script box version of the Stage 4 Prototype control program.

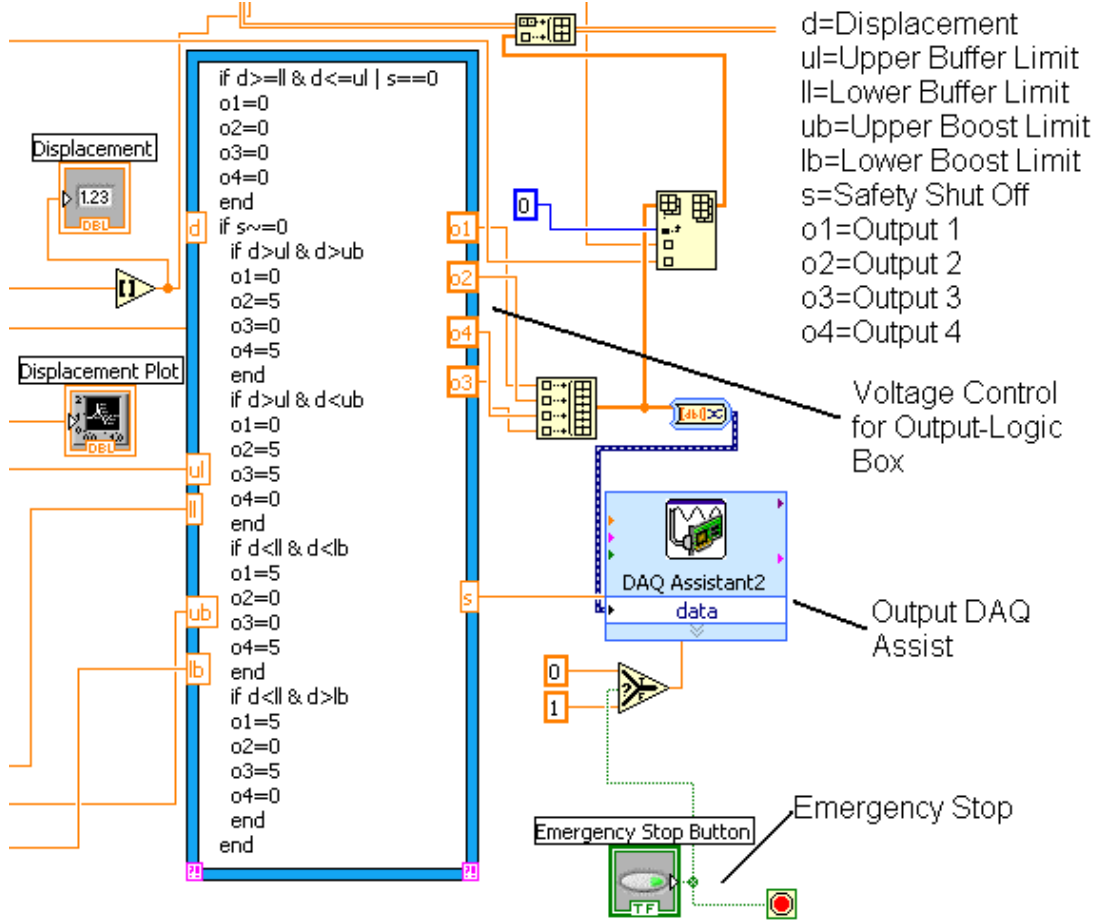


Figure 87: The output control and voltage control-logic box portion of the program.

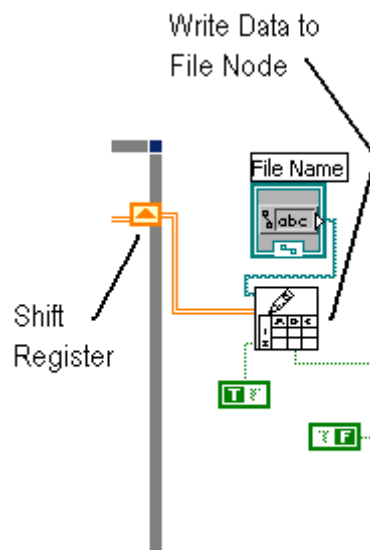


Figure 88: The shift register and data writing node.

Stage 4 Prototype-Logic Switch Based

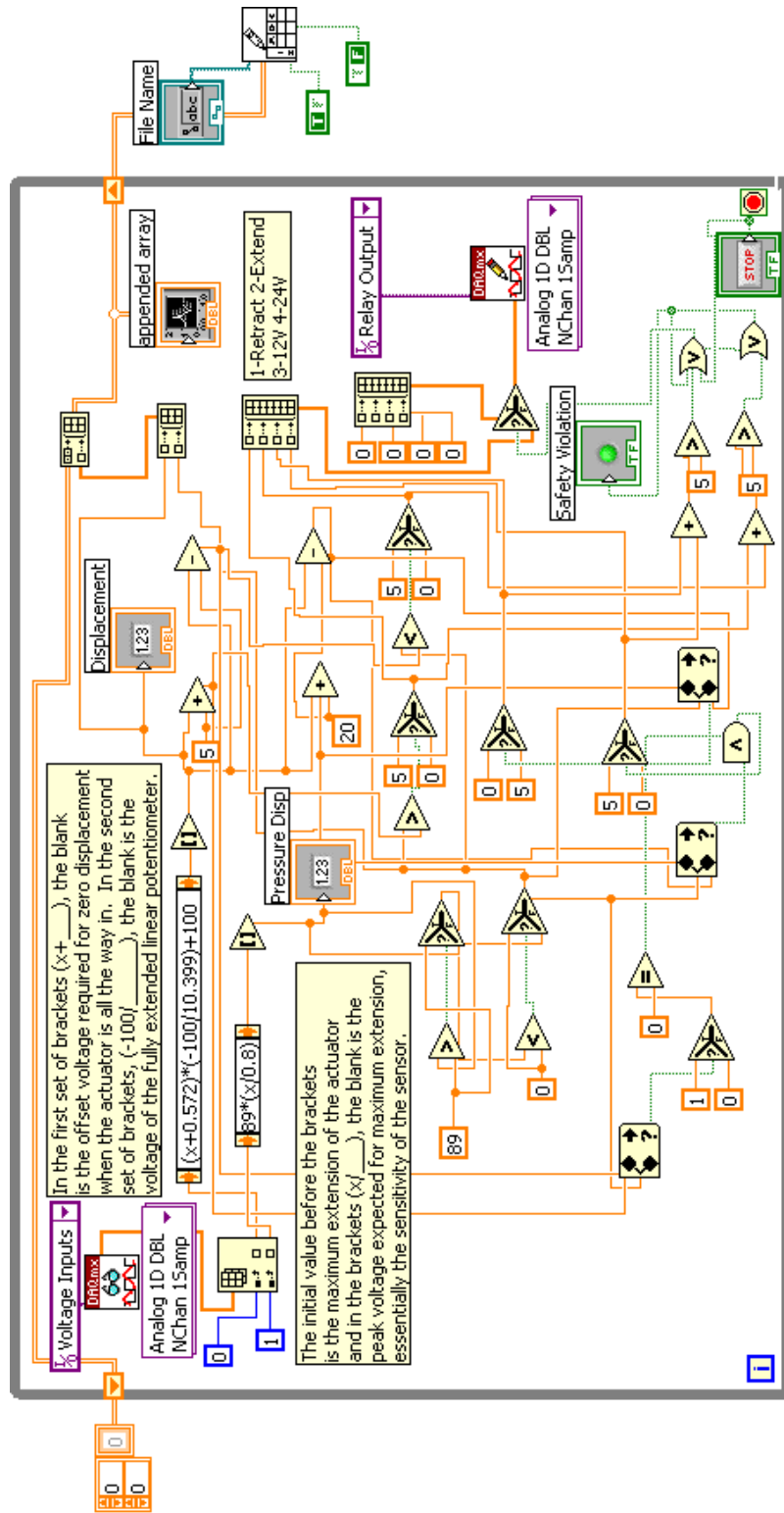


Figure 89: The complete Stage 4 Prototype control program based on logic switches.

The attempt to use Math Script boxes proved to be ineffective so another program was developed which, once again, utilized logic switches (Figure 89). The logic structure was completely reexamined and redesigned to allow for simpler operation (Figure 90), the restructuring required adding several new components and became difficult to organize, resulting in a much messier system, but one which worked more effectively. During the design process, a glitch occurred which would occasionally cause a short to occur, so a safety was added to prevent this from damaging the relays. The glitch was later resolved, but the safety switch was left in, it could likely be removed now and safe operation would remain. To reduce memory requirements further the DAQ assist modules were removed and replaced with the more contemporary DAQ inputs (Figure 91) and DAQ outputs (Figure 92), used in the first two programs. The data manipulation was simplified by the use of what is known as expression nodes (Figure 93) which took the input voltage and plugged it into an equation and output the desired metric, rather than running it through a series of nodes, similar to, but simpler than the Math Script Node. The Stage 4 Prototype also incorporated the pressure transducer which was included into the program by the addition of a second input. The write to file, data output, remained outside of the while loop through the use of a shift register.

Once completed the program was smallest and least memory intensive program produced. Tests of the program also showed it to perform the best of all the programs designed. The performance was not as expedient as desired, but the simplified, yet messier structure proved to be the best answer yet, simpler and better programs may be possible, but they will likely require intensive examination of LabVIEW programming.

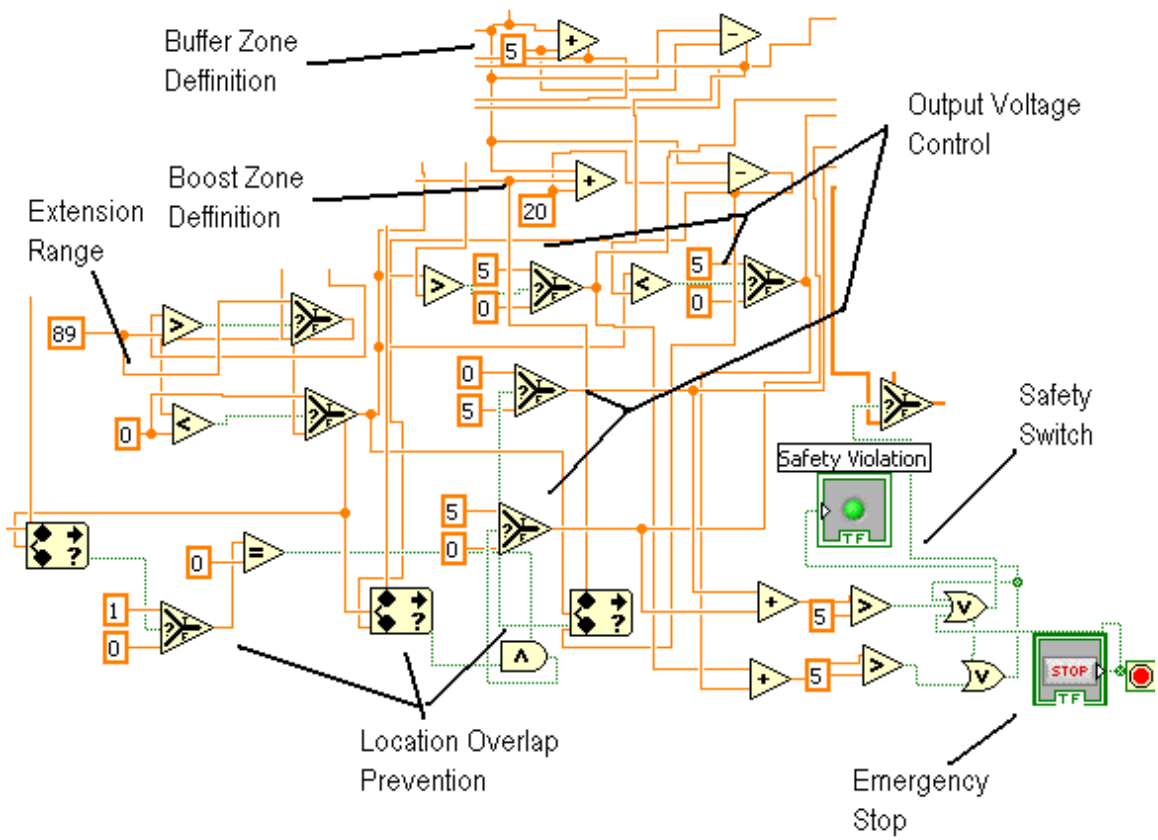


Figure 90: The logic portion of the program, utilizing the logic switches again, completely restructured, allowing faster operation, but becoming cluttered and difficult to follow.

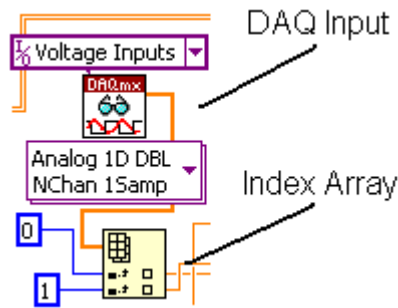


Figure 91: The output voltage control and output DAQ, no longer utilizing the DAQ Assist.

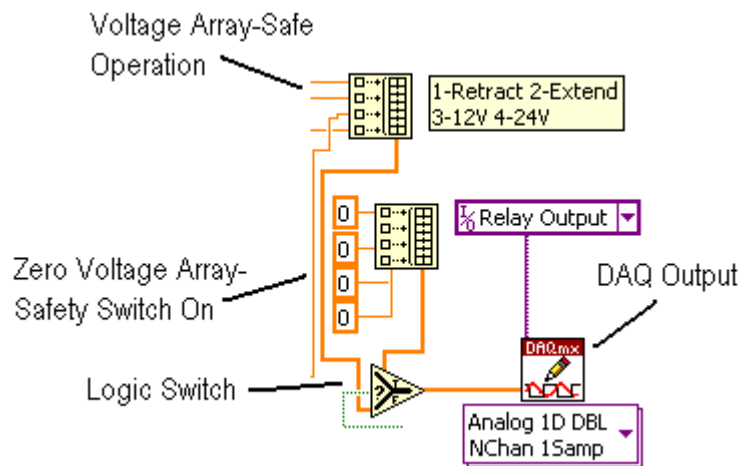


Figure 92: The input section, no longer utilizing the DAQ Assist.

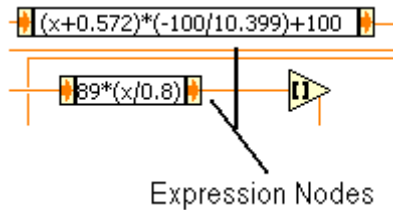


Figure 93: The expression nodes, used to manipulate data.